

Kate Robinson

Experimental and Numerical Investigations of Infiltration into Unsaturated Soil

Large-scale soil column experiment

June 2019



Norwegian University of
Science and Technology

Experimental and Numerical Investigations of Infiltration into Unsaturated Soil

Large-scale soil column experiment

Kate Robinson

Geotechnics and Geohazards

Submission date: June 2019

Supervisor: Thakur, Vikas

Co-supervisor: Depina, Ivan
Oguz, Emir Ahmet

Norwegian University of Science and Technology
Department of Civil and Environmental Engineering

Kate Robinson

Experimental and Numerical Investigations of Infiltration into Unsaturated Soil

Large-scale soil column experiment

Trondheim, June 2019

MASTER'S THESIS: TBA4900

Main supervisor: Dr. Vikas Thakur, NTNU

Co-supervisor: Dr. Ivan Depina, SINTEF

Co-supervisor: Mr. Emir Ahmet Oguz, NTNU Ph.D Candidate

Department of Civil and Environmental Engineering
Norwegian University of Science and Technology (NTNU)



NTNU – Trondheim
Norwegian University of
Science and Technology

Preface

This master's thesis was conducted in partial completion of the Master of Geotechnics and Geohazards at the Norwegian University of Science and Technology (NTNU) in the spring of 2019. The main supervisors of this project were Professor Vikas Thakur from NTNU, Dr. Ivan Depina from SINTEF and Ph.D. Candidate Emir Ahmet Oguz. This thesis was completed in conjunction with the KlimaDigital project, which is a collaboration between NTNU, SINTEF, MET and others.

The goal of this thesis was to design and construct a large-scale infiltration column test setup in the laboratory, and investigate the unsaturated characteristics of a soil by using instrumentation to monitor constant head infiltration tests. The unsaturated properties of a soil are important for effective stress calculations in slope stability analysis of unsaturated slopes, and this thesis was an investigation into evaluating if a valid relationship between soil suction and moisture content could be determined from installed instrumentation. The results of the infiltration tests were also evaluated with numerical analysis.

Trondheim, 2019-06-11



Kate Robinson

Acknowledgements

I would like to thank those who provided assistance to me during completion of my master thesis. Without your support and guidance during this semester I would have had a much more difficult journey to completing my thesis.

My supervisor Professor Vikas Thakur from NTNU and co-supervisor Dr. Ivan Depina from SINTEF were instrumental in completion of this thesis. They provided the topic for this thesis and helped to organize construction of the infiltration column and acquisition of the instrumentation, in addition to feedback and recommendations on testing procedures and interpretation of results.

Ph.D. candidate and co-supervisor Emir Ahmet Oguz was a great mentor during my thesis work. Thank you for your help in the laboratory and all the advice and information you provided during my thesis. Good luck with the rest of your research.

Professors Gudmund Eiksund, Gustav Grimstad and Steinar Nordal gave recommendations on the numerical modeling of unsaturated soils when numerical problems were encountered. Arnfinn Emdal provided the initial suggestion to construct an infiltration column for testing of unsaturated soil infiltration.

Espen Andersen and Karl Ivar Kvisvik helped with coordinating the laboratory work for the initial testing and material selection part of the thesis. Per Asbjørn Østensen spent many hours setting up the dataloggers to connect the instruments to the computer and writing the program to record instrument readings. Frank Stæhli gave advice and recommendations on the design of the infiltration column and constructed the entire test setup. Bent Lervik provided access to equipment in the roads department and instructions on use.

I would also like to thank my friends and family for the moral support through this semester. There were some challenging moments and it always helped to talk it through with those who were always willing to listen.

K.R.

Abstract

Many places around the world are affected by rainfall-induced landslides. These types of landslides often occur in unsaturated soil slopes, and conventional soil mechanics does not commonly consider the effects of negative pore-pressure, or suction, in effective stress calculations for slope stability. The soil water characteristic curve (SWCC) defines the relationship between moisture content and suction in a soil due to interaction between the air and water phases in a saturating or desaturating soil, and can be used to derive relationships for unsaturated soil permeability and water storage. This relationship has been found pivotal in describing unsaturated soil behaviour and was explored in detail in this thesis.

Rainfall-induced landslides frequently occur in remote or difficult to access locations, which still remain capable of impacting human life, infrastructure and the environment. These areas can be monitored with sensors connected via the Internet of Things to a local server. Moisture content and suction sensors were purchased by NTNU for this work with the purpose of assessing measurement accuracy and reliability in a laboratory setting, and the possibility of developing an in-situ SWCC during infiltration testing.

During this thesis a large-scale infiltration column was designed and constructed, standing 1.3 m tall with 0.24 m internal diameter. Material selection was conducted prior to delivery of the instruments and completion of the large-scale column through initial testing consisting of small-scale infiltration testing and numerical analysis using PLAXIS. The results of the initial testing concluded a combination of three materials available at NTNU was required to obtain a soil suction range compatible with the measurement range of the ordered suction sensor while maintaining reasonable infiltration times. The combined material contained 45% sand fraction, 45% silt fraction and 10% clay fraction and was classified as a clayey, sandy silt according to Norwegian standards.

The infiltration column was filled with 1 m of unsaturated soil and a constant head of water was applied to the top surface until the column became fully saturated through infiltration. Saturated permeabilities were measured from the flow of water exiting the base of the column. Five pairs of sensors were installed at various depths in the column to monitor the suction and moisture content change with time during infiltration. The sensors were connected to a computer through dataloggers, and a software program was written to record sensor readings at set intervals.

Three column infiltration tests were completed during this semester. The sensor data collected was used to create an average SWCC for the tested material using the van Genuchten-Mualem curve fitting model. From the SWCC, three methods were used to estimate the unsaturated Soil Permeability Function (SPF) for the material, using a combination of statistical methods, instrument data and visual measurements. The derived SPFs gave differing results due to assumptions

made in each method definition, but gave a trend within each infiltration test. An attempt was made to calibrate a Green-Ampt infiltration model to the infiltration rate, however the material did not fit with established datasets for obtaining the suction at the wetting front.

The finite element software PLAXIS 2D was used for numerical analysis of the infiltration tests to evaluate laboratory infiltration results. The derived SWCC was input as a hydraulic property of the material with the obtained saturated permeability, and a flow only analysis with transient groundwater flow conducted. The infiltration times were overestimated by 2.6 to 4 times that of the column test results. A sensitivity analysis was run on the van Genuchten-Mualem curve fitting parameters " a " and " n " to determine the impact on the infiltration time by modification of the parameters. The analysis concluded slight modifications to the SWCC can have large impacts on infiltration time, and due to the scatter in the sensor data it is difficult to estimate the appropriate SWCC for the material to match numerical analysis results.

The main conclusion from this thesis is the suction sensor ordered was not appropriate for the tested material. The sensor is not capable of measuring suctions below 9 kPa, which in this thesis meant the air entry value for the test material could not be found through sensor measurements. The transitional zone of the SWCC was also on the lower boundary of the suction sensor range and showed large scatter. Soils which desaturate more slowly and at higher suctions could be measured with this sensor, however infiltration times in a 1 m tall clay column would take significant time and may not be suitable for master thesis work. Additionally, the suction sensor appeared to have a slow reaction time to quickly changing moisture contents, which was shown by SWCCs differing between higher and lower sensor pairs as the infiltration rate slowed with depth.

Additional work could be conducted on the response time of the sensors during infiltration to conclude if they are suitable for accurate monitoring of infiltration in a field setting. This thesis was completed in conjunction with the KlimaDigital project, a collaboration between NTNU and SINTEF, among other industry and public partners ([SINTEF](#)). The KlimaDigital project aims to create a digitally supported framework to assess geohazard risks around Norway, and is currently focusing on rainfall-induced landslides. Based on the results of this thesis, the instruments may be installed in a field setting around Trondheim in the summer for further evaluation.

Contents

Preface	i
Acknowledgements	ii
Abstract	iii
1 Introduction	1
1.1 Background	2
1.2 Problem Formulation	4
1.3 Objectives	4
1.4 Limitations	4
1.5 Structure of the Report	5
2 Unsaturated Soil Theory	6
2.1 Landscape of an Unsaturated Soil	6
2.1.1 Capillary Theory	7
2.1.2 Stress State	9
2.1.3 Slope Stability	10
2.2 Soil Water Characteristic Curves	12
2.2.1 Description	13
2.2.2 Determination of SWCC points	14
2.2.3 Curve Fitting of SWCC points	15
2.3 Water Flow	19
2.3.1 Transient Flow	20
2.3.2 Green-Ampt Infiltration Model	21
2.4 Soil Permeability Functions	23
2.4.1 Instantaneous Profile Method	23
2.4.2 Wetting Front Advance Method	25
2.4.3 Empirical and Statistical Methods	27
3 Preparation for Large-scale Column Testing	29
3.1 Permeameter Testing	29
3.2 Numerical Model	31

3.2.1	Model Parameters	31
3.2.2	Model Trials	33
3.2.3	Discussion on Initial Testing	35
3.3	Material Selection	36
3.4	Selection of Instrumentation	40
3.4.1	Volumetric Water Content Sensors	40
3.4.2	Suction Sensors	44
3.5	Soil Water Characteristic Curve from Initial Testing	48
4	Large-Scale Infiltration Column Testing	51
4.1	Design of Infiltration Column	51
4.2	Experiment Preparation	53
4.2.1	Sample Preparation	53
4.2.2	Instrumentation Setup	54
4.2.3	Compaction into Column	55
4.2.4	Test Initiation	56
4.2.5	Test Completion	56
4.3	Large-scale Column Test Results and Discussion	58
4.3.1	Testing conditions	59
4.3.2	Instrument Readings	59
4.3.3	Saturated Permeability Measurements	64
4.3.4	Physical Observations	64
4.4	Derivations from Results and Discussion	67
4.4.1	Soil Water Characteristic Curve from Column Testing	67
4.4.2	Unsaturated Soil Permeability Function	70
4.4.3	Infiltration Model Comparison	74
5	Numerical Infiltration Study	77
5.1	Model Description	77
5.2	Numerical Control Parameters	79
5.3	Model Results and Discussion	80
5.4	Sensitivity Analysis	81
5.4.1	Curve Fitting Parameter Modification	82
5.4.2	Effect of Curve Fitting Parameters on Infiltration Time	84
5.4.3	Results and Discussion	87
5.5	Limitations of Numerical Model	88
6	Summary and Main Conclusions	91
7	Recommendations for Future Work	94

Bibliography	96
Appendix A Drawings	100
Appendix B Laboratory Testing Results	103
Appendix C Sample Photos from Test 2	110

List of Figures

1.1 Fatal landslides in Europe showing an increasing trend after 2008 (Haque et al., 2016)	2
1.2 Number of fatalities versus economic loss for countries around Europe (Haque et al., 2016)	3
2.1 Zones of an unsaturated soil (Makonto, 2013)	6
2.2 Phases of an unsaturated soil (Fredlund et al., 2012)	7
2.3 Matric suction as a function of pore radius (Fredlund et al., 2012)	9
2.4 Infinite slope sliding block (Cho and Lee, 2002)	11
2.5 Typical Soil Water Characteristic Curve (Soltani et al., 2019)	13
2.6 Hysteresis of SWCCs (Fredlund et al., 2012)	14
2.7 Suction ranges of various methods used to determine a SWCC in the laboratory (Tuller and Or, 2003)	15
2.8 Variation in Fredlund-Xing SWCC by modifying each curve fitting parameter (Fredlund and Xing, 1994)	19
2.9 Distinct wetting front for Green-Ampt infiltration calculations (Zhang et al., 2016)	22
2.10 Variables for wetting front advance method calculations (Li et al., 2009)	26
3.1 Permeameter cell used for initial testing	30
3.2 Grainsize distribution of initial material	31
3.3 PLAXIS model for initial testing	32
3.4 Comparison of van Genuchten SWCCs	34
3.5 Comparison of infiltration times between laboratory and PLAXIS analyses	35
3.6 Typical SWCCs for sand, silt and clay material (Fredlund et al., 2012)	35
3.7 USDA soil types (stackoverflow)	36
3.8 SWCCs from USDA dataset	37
3.9 Grainsize distributions of sand and gravel, sand, silt and clay materials	38
3.10 Combined grainsize distribution used in testing	39
3.11 ECH ₂ O Sensor from METER Group, Inc.	41
3.12 VWC calibration curves from laboratory testing and METER group	43

3.13 Performance of VWC sensors during initial testing	44
3.14 TEROS 21 suction sensor from METER Group, Inc.	45
3.15 SWCC of porous discs in TEROS 21 suction sensors (METER Group, 2019d)	46
3.16 Performance of suction sensors during initial testing	47
3.17 Initial testing points for SWCC with van Genuchten-Mualem fit	49
3.18 Fitted SWCCs comparison	49
4.1 Instrumented column used for infiltration testing	52
4.2 Components of the column base	53
4.3 Machine used for mixing and conditioning material	54
4.4 Instrument arrangement during soil placement and compaction	55
4.5 Compaction of soil lifts and placement of instruments in column	56
4.6 Column tilted for soil removal from base	57
4.7 Rinsing the column in the sink	57
4.8 Experiment setup	58
4.9 Grainsize distributions for large-scale column testing	60
4.10 Instrument readings from column test 1	61
4.11 Instrument readings from column test 2	62
4.12 Instrument readings from column test 3	62
4.13 Comparison of VWCs with depth	63
4.14 Surface settlement with time during column tests	65
4.15 Movement of soil, sensors and wetting front during testing	66
4.16 SWCCs plotted from large-scale test data	67
4.17 Optimization to find Brooks and Corey pore size distribution index and air entry value	69
4.18 Fitted SWCCs using column testing data	70
4.19 Upper and lower bound of van Genuchten-Mualem SWCCs from testing data	71
4.20 SPFs generated using three different methods from column test data	72
4.21 VWC and suction measurements with depth at instantaneous profile method time increments	73
4.22 Range of SPFs based on van Genuchten-Mualem formulation of the SWCC	74
4.23 Comparison of Green-Ampt model with column testing infiltration	75
4.24 Wetting front suction based on soil fractions (from Dingman (2015) after Rawls et al. (1983))	76
5.1 PLAXIS large-scale column test model	78
5.2 Numerical control parameters giving stable infiltration times	80
5.3 Suction and saturation profiles, and flow vectors after 2 minutes of infiltration dur- ing Test 2	81
5.4 Sensitivity of SWCC due to variation in van Genuchten-Mualem " α " parameter	82

5.5	Sensitivity of SWCC due to variation in van Genuchten-Mualem " n " parameter . .	83
5.6	Sensitivity of SPF due to variation in van Genuchten-Mualem " a " parameter	83
5.7	Sensitivity of SPF due to variation in van Genuchten-Mualem " n " parameter . . .	84
5.8	Variation of infiltration time by curve fitting parameter modification	85
5.9	Comparison of curve fitting parameter combinations to match column infiltration time	86
5.10	SWCCs giving infiltration time close to column experiments	86
5.11	SPFs giving infiltration time close to column experiments	87
5.12	SPF plotted against saturation level	89

List of Tables

3.1	Initial permeameter testing parameters and results	30
3.2	van Genuchten parameters used in PLAXIS initial modeling	34
3.3	Infiltration time and grainsize distributions for selected USDA soil types	37
3.4	Material combination and final fractions used in testing	40
3.5	SWCC parameters for initial testing fitting equations	48
4.1	Variables for large-scale column tests	59
4.2	Saturated permeabilities from column testing	64
4.3	Saturation levels in soil columns after infiltration completion	64
4.4	SWCC fitting equation parameters from column testing data	68
5.1	van Genuchten-Mualem SWCC parameters used in PLAXIS model	78
5.2	Comparison of infiltration times between PLAXIS model and large-scale column testing	81

List of Acronyms and Symbols

Acronyms

AIC Akaike Information Criterion

ASTM American Society for Testing and Materials

FS Factor of safety

GSD Grainsize Distribution

LA Abrasion Los Angeles Abrasion

MET Norwegian Meteorological Institute

NGTS Norwegian Geo-Test Site

NTNU Norwegian University of Science and Technology

POM Polyoxymethylene

SPF Soil Permeability Function

SWCC Soil Water Characteristic Curve

USCS Unified Soil Classification System

USDA United States Department of Agriculture

VWC Volumetric Water Content

Greek Symbols

α Slope angle [°]

χ Bishop effective stress parameter

ϵ_a Dielectric permittivity [F/m]

γ Unit weight of water [kN/m³]

λ_{bc} Brooks and Corey pore-size distribution index
 ϕ' Effective internal friction angle [°]
 ψ Total suction head [kPa]
 $\psi_m = u_a - u_w$ Matric suction [kPa]
 ψ_p Pressure suction head [kPa]
 ψ_g Gravitational suction head [kPa]
 ψ_o Osmotic suction head [kPa]
 ψ_{aev} Air-entry value suction [kPa]
 ψ_r Residual suction [kPa]
 ψ_f Suction at the wetting front [m]
 ρ Density of material [kg/m³]
 ρ_w Density of water [kg/m³]
 ρ_d Dry bulk density [kg/m³]
 σ' Effective stress [kPa]
 σ Total stress [kPa]
 τ Shear stress [kPa]
 Θ Normalized volumetric water content
 θ Volumetric water content
 $\theta_s, \theta_r, \theta_i$ Saturated, residual and initial volumetric water content
 u_a Air pressure [kPa]
 u_w Water pressure [kPa]

Roman Symbols

A Area of column [m²]
 a, n, m Curve fitting parameters in Van Genuchten-Mualem equation [units of a : 1/kPa or 1/m]
 a_f, n_f, m_f Curve fitting parameters in Fredlund-Xing equations [units a_f : kPa]
 $C(\psi)$ Fredlund-Xing correction factor
 c' Effective cohesion [kPa]

$f(t)$ Infiltration rate [m/s]
 $F(t)$ Cumulative infiltration [m]
 F_p Infiltration depth at ponding time [m]
 H Total head [m]
 h Hydraulic head [m], or column height in wetting front advance method [m]
 h_c Capillary height [m]
 i Hydraulic gradient
 m End of profile in instantaneous profile method
 j Point of interest in instantaneous profile method
 h Hydraulic head [kPa]
 k Permeability [m/s]
 k_s Saturated permeability [m/s]
 $k(\psi)$ Permeability as a function of soil suction
 r Radius of capillary tube when the liquid is water [m]
 S Degree of saturation
 S_r Residual saturation
 S_s Full saturation
 t Time [units vary]
 t_p Time to ponding [h]
 T_s Surface tension of a liquid [N/m]
 V_w Volume of water [m³]
 w Gravimetric moisture content
 v Velocity [m/s]
 W Soil weight [kPa]
 z Elevation head [m]

Chapter 1

Introduction

Shallow landslides are frequently triggered around Norway and the world due to rainfall infiltration. Slopes which are relatively steep and initially dry are sometimes stable due to the contributions of suction, or negative pore water pressure, on the effective stress in the soil. Soils near the surface have low effective stress due to less overburden pressure and may rely on suction stresses to remain stable. Suction is related to the moisture content in a soil by the Soil Water Characteristic Curve (SWCC), which describes the interaction between the water and air phases in an unsaturated soil. As soils begin to saturate through rainfall infiltration, suction levels in a soil tend to decrease which can lead to slope destabilization.

Soil sensors can be installed in slopes of interest to monitor site conditions in near real time, and communicate data via the Internet of Things to a local server for interpretation. Sensors to monitor soil suction and soil moisture content were purchased for use in this thesis by NTNU and were evaluated for potential future use in a field setting.

A large-scale infiltration column was designed and constructed for performing constant head infiltration tests on unsaturated soil. The column was instrumented with moisture content and suction sensors to monitor the change in soil conditions with time during infiltration. The material used in testing was a mixture of three soils available at NTNU, combined to create a soil reasonable for Norwegian conditions while maintaining acceptable testing times. Three infiltration tests were conducted in the large-scale column during this semester.

The sensor data from infiltration testing was used to create a SWCC for the tested material. Soil permeability functions (SPFs) were derived using combinations of three methods: statistical SWCC interpretation, sensor measurements, and visual interpretation. Finally the infiltration advance rate was fit to an infiltration model.

The laboratory infiltration time was compared to a numerical simulation using the SWCC estimated from sensor data and the saturated permeability. A sensitivity analysis was conducted on the SWCC model curve fitting parameters to assess the parameter influence on infiltration time.

1.1 Background

During the period of 2004-2016, approximately 56,000 people were killed in over 4,800 non-seismically induced landslides around the world (Froude and Petley, 2018). According to Chae et al. (2017), landslides are responsible for a minimum of 17% of fatalities due to natural hazards worldwide. In addition to these deaths, many more people were likely affected through injury or property damage. Infrastructure such as transportation and communication networks around countries are also affected by landslide damage every year (Haque et al., 2016).

Haque et al. (2016) compiled a list of fatal landslides between 1995 and 2014 encompassing 27 countries in Europe. In this time, 1,370 deaths and 784 injuries were reported following 476 landslides occurring all over Europe. Figure 1.1 shows an increasing number of fatal landslides in the years 2008 onward, however the authors note this may be due to increased reporting during that period.

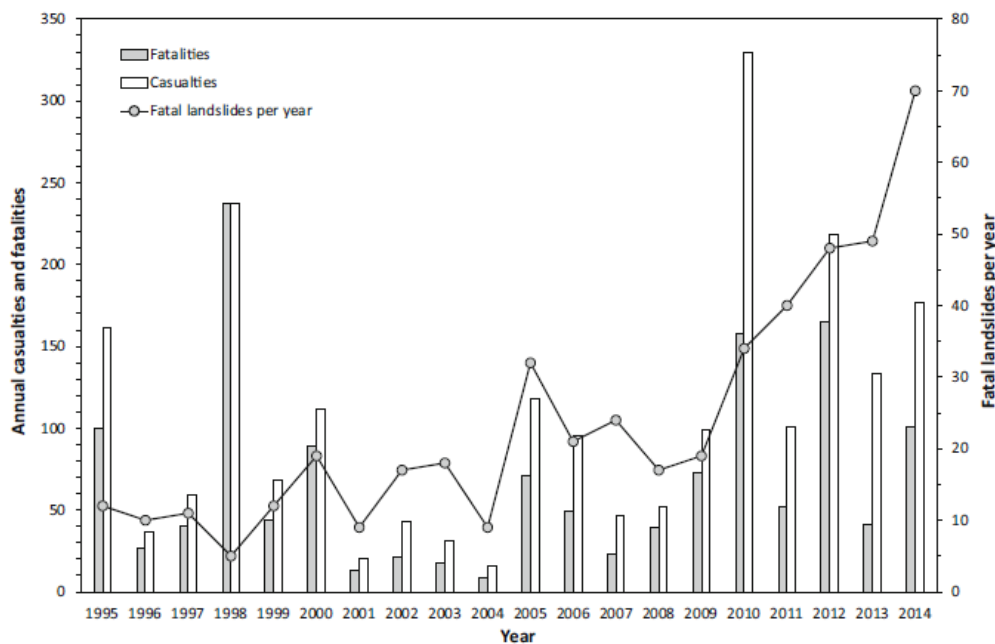


Figure 1.1: Fatal landslides in Europe showing an increasing trend after 2008 (Haque et al., 2016)

The average economic loss is 4.7 billion Euros annually throughout Europe due to landslides. Figure 1.2 shows a graph of number of fatalities versus economic loss for some European countries. In Norway, over 40 fatalities were reported, totalling around 5 million Euros. Additionally, over 8000 kilometers of roads, railways and other linear infrastructures are exposed to landslide hazards around Europe (GeoCybersafe, 2018).

This thesis was conducted in conjunction with the KlimaDigital project, which is a collaboration between NTNU and SINTEF, among other industry and public partners. The KlimaDigital project is investigating the use of Internet of Things enabled sensors to monitor remote or diffi-

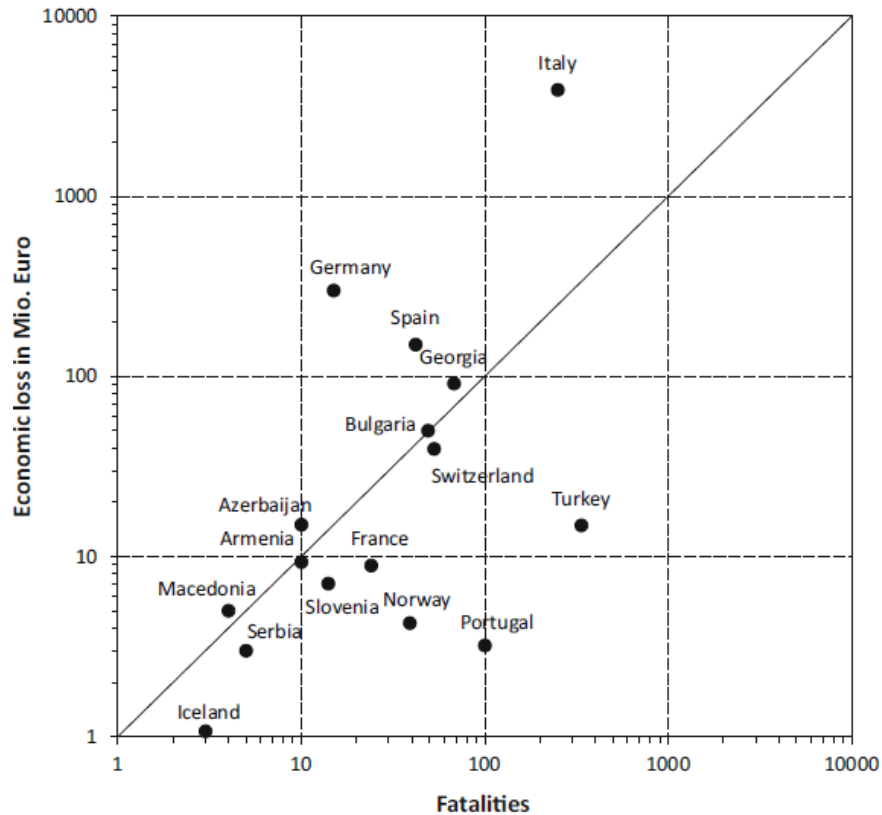


Figure 1.2: Number of fatalities versus economic loss for countries around Europe (Haque et al., 2016)

cult to access site locations where shallow landslides are of concern. Currently, the application of IoT solutions for monitoring landslides in Norway is at an early stage, mainly within the research domain.

Norway has a regional landslide forecasting system operated by Varsom (Devoli et al., 2018), however the forecasts are based on conceptual hydrologic models which simulate and update conditions based on forecasted regional precipitation and temperature, instead of monitoring site specific conditions. Given the high number of remote or challenging to access landslide sites around Norway, there is a desire to develop an IoT device or system that can operate independently, and without large maintenance requirements, to monitor site conditions and send data to a specified location for interpretation. Additionally, the population of Norway is growing and people are moving to areas potentially in danger of landslides (SINTEF). Combined with a predicted increase in frequency of landslide triggering events due to changing climate, there is a need to develop a robust monitoring system. The relevance of this thesis was to assess the performance of soil sensors in providing accurate information on site conditions and if the data provided could be used to generate unsaturated soil relationships.

1.2 Problem Formulation

The focus of this thesis was to design and construct a large-scale infiltration column to perform constant head infiltration tests which could be monitored with moisture content and suction sensors. The sensor performance was to be evaluated for accuracy, reliability, response time and measurement range applicability for potential future use in shallow landslide field monitoring.

The data retrieved from the sensors after infiltration testing was to be evaluated for use in creating unsaturated soil relationships such as the soil water characteristic curve and soil permeability function. Numerical analysis was to be conducted on the derived relationships and infiltration times compared to large-scale column testing results to assess to assess if a simplified numerical model could accurately reproduce laboratory results.

1.3 Objectives

The main objectives of this thesis include:

1. Design and construct a large-scale infiltration column test setup
2. Select and order sensors to install into the infiltration column
3. Develop a gradation curve and material fractions for soil to be tested
4. Conduct infiltration testing in large-scale model
5. Evaluate accuracy of sensors and quality of sensor data
6. Determine soil-water characteristic curve for tested material
7. Establish soil permeability function for tested material
8. Verify laboratory infiltration process with numerical modelling

1.4 Limitations

Some limitations related to this thesis work include:

- Although the background of this thesis is related to shallow landsliding, only 1D column infiltration testing took place and slope stability analysis was not conducted.
- Infiltration testing took place in a laboratory setting, so wireless sensor communication was unnecessary and sensors were directly connected to a laptop. Thus the wireless communication capacity of the sensors was not considered and should be investigated prior any future field installation.

- This thesis focused on instruments monitoring rainfall infiltration leading to shallow landsliding in unsaturated soils. No testing was completed where a groundwater table was present or where the effects of a rising groundwater table (i.e. from an impermeable surface) led to slope failure.
- Soil water characteristic curves can exhibit hysteresis between wetting and drying curves. Only infiltration testing took place, so only the wetting curve for the tested material was estimated.

1.5 Structure of the Report

The remainder of the report is structured as follows.

- Chapter 2 gives an introduction to unsaturated soil mechanics relating to rainfall-induced landslides, and equations used for calculations.
- Chapter 3 explains the initial testing conducted in the laboratory to create the material to be used for testing, describes the sensors and provides initial results from sensor data in the combined material.
- Chapter 4 gives the results from the large-scale infiltration column testing, and provides discussions on the derived unsaturated soil relationships using sensor output data.
- Chapter 5 outlines the verification of infiltration results from the column testing using finite element software, a sensitivity analysis on the curve fitting parameters, and a back analysis to find parameters giving equivalent infiltration times.
- Chapter 6 provides a summary of work completed and final conclusions.
- Chapter 7 outlines recommendations for test setup and sensor improvements, and future work which could be conducted using the infiltration column and sensors.

Chapter 2

Unsaturated Soil Theory

2.1 Landscape of an Unsaturated Soil

Classical soil mechanics assumes a two phase soil system at all points in the soil deposit. Above the water table, the soil is completely dry, leaving only solid and gas phases. Below the water table no air exists and the two phases are solid and liquid. However, true soil slopes contain zones of various saturation levels, as shown in Figure 2.1.

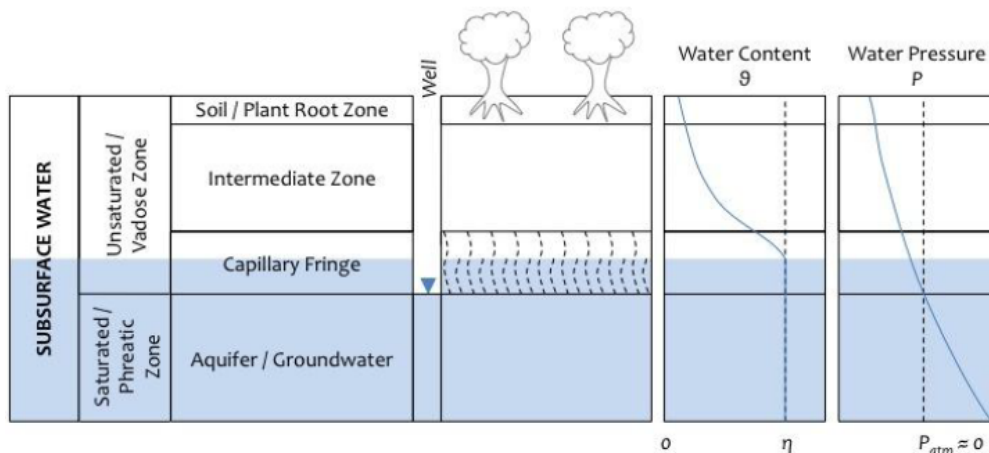


Figure 2.1: Zones of an unsaturated soil (Makonto, 2013)

The unsaturated zone above the water table is also termed the vadose zone, and includes the capillary fringe, intermediate zone and soil/plant root zone, which generally decrease in moisture content towards surface. In these unsaturated zones, four phases exist: solid, liquid, gas and contractile skin, as shown in Figure 2.2. The contractile skin is defined as the air-water interface, or interaction between the air and water phases, and causes capillarity in the vadose zone, or the phenomenon of water rising above the water table due to surface tension (Fredlund et al., 2012).

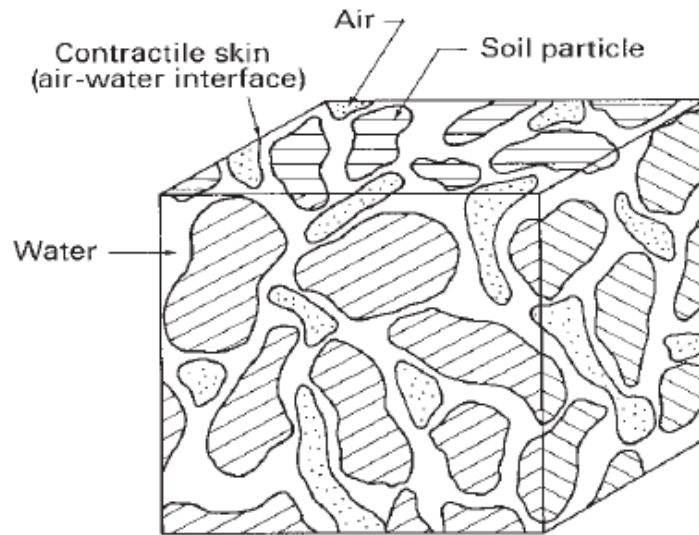


Figure 2.2: Phases of an unsaturated soil (Fredlund et al., 2012)

2.1.1 Capillary Theory

According to Bernoulli's principle, in steady state conditions, the total head along a soil column is constant. Total head is composed of three components: elevation head (z), pressure head ($\frac{p}{\rho g}$) and velocity head ($\frac{v^2}{2g}$), shown in Equation 2.1. In soils, the velocity head is generally a small component of the total head and is often removed. The sum of the elevation and pressure heads is commonly referred to as hydraulic head, where the pressure, p , is equal to water pressure, u_w .

$$H = z + \frac{p}{\rho g} + \frac{v^2}{2g} = \text{constant} \quad (2.1)$$

where:

H = total head [m]

z = elevation head [m]

p = pressure [kPa]

ρ = density of fluid [kg/m^3]

g = acceleration due to gravity [m/s^2]

v = velocity of fluid [m/s]

If the elevation datum is set to the groundwater table, where the pressure head is zero, any water pressure above the groundwater table must be negative to negate the positive elevation head, and water pressure below the groundwater table is positive due to negative elevation head. Thus, porewater pressure above the groundwater table in the vadose zone is negative, provided the pore air pressure is taken as atmospheric and equal to 0. Matric suction is defined to be the difference between the pore air and pore water pressure, shown in Equation 2.2.

$$\psi_m = (u_a - u_w) \quad (2.2)$$

where:

ψ_m = matric suction [kPa]

u_a = pore air pressure [kPa]

u_w = pore water pressure [kPa]

The height of capillary rise above the groundwater table is a function of the surface tension on the contractile skin, which is a function of the adhesion between the contractile skin and the material of the capillary tube. Fredlund et al. (2012) give an equation for the height of capillary rise in a clean glass tube, shown in Equation 2.3.

$$h_c = \frac{2 \cdot T_s}{\rho_w \cdot g \cdot r} \quad (2.3)$$

where:

h_c = capillary rise height [m]

T_s = water surface tension [N/m]

ρ_w = density of water [kg/m³]

g = acceleration due to gravity [m/s²]

r = meniscus radius of the capillary tube when the liquid is water [m]

If the equation for water pressure ($u_w = \rho_w g h_c$) is substituted into Equation 2.3, and air pressure is considered to be atmospheric (i.e. $u_a = 0$), then matric suction can be related to pore radius and surface tension by Equation 2.4.

$$u_a - u_w = \frac{2 \cdot T_s}{r} \quad (2.4)$$

Fredlund et al. (2012) show a plot of pore radius for various soil grain sizes against matric suction using Equation 2.4, indicating smaller grain sizes such as clays induce larger matric suctions than coarser grains such as sands (Figure 2.3).

Equation 2.4 was developed for use in a uniform material with equal grain radii throughout the sample. However, in natural deposits, the grain radii, and therefore capillary pore radii, exist in non-uniform distributions and require complex formulations to describe pore size distributions. These distributions provide the basis for relationships between soil suction and moisture content and are further discussed in Section 2.2.

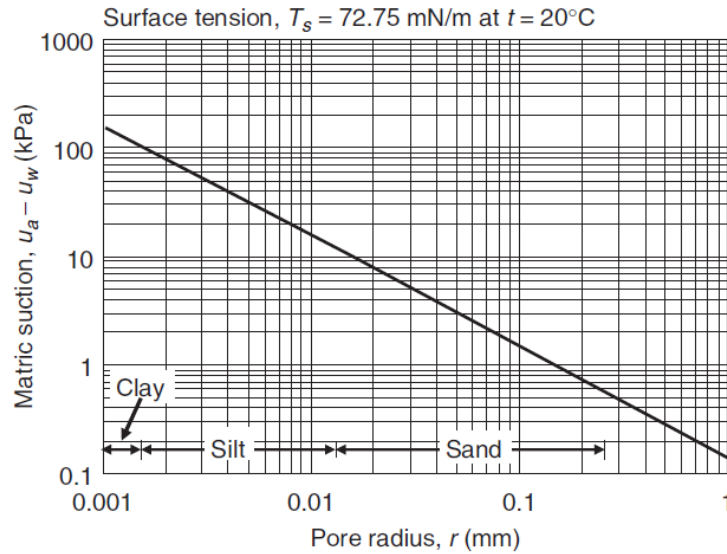


Figure 2.3: Matric suction as a function of pore radius (Fredlund et al., 2012)

2.1.2 Stress State

When analyzing unsaturated soils it becomes important to consider the effective stress state including the contributions of suction. The effective stress in a soil was first defined by Karl Terzaghi in 1936 as the difference between the total soil stress and the pore water pressure at a point of interest in the soil deposit (Equation 2.5).

$$\sigma' = \sigma - u_w \quad (2.5)$$

where:

σ = total stress [kPa]

σ' = effective stress [kPa]

u_w = pore pressure [kPa]

An unsaturated soil, as discussed in Section 2.1, contains an gas phase in addition to the solid and liquid phases, which in combination with liquid creates a contractile skin. Researchers identified a need to distinguish between total stress changes and pore water pressure changes when analyzing an unsaturated soil, which resulted in the definition of three stress state variables considering soil, air and water phases, to be $(\sigma - u_a)$, $(\sigma - u_w)$ and $(u_a - u_w)$ (Fredlund et al., 2012). Of these, the combination of $(\sigma - \sigma_a)$ and $(\sigma_a - \sigma_w)$, or net normal stress and matric suction, are most widely accepted to describe the stress state in an unsaturated soil.

As described by Lu and Likos (2006), true effective stress should take into account macroscopic stresses such as total stress, pore air and porewater pressures in addition to microscopic stresses from physicochemical and capillary forces. However, microscopic stresses are often taken into

account as cohesion in shear strength envelope equations (i.e. the Mohr-Coulomb envelope) and are therefore excluded in effective stress formulations. The concept of cohesion is further discussed in Section 2.1.3.

Terzaghi's original effective stress equation is sufficient to describe the stress state in a saturated soil medium, but only considers one stress state variable. Bishop proposed an effective stress equation in 1959 for unsaturated soils, shown in Equation 2.6. This formulation uses an effective stress parameter, χ , to modify the effective stress in the soil as a result of matric suction.

$$\sigma' = (\sigma - u_a) + \chi(u_a - u_w) \quad (2.6)$$

where:

σ' = effective stress [kPa]

σ = total stress [kPa]

u_a = pore air pressure [kPa]

χ = Bishop effective stress parameter

u_w = pore water pressure [kPa]

The Bishop effective stress parameter is often defined as the effective saturation (i.e. ranging from 0 to 1) in the soil, however this has been expressed as a limitation by some (Fredlund et al., 2012). The relationship of χ to a soil property (saturation level) excludes the Bishop equation from designation as a stress state variable, as stress states must be independent of soil properties. The finite element software package PLAXIS takes χ to be the effective saturation in effective stress calculations in unsaturated soils when suction is enabled (PLAXIS bv, 2019a).

2.1.3 Slope Stability

Shallow landslides are often analysed using infinite slope theory, which assumes the depth of a failing mass is small compared to the length and width. Since the failure surface is generally parallel to the ground surface, the stability can be simplified to a sliding block as shown in Figure 2.4.

The factor of safety for a slope is given as the ratio of resisting stresses to driving stresses, or shear strength to shear stress. For the slope shown in Figure 2.4, the factor of safety could be calculated by Equation 2.7, with the shear strength of a soil as the numerator. In this equation the shear strength is expressed as the Mohr-Coulomb criterion. As there is no groundwater table illustrated in Figure 2.4, it can be assumed the failure surface occurs near to surface, and above the groundwater table. Shallow landslides often occur in this partially saturated zone, and therefore it is important to properly characterize the shear resistance along the sliding plane (Lu and Godt, 2008). As discussed earlier, the effective stress acting at the failure surface should take into account the negative pore pressure in the unsaturated soil.

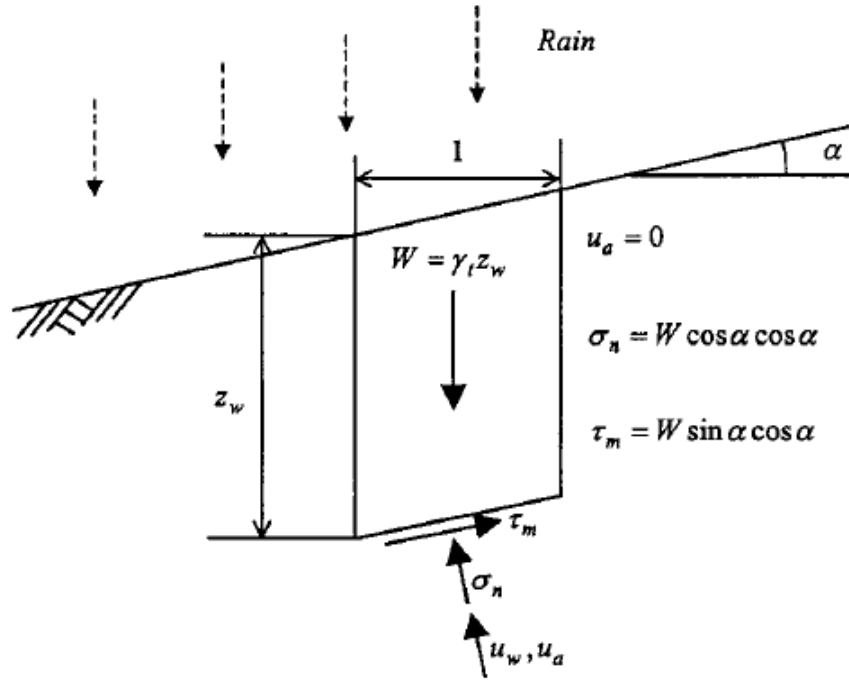


Figure 2.4: Infinite slope sliding block (Cho and Lee, 2002)

$$FS = \frac{\tau_{\text{resisting}}}{\tau_{\text{driving}}} = \frac{c' + \sigma' \cdot \tan \phi'}{W \cdot \sin \alpha \cdot \cos \alpha} \quad (2.7)$$

where:

FS = factor of safety

τ = shear stress [kPa]

c' = effective cohesion [kPa]

σ' = effective stress [kPa]

ϕ' = effective friction angle [°]

W = weight of soil [kPa]

α = slope angle [°]

The required input parameters in the Mohr-Coulomb failure criterion are the effective stress at the shearing boundary, cohesion and friction angle. The friction angle can be experimentally determined and the Bishop effective stress can be used in place of Terzaghi's effective stress in unsaturated soil situations to account for matric suction contributions to shear strength. Equation 2.8 shows the Mohr-Coulomb failure criterion used in the factor of safety equation with the Bishop effective stress for an infinite slope.

$$FS = \frac{c' + [(\sigma - u_a) + \chi(u_a - u_w)] \cdot \tan \phi' \cdot \cos^2 \alpha}{W \cdot \sin \alpha \cdot \cos \alpha} \quad (2.8)$$

Cohesion is defined in soil mechanics as the shear strength of a material without any applied normal stress, or the act of soil grains sticking together without external load (Lu and Likos, 2013). Cohesion can occur through several processes:

1. Van der Waals attraction
2. Double layer repulsion
3. Cementation
4. Particle interlocking
5. Capillary attraction

Items [1] to [3] are commonly referred to as interparticle physicochemical forces due to the dependence on both physical and chemical properties of the soil and water (Lu and Likos, 2006). Item [4] results from particle surface condition. All items [1-4] are dependant on material type and degree of saturation, but can exist at all saturation levels.

In shear strength equations for saturated soils, cohesion only takes into account items [1] through [4], because in a saturated state, capillary attraction is negligible. However, in unsaturated soils, cohesion is also influenced by the capillary attraction, or matric suction, in a soil and item [5] should be taken into consideration (Lu and Likos, 2013). The capillary attraction is often incorporated into shear strength equations as the stress state variable matric suction, such as in Bishop's effective stress equation.

2.2 Soil Water Characteristic Curves

The Soil Water Characteristic Curve (SWCC) is typically a sigmoidal shaped function (i.e. S-shaped curve) which relates matric suction to the moisture content (gravimetric or volumetric moisture content, or degree of saturation) in the soil. This function has been described as a pivotal relationship of soil behaviour during change in saturation levels due to the interaction of the air and water phases in an unsaturated soil (Fredlund et al., 1996), and is therefore necessary when solving transient problems in the unsaturated (vadose) zone (Sillers and Fredlund, 2001). Other functions which are based on the SWCC include permeability and water storage functions, discussed in Section 2.4. Lastly, the SWCC provides information required for analysis of seepage, shear strength, volume change and other problems related to unsaturated soils (Fredlund et al., 2012).

It should be noted the SWCC is often referred to by other names (e.g. in soil science disciplines) such as the soil water retention curve, moisture retention curve or others, however in this thesis will be referred to as the soil water characteristic curve or SWCC.

2.2.1 Description

The SWCC can be broken down into three ranges of soil saturation, known as the boundary effect zone, the transition zone and the residual zone, shown in Figure 2.5.

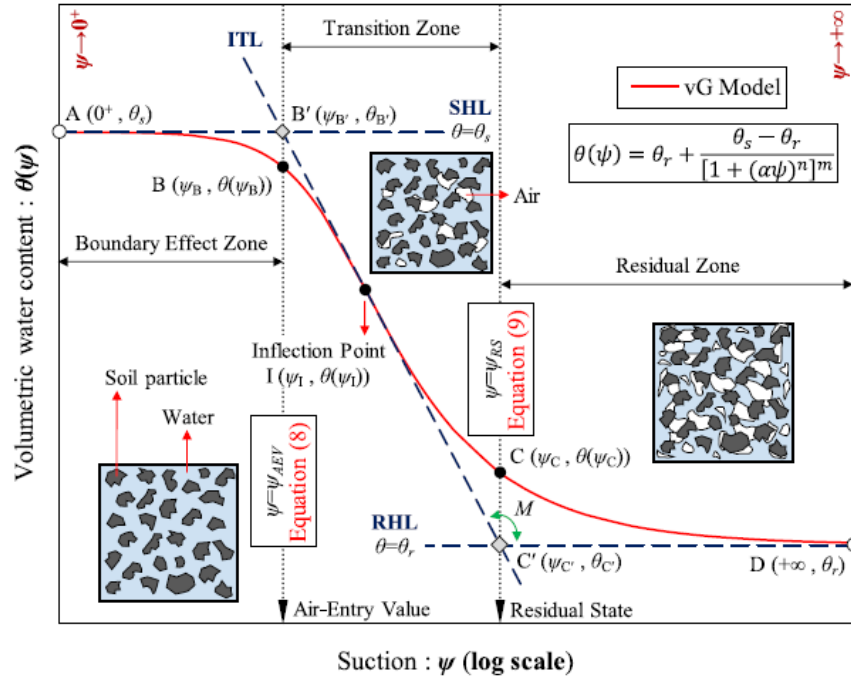


Figure 2.5: Typical Soil Water Characteristic Curve (Soltani et al., 2019)

The boundary effect zone, or capillary saturation zone, is the wettest part of the SWCC, where the pore water is in tension and holding the soil nearly saturated. As drying occurs the soil approaches the air entry suction value (i.e. bubbling pressure), at which point air bubbles begin to enter the soil pores (Sillers et al., 2001). As can be seen in Figure 2.5, the soil has only two phases in this zone of the SWCC: water and soil.

In the transition (desaturation) zone the pore water continues to be replaced by air, and approaches the residual moisture content. The soil pores in this zone are filled with a mixture of air and water. In this zone small changes in suction show large moisture content changes, however the steepness of the curve varies depending on soil type (Fredlund et al., 2012).

The residual saturation zone is where the moisture content dips below the residual moisture content. The remaining pore water is difficult to remove, even with large changes in suction, and any movement of moisture is typically associated with vapour (Sillers et al., 2001). In this zone most pore space is air filled; any remaining water is discontinuous and does not flow easily.

Figure 2.5 only shows one SWCC, however SWCCs may follow different paths when wetting and when drying. Figure 2.6 shows two SWCC lines, labelled desorption, or drying, and adsorption, or wetting. The difference between these drying and wetting curves is due to hysteresis. Not all

SWCCs will exhibit hysteresis, as it depends on factors such as non-uniform pore cross sections, differing contact angles between soil grains and water during wetting and drying, and trapped air (Zhang et al., 2016; Fredlund et al., 2012). For example, the radius of curvature of the water meniscus is smaller during drying than wetting, giving larger suction values on the drying curve (Albadri et al., 2018). The starting point of the wetting and drying curves may also begin from different points along the moisture content axis due to trapped air in the pores (Fredlund and Xing, 1994).

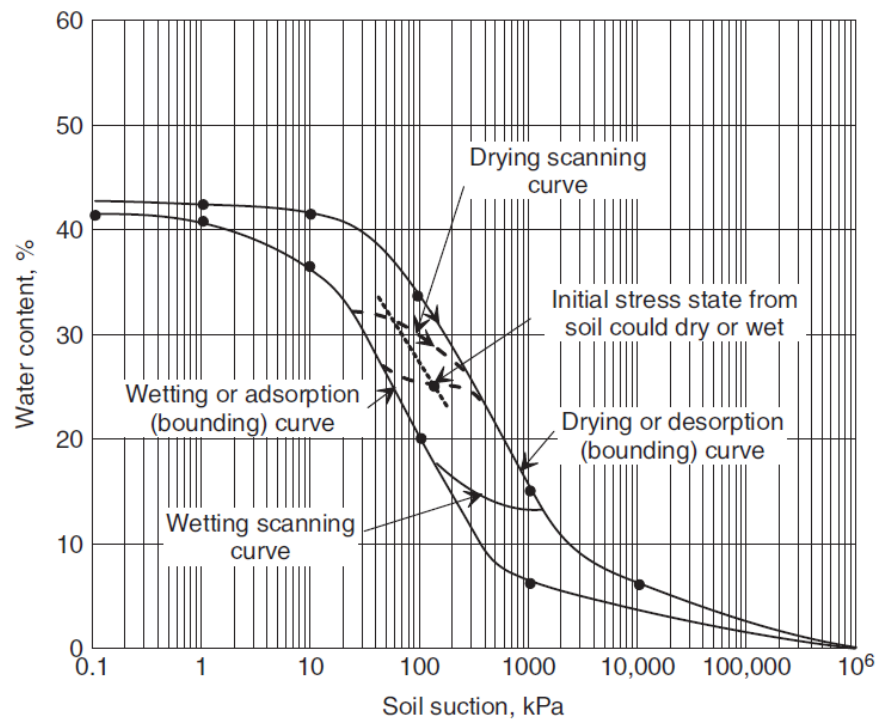


Figure 2.6: Hysteresis of SWCCs (Fredlund et al., 2012)

SWCCs are not unique curves, even for the same soil, as they will form differently depending on the history of wetting and drying (i.e. stress history), and the current soil stress state (Fredlund et al., 2012). There are bounding curves for the extreme cases (i.e. initial drying and wetting) and scanning curves within the bounding curves. In this thesis, only the wetting curves will be considered as rainfall infiltration would follow a wetting curve.

2.2.2 Determination of SWCC points

SWCCs can be developed from various estimation techniques based on soil index parameters, or can be measured in the field or laboratory by direct or indirect methods (Zapata et al., 1999). Typically several methods are required to define the entire SWCC, as each method is only applicable over a certain range of suction values. Figure 2.7 shows various available testing methods and the range of the moisture content and suction covered by each method.

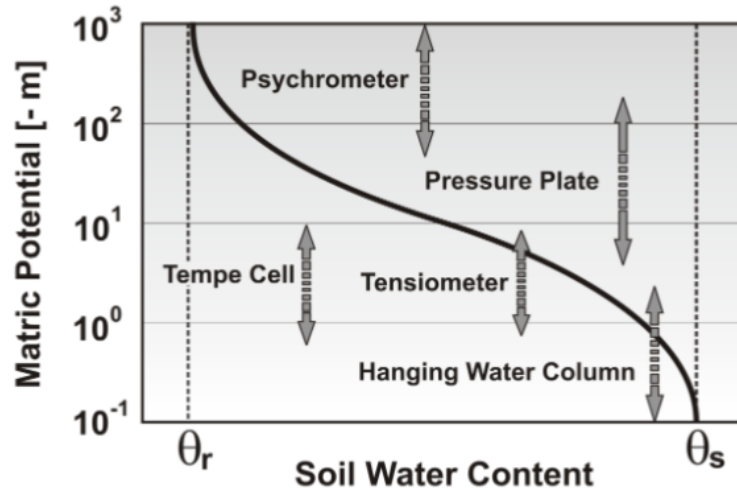


Figure 2.7: Suction ranges of various methods used to determine a SWCC in the laboratory (Tuller and Or, 2003)

In this thesis a direct method was used in the laboratory to determine a portion of the SWCC, by use of a tensiometer in combination with oven-drying moisture content measurements and volumetric water content (VWC) sensor measurements. Tensiometers are instruments used to measure soil suction, and typically consist of a water filled tube with a porous tip on one end. An attached gauge measures the suction pressure as water is drawn out of the porous tip by contact with unsaturated soil. Tensiometers are in direct contact with the soil skeleton and can generally measure suctions from 0 kPa up to 100 kPa, at which point the water inside the instrument begins to cavitate. Suctions above 100 kPa must be measured using other methods, such as a pressure plate or Tempe cell, both of which are also direct measurements of suction. For the measurements in this thesis a different type of tensiometer was used which could measure suctions above 100 kPa, discussed in Section 3.4.2. From any of these testing methods, points along the SWCC at various suction levels are found and curve fitted using models developed by various researchers.

In many of these laboratory methods it is most common to measure the drying curve of the SWCC, and use empirical methods to estimate the wetting curve (Fredlund et al., 2011). In this thesis only a wetting curve was estimated due to the testing method.

2.2.3 Curve Fitting of SWCC points

Many SWCC models are developed based on the theories of pore size distribution and capillarity. Pore size distribution is the relationship between the effective pore size and the soil suction (Sillers et al., 2001). The pores within a soil can be considered randomly distributed and interconnected, and can be described by statistical functions which are then incorporated into equations describing the SWCC (Fredlund and Xing, 1994; Fredlund et al., 2012). The differences between SWCCs proposed by various researchers are the assumptions made in developing the

pore size distribution functions.

For a SWCC to be complex enough to accurately describe soil behaviour, the pore size distribution function must be highly flexible (Sillers et al., 2001), which in terms of equations means a larger number of curve fitting parameters. Early equations for the SWCC were bi-linear and contained fewer curve fitting parameters, such as the equation by Brooks and Corey (1964). Later equations became continuous with greater flexibility, such as the equations by van Genuchten (1980) and Fredlund and Xing (1994). There are many other models which have been developed to model the SWCC, however only these three example models are briefly discussed.

Brooks and Corey

The SWCC model developed by Brooks and Corey (1964) is a power law equation describing the desaturation of the soil once the suction is greater than the air entry value (i.e. bubbling pressure). When the suction is less than the air entry value the moisture content is constant at the saturated value, as shown in Equation 2.9.

$$\Theta = \frac{\theta - \theta_r}{\theta_s - \theta_r} = \begin{cases} 1, & \psi_m \leq \psi_{aev} \\ \left[\frac{\psi_{aev}}{\psi_m} \right]^{\lambda_{bc}}, & \psi_m > \psi_{aev} \end{cases} \quad (2.9)$$

where:

Θ = normalized VWC between residual and saturated VWC

θ_s , θ_r and θ = saturated, residual and measured VWCs

ψ_{aev} = matric suction at the air entry value [kPa]

ψ_m = matric suction [kPa]

λ_{bc} = constant related to the pore-size distribution

The pore-size distribution index, λ_{bc} is found by plotting, on a log-log plot, the effective saturation versus suction for a sample set. λ_{bc} is defined as the slope of the linear portion of the curve on the log-log plot. The air entry value, ψ_{aev} , is found as the suction intercept of the linear portion of the curve at 100% effective saturation.

Although the Brooks and Corey model is popular and simple to use, the discontinuous nature of the model when ψ_m passes ψ_{aev} can lead to instabilities during modelling (Sillers et al., 2001). It has also been suggested by Fredlund et al. (2012) suggests this model has validity for coarser grained soils with quick changes in moisture content at low suctions, but less validity for finer grained soils which show a more gradual slope change in the transitional zone.

van Genuchten

van Genuchten (1980) developed a continuous model for the SWCC which uses three curve fitting parameters, shown in Equation 2.10. The fitting parameter " a " adjusts the inverse of the air entry value, " n " is related to the distribution of pore sizes in the soil and " m " is related to the model asymmetry (Sillers et al., 2001).

$$\Theta = \frac{\theta - \theta_r}{\theta_s - \theta_r} = \left[\frac{1}{1 + (a |\psi_m|)^n} \right]^m \quad (2.10)$$

where:

Θ = normalized VWC between residual and saturated VWC

θ_s , θ_r and θ = saturated, residual and measured VWCs

ψ_m = matric suction [kPa]

a [1/kPa], n and m = van Genuchten curve fitting parameters

The van Genuchten model has also been combined with the Mualem (1976) and Burdine (1953) models for hydraulic conductivity, which simplify the van Genuchten model as they both eliminate one of the curve fitting parameters. The Mualem model relates " m " and " n " by $m = 1 - \frac{1}{n}$, and the Burdine model by $m = 1 - \frac{2}{n}$. As described by Silles et al. (2001), the advantage to the full van Genuchten model over the van Genuchten-Mualem and van Genuchten-Burdine models is increased flexibility of the SWCC shape by maintaining three curve fitting parameters.

Fredlund et al. (2012) note that van Genuchten did not appear to verify the proposed relationship between the " m " and " n " parameters using laboratory results, and a test on the relationship using regression analysis to determine independent " m " and " n " parameters using available SWCC data showed the proposed relationship was not representative for most curves. However, in a study completed by Silles and Fredlund (2001), the van Genuchten-Mualem equation performed comparably to other SWCC models as rated by the Akaike Information Criterion (AIC).

In this thesis the van Genuchten-Mualem model was selected to fit the experimental data. An advantage to selecting the van Genuchten-Mualem SWCC model is the finite element software package PLAXIS accepts this model as an input for unsaturated soil.

Fredlund-Xing

The SWCC model developed by Fredlund and Xing (1994) also uses three curve fitting parameters: " a_f ", " n_f " and " m_f ", to define the full SWCC from data points, shown in Equation 2.11.

$$\theta = C(\psi_m) \frac{\theta_s}{\left[\ln \left(e + \left(\frac{\psi_m}{a_f} \right)^{n_f} \right) \right]^{m_f}} \quad (2.11)$$

where:

θ_s, θ = saturated and measured VWCs

$C(\psi_m)$ = correction factor, defined below

ψ_m = matric suction [kPa]

a_f [kPa], n_f and m_f = Fredlund-Xing curve fitting parameters

This model attempts to better represent the SWCC in the residual suction zone. Both the Brooks and Corey and van Genuchten series of models only properly represent the SWCC in the transition zone due to the sigmoidal curve shape. Sigmoidal functions have been shown to be accurate between this range, however outside this range sigmoidal functions give poor results in the form of horizontal asymptotes (Rossi and Nimmo, 1994). According to Fredlund and Xing (1994), many of the earlier equations for SWCCs were also only valid for certain groups of soils (i.e. across a certain range of suction or moisture content values), so this proposed pore size distribution function covers a larger range of suction values.

Based on experimental results and laws of thermodynamics, Fredlund and Xing (1994) set the maximum value of suction at zero VWC to 10^6 kPa (Fredlund et al., 2012), such that if $\psi_m = 1,000,000$ kPa then $\theta = 0$. A correction factor, $C(\psi_m)$ was added to the equation to limit the upper bound of suction between the residual moisture content and dry soil (Equation 2.12).

$$C(\psi_m) = 1 - \frac{\ln \left(1 + \frac{\psi_m}{\psi_r} \right)}{\ln \left(1 + \frac{10^6}{\psi_r} \right)} \quad (2.12)$$

where:

$C(\psi_m)$ = correction factor

ψ_m = matric suction [kPa]

ψ_r = residual suction value [kPa]

As with the van Genuchten model, this model contains three curve fitting parameters which gives the model flexibility in curve fitting ability. The curve fitting parameters affect the shape of the SWCC as shown in Figure 2.8.

Sillers et al. (2001) noted this model may require fewer iterations to converge than the van Genuchten model. Zapata et al. (1999) noted the Fredlund-Xing model performed the best for

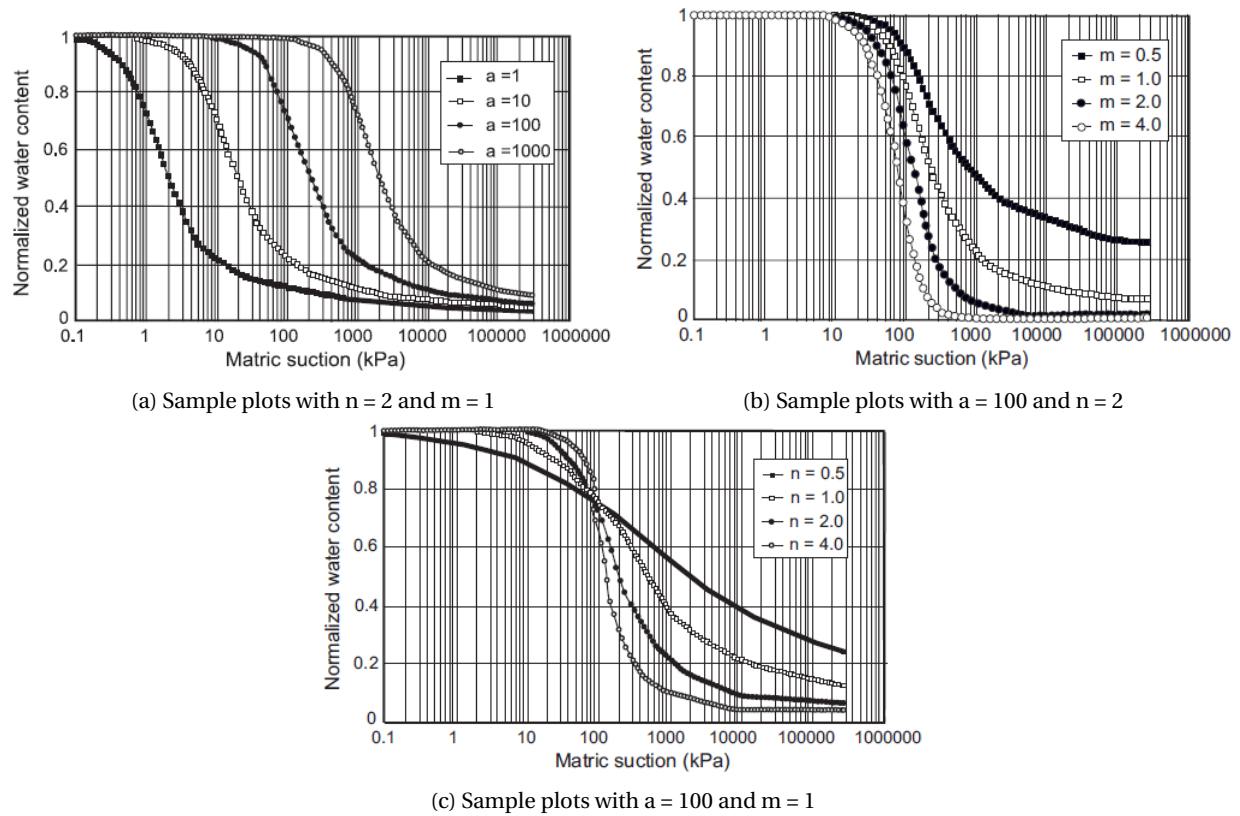


Figure 2.8: Variation in Fredlund-Xing SWCC by modifying each curve fitting parameter (Fredlund and Xing, 1994)

sand materials, but was surpassed by the 3-parameter van Genuchten model for silt and clay materials such as the ones used in this thesis.

Despite the greater flexibility with a 3-parameter equation and improved curve fitting above the residual suction value, the van Genuchten-Mualem SWCC equation was selected for use in this thesis due to simplicity and compatibility with the finite element software PLAXIS.

2.3 Water Flow

Flow through soils is driven by a gradient in hydraulic head. Henry Darcy developed a relationship for the flow of water through a soil mass based on the hydraulic head gradient and the coefficient of permeability, shown in Equation 2.13 (Zhang et al., 2016). Darcy discovered the flow of water, v , is proportional to the hydraulic head gradient, i by the permeability, k . The negative sign in Equation 2.13 is due to the fact water flow occurs from a high hydraulic head to low hydraulic head, and thus the change in hydraulic head will be negative.

$$v = -ki = -k \frac{dh}{dx} \quad (2.13)$$

where:

v = flow rate [m/s]

k = coefficient of permeability [m/s]

i = hydraulic gradient

h = hydraulic head [m]

x = distance along flow path [m]

The coefficient of permeability, k , is a constant for saturated soils and depends on factors such as porosity, fluid properties and soil type (Dingman, 2015; Fredlund et al., 2012). Flow will only occur through pore channels which are filled with water, therefore in a saturated soil all pore channels are available for flow and permeability will be at a maximum. As a soil desaturates and air enters the pore space, the permeability of a soil will decrease as the number of water filled pore spaces decreases.

2.3.1 Transient Flow

Transient flow through an unsaturated soil is governed by a partial differential equation known as Richards equation (Equation 2.14). This equation was developed based on mass balance and Darcy's law (Richards, 1931; Zhang et al., 2016), and was verified by Childs et al. (1950) to be valid for unsaturated soils. Childs et al. (1950) kept a soil medium at a constant moisture content and applied varying hydraulic heads, and determined the permeability of a soil is constant at a constant moisture content.

$$\nabla(-ki) = -\frac{\partial \theta}{\partial t} \quad (2.14)$$

where:

k = coefficient of permeability [m/s]

i = hydraulic gradient

θ = VWC

t = time [s]

Expanding Richards equation for 1-dimensional (vertical) infiltration to unsaturated soils gives Equation 2.15 (Srivastava and Jim Yeh, 1991; Zhang et al., 2016). This equation for flow through unsaturated soil shows that the rate of change of VWC with time in a unit volume is equal to the change in water flux in and out of the volume, and that permeability is a function of soil suction.

$$\frac{\partial}{\partial z} \left[k(\psi_m) \frac{\partial \left(\frac{\psi_m}{\rho_w g} + z \right)}{\partial z} \right] = \frac{\partial \theta}{\partial t} \quad (2.15)$$

where:

z = elevation [m]

$k(\psi_m)$ = coefficient of permeability as a function of soil suction [m/s]

ψ_m = negative pressure head, or suction head [kPa]

ρ_w = density of water [kg/m³]

g = acceleration due to gravity [m/s²]

θ = VWC

t = time [s]

Although Richards equation is the full solution for unsaturated water flow, it is complex and is not guaranteed to converge due to highly non-linear permeability functions (Zhang et al., 2016). Analytical solutions are also challenging to obtain due to the non-linearities in soil hydraulic properties, however solutions are provided in Srivastava and Jim Yeh (1991) for homogeneous and two-layered soils, based on the exponential hydraulic parameter model proposed by Gardner (1958). Many other models have been developed to describe infiltration; a comparison of 14 different empirical and conceptual models is made by Mishra et al. (2003). Although in this comparison of infiltration models the Green-Ampt model is poorly ranked in terms of efficiency compared to other models, it is still commonly used in practice and was explored in this thesis.

2.3.2 Green-Ampt Infiltration Model

The Green-Ampt model is a conceptual infiltration model developed from Darcy's law and contains parameters which are physically based (Zhang et al., 2016). This model assumes that there is a distinct wetting front below the soil surface, as shown in Figure 2.9, where the soil below the wetting front is unsaturated and the soil above the wetting front is saturated, when wetting occurs from surface. Despite assumptions made in the formulation of the Green-Ampt model, predictions have been shown to agree with numerical solutions of Richards equation (Dingman, 2015).

The Green-Ampt model takes into account varying hydraulic boundary conditions and can be used to calculate the time for ponding to occur. The infiltration rate before and after ponding occurs can also be calculated. In this thesis only the infiltration rate after ponding is relevant as there was a constant head of water applied to the soil surface. The infiltration rate after ponding occurs is given in Equation 2.16 (Mein and Larson, 1973).

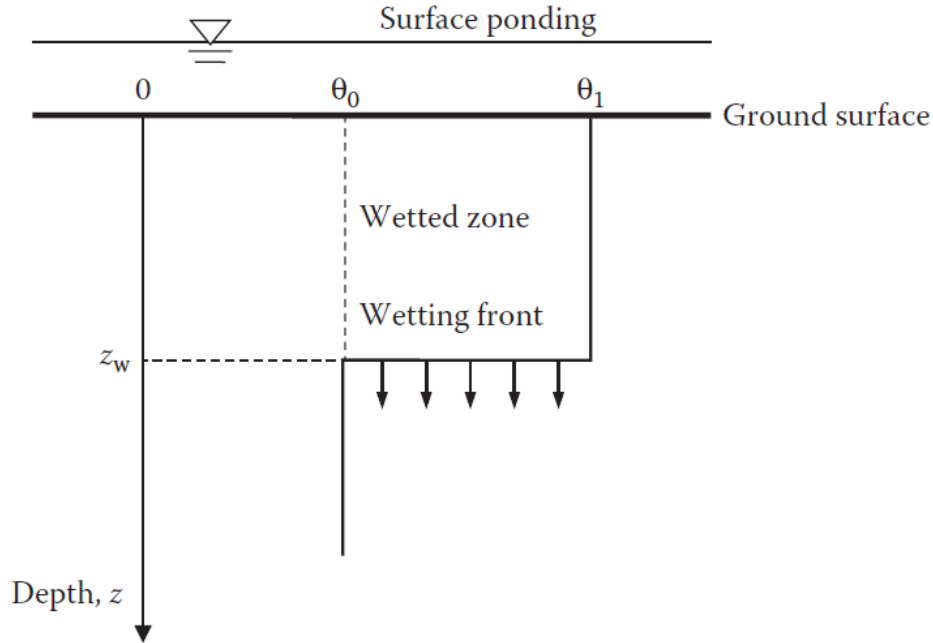


Figure 2.9: Distinct wetting front for Green-Ampt infiltration calculations (Zhang et al., 2016)

$$f(t) = k_s \left[1 + \frac{|\psi_f|(\theta_s - \theta_i)}{F(t)} \right] \quad (2.16)$$

where:

$f(t)$ = infiltration rate [m/s]

k_s = saturated permeability [m/s]

ψ_f = suction head at the wetting front [m]

θ_s = saturated moisture content

θ_i = initial moisture content

$F(t)$ = cumulative infiltration [m]

Since there is no time variable in Equation 2.16 it is useful to further expand by using the relationship $f(t) = dF/dt$ to obtain Equation 2.17, which gives the time at which the wetting front reaches each infiltration depth.

$$t = t_p + \frac{1}{k_s} \left[F(t) - F_p + |\psi_f|(\theta_s - \theta_i) \ln \left(\frac{|\psi_f|(\theta_s - \theta_i) + F_p}{|\psi_f|(\theta_s - \theta_i) + F(t)} \right) \right] \quad (2.17)$$

where:

t = time when wetting front reaches depth $F(t)$ [h]

t_p = time to ponding [h]

F_p = depth of wetting front when ponding begins [m]

For the column testing in this thesis ponding was taken at time $t = 0$ h, and therefore $F_p = 0$ m, as a constant water head was applied nearly instantly at the beginning of the test. The suction at the wetting front can be approximated in several ways. [Mein and Larson \(1973\)](#) suggest taking an average value of suction equal to the integral of the suction across the relative permeability range from the residual to the saturated moisture condition. [Rawls et al. \(1983\)](#) created a table of suggested parameter ranges for porosity, wetting front soil suction and saturated hydraulic conductivity for the 12 soil textures outlined by the United States Department of Agriculture (USDA) based on 1200 soils of various horizons. The parameters of saturated conductivity and porosity were measured in this thesis and do not require estimation.

The infiltration rate of a material is an important factor when considering rainfall induced landslides. Certain intensities of rainfall may lead to infiltration or surface runoff, depending on the permeability of the soil. Depending on the length of rainfall, the ratio of infiltration to runoff will also vary.

2.4 Soil Permeability Functions

Soil Permeability Functions (SPFs) describe the change in permeability of a soil with respect to the soil moisture content, or suction. Experiments by [Childs et al. \(1950\)](#) showed that the coefficient of permeability, k , was constant when the unsaturated soil was kept at a specific moisture condition and the hydraulic head gradient was modified, however, the permeability would vary with changing moisture content. SPFs are therefore developed which relate the permeability of a soil to the moisture content (or suction) of the soil ([Fredlund et al., 2012](#)).

These functions can be used to predict infiltration into unsaturated soils and are used in software packages such as PLAXIS. SPFs can be determined directly by field or laboratory measurements, or indirectly by empirical or statistical methods ([Fredlund et al., 2012](#); [Zhang et al., 2016](#)).

Three methods were applied to develop the permeability function:

1. Instantaneous profile method using instrumentation data ([Watson, 1966](#); [Hamilton et al., 1981](#); [ASTM International, 2010](#))
2. Wetting front advance method using instrumentation data and visual wetting front advance measurements (proposed by [Li et al. \(2009\)](#))
3. Empirical and statistical relationships based on the SWCC

2.4.1 Instantaneous Profile Method

The instantaneous profile method is an unsteady state method presented by [Watson \(1966\)](#); [Hamilton et al. \(1981\)](#); [ASTM International \(2010\)](#) to determine the relationship between water

velocity and water potential gradient at a specific point (i.e. "instant") in time. This method requires either measurement of both suction and moisture content at points along a length of soil, or measurement of one parameter and knowledge of the SWCC for the soil to obtain the other parameter.

In this method moisture content and suction values are plotted against distance along the profile at selected points in time, as isochrones. The water velocity at a specific point is computed by the volume of water passing by the point in a time increment. The volume of water passing by is equal to the moisture content change between that point and the end of the profile, provided no water is exiting the end of the profile. The hydraulic head gradient is the change in hydraulic head (suction head and gravitational head) across a distance along the profile. The permeability coefficient is the water velocity divided by the average hydraulic head gradient in the time period used to compute the water velocity. Equations 2.18, 2.19, 2.20 and 2.21 show the calculation steps for the instantaneous profile method, following [Hamilton et al. \(1981\)](#).

$$i = \frac{dh}{dx} \quad (2.18)$$

$$V_w = \int_j^m \theta(x) \cdot A \, dx \quad (2.19)$$

$$v = \frac{dV_w}{A \, dt} \quad (2.20)$$

$$k = \frac{v}{i_{ave}} \quad (2.21)$$

where:

i = hydraulic head gradient

h = hydraulic head [m]

dx = change in distance along profile [m]

V_w = volume of water between point j and point m [m³]

j = point of interest

m = end of profile

θ = measured VWC

A = area of cylinder [m²]

v = velocity of water passing point j in time increment dt [m/s]

dt = time increment for calculating water velocity [s]

k = permeability at point j between period dt [m/s]

i_{ave} = average of hydraulic head gradients at point of interest from t to $t + dt$

The hydraulic head, h , should take into account gravitational head in vertically oriented soil columns as presented in the ASTM method. [Hamilton et al. \(1981\)](#) developed the instantaneous profile method using a horizontal column, where gravitational effects were not considered.

Advantages of the instantaneous profile method include (Carter and Gregorich, 2008):

- simplicity of laboratory equipment required, except for cost of sensors
- no assumption of functional form of the permeability function, i.e. no pore size distribution requirement

However, Fredlund et al. (2012) note some disadvantages of this method exist, which include:

- potentially long testing durations
- difficulty in choosing flow rate to obtain appropriately sloping suction profiles (i.e. not too abrupt and not too gradual)
- accuracy dependant on distance between suction and moisture content monitoring points (e.g. closer monitoring gives more accurate results but may cause inaccurate infiltration processes)

A column test performed by Li et al. (2009) noted the instantaneous profile method was not suitable for their sensor separation distance of 200 mm, as calculating the average hydraulic gradient across monitoring points became unrealistic. It was also noted the instantaneous profile method results were quite scattered compared with other methods.

2.4.2 Wetting Front Advance Method

Li et al. (2009) proposed a new method for estimating the SPF called the wetting front advancing method. This method uses a combination of sensor readings and visual observations on the wetting front advancing along the column length. This method requires sensor readings at only one cross-section along the profile, but requires frequent visual interpretation of wetting front advance along the profile.

The large-scale tests in this thesis were monitored mainly by use of a digital camera recording photos of the column at set intervals. Occasionally physical measurements would be made on the column wall throughout the test to verify the results obtained from photo interpretation.

Equations 2.22 and 2.23 are used to compute the unsaturated permeability using the wetting front advance method, with reference to Figure 2.10. The figure shows testing completed in a capillary rise test rather than an infiltration test, however the variables are the same, only wetting begins from the top in the trials conducted in this thesis.

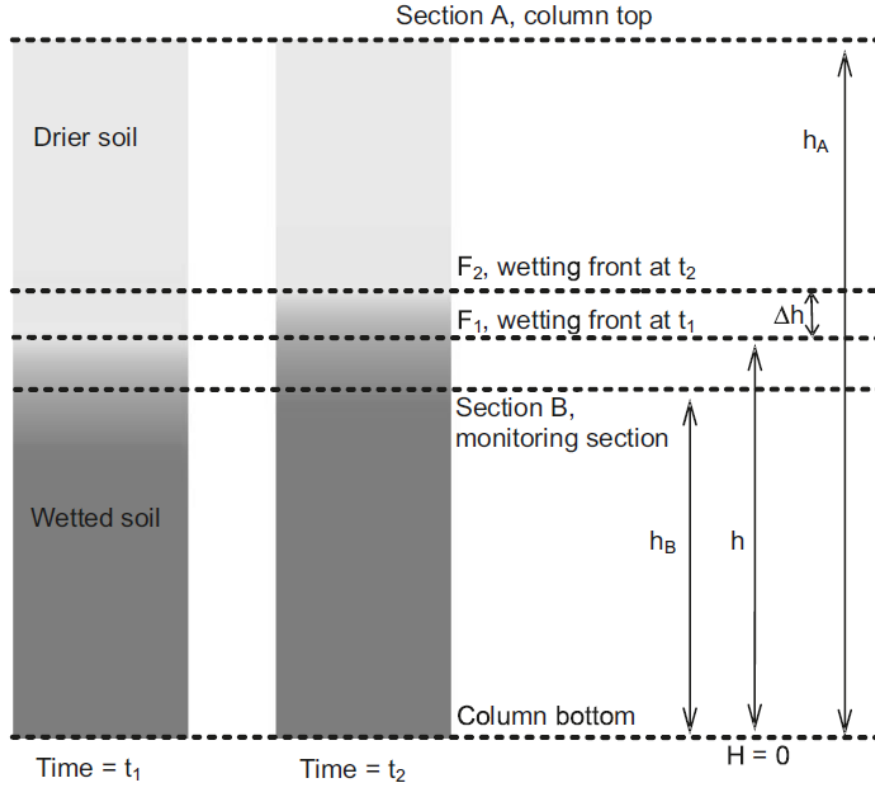


Figure 2.10: Variables for wetting front advance method calculations (Li et al., 2009)

$$k_{ave} = \frac{[\theta(h_B, t_2) + \theta(h_B, t_1) - 2\theta_i] \gamma_w v^2 (t_2 - t_1)}{2 [\psi_m(h_B, t_1) - \psi_m(h_B, t_2) - \gamma_w v (t_2 - t_1)]} \quad (2.22)$$

$$v = \frac{\Delta h}{\Delta t} \quad (2.23)$$

where:

k_{ave} = average permeability between t_1 and t_2 [m/s]

θ = VWC at a specific height and time as outlined by Figure 2.10

h_B = height to monitoring section along soil column as indicated in Figure 2.10 [m]

t = point in time during test [s]

θ_i = initial VWC in sample

γ_w = unit weight of water [kN/m³]

v = wetting front velocity [m/s]

ψ_m = matric suction at specific height and time as outlined by Figure 2.10 [kPa]

h = height along soil column [m]

Some assumptions of the wetting front advance method, discussed in Li et al. (2009), include smooth gradient of moisture content increase in the measured section, and low initial moisture content such that permeability is negligible in non-wetted soil sections. In the tests performed

in this thesis the Δh increments were small enough to consider the moisture content change linear. The initial volumetric moisture content of 9.91% is close to the residual moisture content for the material, and was considered to have a negligible permeability. One advantage to this method over the instantaneous profile method is the applicability over a large range of suctions without requiring a change in flow rate. A limitation to this method is the initial moisture conditions must be near-dry and must produce a visible colour change when wetted.

2.4.3 Empirical and Statistical Methods

Numerous equations exist for calculating the SPF based on SWCCs. Zhang et al. (2016) provide a table showing the various available SPFs based on empirical and statistical methods. In this thesis one empirical and one statistical method were employed. Fredlund et al. (2012) note that there are also equations which can be classified as correlation or regression models, however these will not be discussed.

Empirical SPF models based on SWCCs utilize pore-size distribution theory, and apply curve fitting techniques to fit the parameters. One popular empirically based SPF is the Brooks and Corey (1964) power law equation, shown in Equation 2.24. This equation is bi-linear such that the permeability below the air entry suction value is equal to the saturated permeability, and above the air entry value is a function dependant on the saturated permeability and the pore-size distribution index, which is the same as was used for the SWCC, discussed in Section 2.2.3.

$$k = k_s \begin{cases} 1 & \text{for } \psi_m \leq \psi_{aev} \\ \left[\frac{\psi_{aev}}{\psi_m} \right]^{(2+3\lambda_{bc})} & \text{for } \psi_m > \psi_{aev} \end{cases} \quad (2.24)$$

where:

k = permeability [m/s]

k_s = saturated permeability [m/s]

ψ_{aev} = matric suction at the air entry value [kPa]

ψ_m = matric suction [kPa]

λ_{bc} = a constant related to the pore-size distribution

Statistical SPF models are based on physical models of soil pore-size distributions through which water can flow. The most common model based on physical representation of pore-channels was that from Childs et al. (1950), on which many models have been based. These techniques often rely on integration procedures along the SWCC (Fredlund et al., 2012), and therefore rely on interpretation of the SWCC. In this thesis the van Genuchten-Mualem (1980) equation was used, which is a combination of separate models produced by Mualem (1976) and van Genuchten (1980). The resulting equation contains 3 curve fitting parameters, however van Genuchten

suggested a relationship between the " m " and " n " parameters which then allowed the equation to become a closed-form solution.

$$k(\psi_m) = k_s \frac{\{1 - (a\psi_m)^{n-1} [1 + (a\psi_m)^n]^{-m}\}^2}{[1 + (a\psi_m)^n]^{m/2}} \quad (2.25)$$

where:

$k(\psi_m)$ = coefficient of permeability as a function of suction [m/s]

k_s = saturated permeability [m/s]

a [1/kPa], n and m = the same curve fitting parameters used for the SWCC

ψ_m = matric suction [kPa]

The " m " parameter is found from the relationship $m = 1 - \frac{1}{n}$, per the Mualem formulation. The advantage of the van Genuchten-Mualem formulation is the closed-form solution, as many other statistically formulated SPFs require complex numerical integration along the SWCC. This was the model used to formulate the SPFs from column testing results in this thesis, and is the model used in the numerical software PLAXIS.

Chapter 3

Preparation for Large-scale Column Testing

The first task to prepare for large-scale column testing was to design and construct the column test setup, and order the required instrumentation. During the lead time for column construction and instrument delivery, initial testing was completed to determine the optimal material to be used in large-scale testing. Initial testing consisted of small infiltration tests in a permeameter cell, back-analysis of the material SWCC using finite element software PLAXIS, and determination of optimal material to be used in column testing.

3.1 Permeameter Testing

Initial testing in a permeameter cell was conducted to examine the relationships between infiltration time, porosity and permeability. The purpose of the initial permeameter testing was to select a void ratio and head height combination giving reasonable infiltration times for large-scale testing. The permeameter cell used for experiments is shown in Figure 3.1.

The permeameter setup consisted of the cell itself, a funnel to maintain a constant head of water above the sample, a supply of water (i.e. in a sink under the tap) and hoses to connect to the inlet and outlet of the cell. As shown in the figure, the head of water was maintained constant by allowing water to overflow the funnel at the top.

The material selected for initial testing was a sand and gravel material readily available at the university for use in other research. The material was similar to soils that could be found naturally on slopes susceptible to shallow landsliding. Additionally, since the large-scale model would include a 1 m high soil column and testing time was limited, a sand material would allow water to infiltrate relatively quickly. The Unified Soil Classification System (USCS) description of the material is a poorly graded gravelly sand with trace of fines (SP). In Norway the sand is classified as medium graded. The grainsize distribution (GSD) curves for each test are shown in Figure 3.2, with a GSD summary in Appendix B. Individual sieve analyses were conducted on



Figure 3.1: Permeameter cell used for initial testing

each of the initial testing samples.

The sand material was placed into the permeameter cell at various void ratios before a constant head of water was applied to the top. The time it took for water to infiltrate from the top of the sample to the outlet of the permeameter cell was recorded for each test. Several head heights corresponding to different hydraulic gradients were investigated with multiple void ratios at each head height to develop relationships between infiltration time and porosity for each gradient. Additionally, after the infiltration was completed, the saturated permeability was determined for each test. The results from initial testing are shown in Table 3.1.

Table 3.1: Initial permeameter testing parameters and results

Test	Hydraulic gradient	Void ratio	Saturated permeability [m/min]	Infiltration time [min]
1	2.40	0.58	n/a	6.60
2	2.31	0.50	n/a	15.72
3	7.31	0.45	5.28E-04	n/a
4	2.00	0.42	2.05E-04	36.25
5	2.00	0.53	5.65E-04	13.50
6	2.00	0.49	4.63E-04	17.40
7	1.69	0.43	3.49E-04	24.83
8	1.69	0.52	5.72E-04	14.27
9	1.69	0.42	2.92E-04	32.17
10	1.69	0.48	4.37E-04	18.73

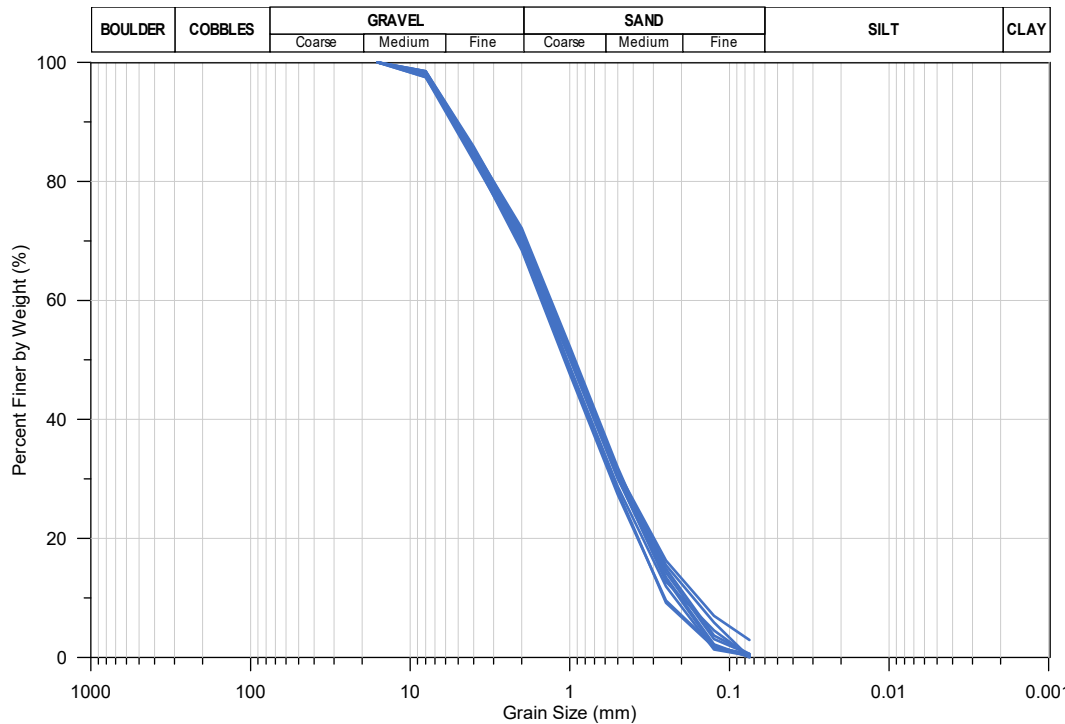


Figure 3.2: Grainsize distribution of initial material

The results in Table 3.1 show the saturated permeability decreases with decreasing void ratio, resulting in increased infiltration time. This follows the theory of water flow, where less void space results in slower permeability and longer infiltration times.

3.2 Numerical Model

In conjunction with laboratory testing, a numerical model was created to simulate infiltration in the same permeameter cells. The finite element software PLAXIS 2D, version 2017.01 was used in this thesis.

3.2.1 Model Parameters

The PLAXIS model was axisymmetric and used a fine mesh with 15-noded elements, shown in Figure 3.3a. The width of the model was the interior radius of the permeameter cell, and the height varied with each test depending on the amount of soil placed into the cell. The default time units were also changed to minutes from days. Node A was selected at the base of the column at coordinate (0,0) for finding the time to full saturation (Figure 3.3b).

The hydraulic boundary conditions were set in the initial conditions to have all boundaries closed and the soil volume set to the unsaturated option. The soil was set to the residual satura-

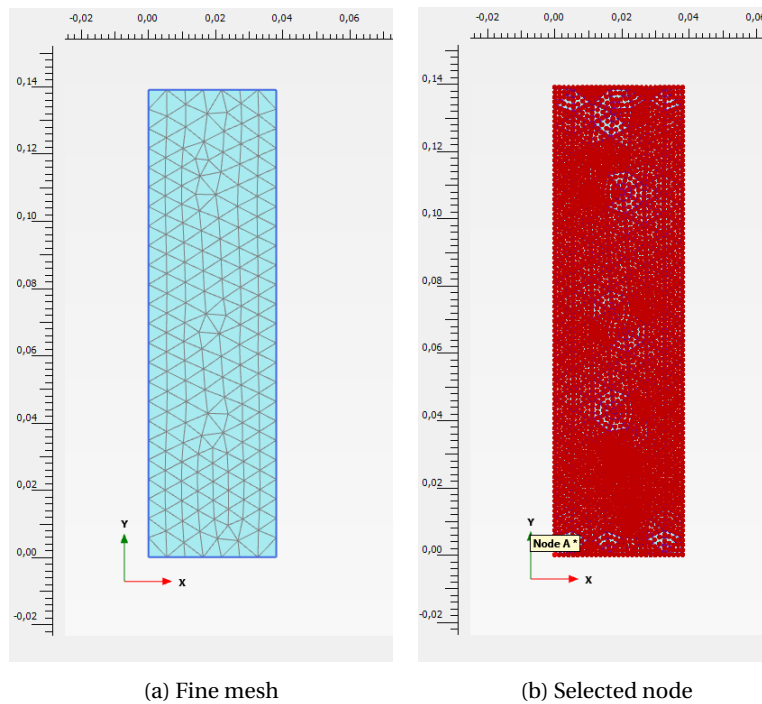


Figure 3.3: PLAXIS model for initial testing

tion value in the selected SWCC, as PLAXIS does not allow initial conditions below the residual value. The calculation type was set to flow only and the pore pressure calculation type set to phreatic.

In the infiltration phase, the top boundary and the soil volume were set to the head height of the laboratory test. The calculation type remained as flow only, however the pore pressure calculation type was changed to transient groundwater flow. In this calculation type a time interval is required, and for these models a time frame of 60 minutes was selected.

Since the calculation type was set to flow only, displacements and stresses are not considered. Therefore, the material parameters that were modified for each test included the void ratio and the saturated permeability, as outlined in Table 3.1.

Transient flow of water is governed by the relationship between permeability and moisture content or suction, the SPF. In PLAXIS, the van Genuchten-Mualem formulation was used as described in Section 2.4, maintaining the same curve fitting parameters as the SWCC. At the time of initial modeling, the instruments had not arrived, and therefore a soil-specific SWCC had not been developed. As such, a trial and error method was employed to back-calculate a SWCC which gave an infiltration time in PLAXIS similar to that obtained in the laboratory study.

3.2.2 Model Trials

One of the laboratory permeameter trials was selected for developing the SWCC required in PLAXIS to have an equal infiltration time as in the permeameter cell. The appropriate soil and applied head heights were set in PLAXIS, with the initial void ratio and saturated permeability found in the laboratory for this trial.

To start, a standard SWCC for sand from the United States Department of Agriculture (USDA) data set was selected, based on the van Genuchten-Mualem model, while maintaining the permeability and void ratio of the selected laboratory trial. In this data set for sand, the GSD comprised 4% < 2 μm , 4% between 2 μm and 50 μm , and 92% from 50 μm to 2 mm. However, using this data set the infiltration time was overestimated by nearly double the laboratory trial.

The sieve analyses conducted from the laboratory samples showed very little fines in the sand sample (Figure 3.2), where the standard sand data set from the USDA contained minimum 8% fines. Since there are no pre-defined SWCCs in PLAXIS with smaller fines content, the next step was to create a user-defined SWCC which brought the infiltration time down to that of the laboratory trial.

A user-defined van Genuchten-Mualem model was created starting from the USDA sand model, however since no information was known of the residual saturation in the sand, it was kept the same as the USDA sand model and only the curve fitting parameters " n " and " a " were modified. In the van Genuchten-Mualem model, three curve fitting parameters are utilized, as explained in Section 2.2.3, however the PLAXIS model uses the Mualem (1976) simplification where two of the curve fitting parameters are related. The " l " parameter is equal to 0.5 in the van Genuchten-Mualem model (van Genuchten, 1980; PLAXIS bv, 2019b). PLAXIS inputs require moisture content in terms of effective saturation instead of VWC, shown in Equation 3.1, so any parameter inputs listed for PLAXIS will be in terms of effective saturation.

$$S = S_{res} + (S_{sat} - S_{res}) \left(1 + (a|\psi_m|)^n\right)^m \quad (3.1)$$

where:

S_{sat} , S_{res} and S = saturated, residual and measured saturation level

a [1/m], n and m = van Genuchten curve fitting parameters

ψ_m = matric suction [kPa]

The " m " parameter is computed using the Mualem relationship, where $m = 1 - \frac{1}{n}$. The " a " and " n " parameters were modified until a similar infiltration time was found between the laboratory trial and PLAXIS. Table 3.2 shows the van Genuchten-Mualem parameters in the USDA sand model and the user-defined parameters established. Figure 3.4 shows the comparison between the USDA sand SWCC and the user-defined curve.

Table 3.2: van Genuchten parameters used in PLAXIS initial modeling

Parameter	USDA sand model	User-defined model
S_{res}	0.1047	0.1047
S_{sat}	1.00	1.00
n	2.68	5.00
a [1/m]	14.50	5.00
l	0.50	0.50
k_s [m/min]	4.95×10^{-3}	See Table 3.1

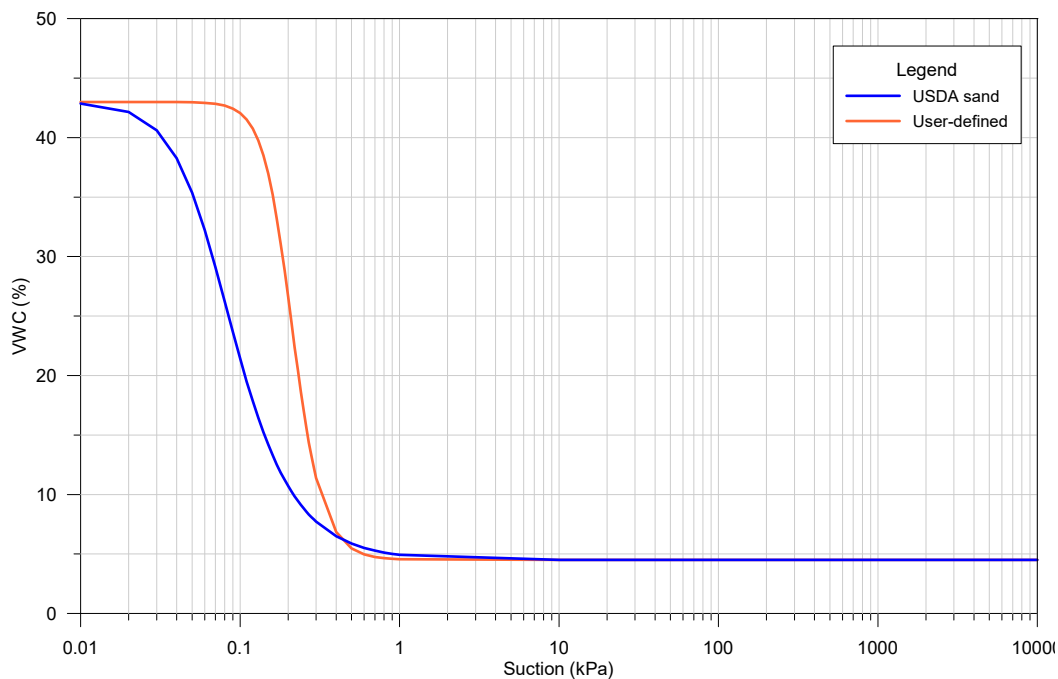


Figure 3.4: Comparison of van Genuchten SWCCs

Once the user-defined SWCC matched the infiltration time of the selected laboratory trial, subsequent PLAXIS analyses were run for each of the laboratory trials to check if the SWCC was appropriate in all cases. In each simulation the soil column and head height, and saturated permeability was updated to the relevant laboratory trial. Figure 3.5 shows the comparison of infiltration times between laboratory and PLAXIS models. PLAXIS simulations were not conducted on the hydraulic gradients $i=2.31$ or $i=2.40$ due to lack of saturated permeability measurements in the laboratory testing.

The PLAXIS model matched quite well the laboratory analyses, and thus the SWCC was accepted as an initial assumption for the sand and gravel material without any physical moisture content or suction measurements from sensors. Furthermore, the shape of the SWCC matches well with curves for typical sandy material, which generally have steep curves at lower suction values, and have saturated moisture contents around 40%. Figure 3.6 from Fredlund et al. (2012) shows typical SWCCs for sand, silt and clay material.

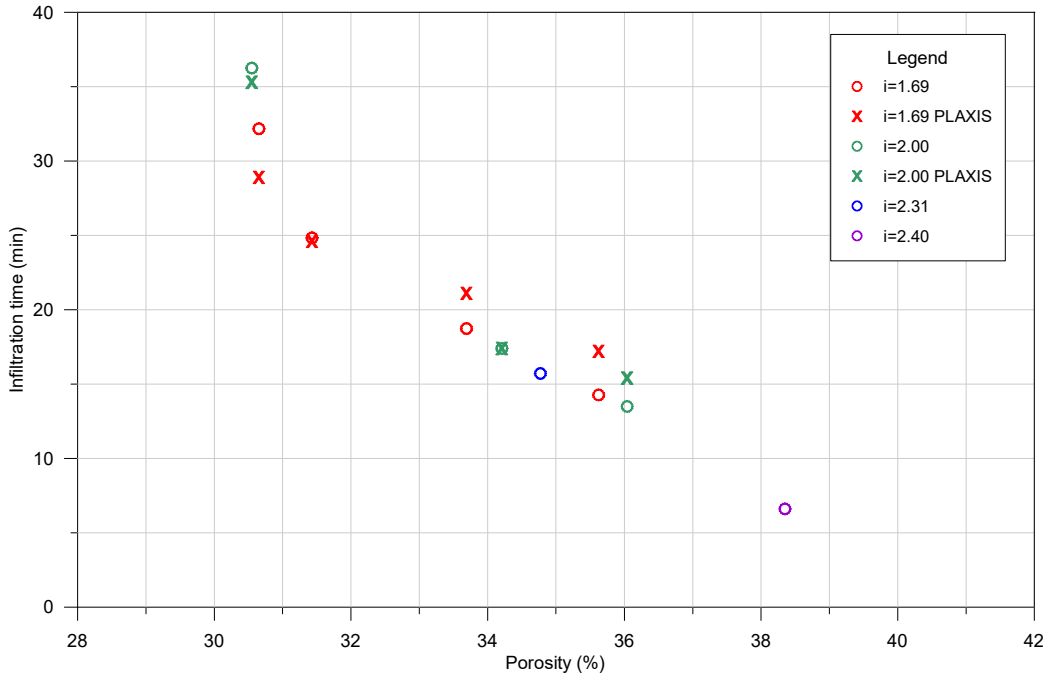


Figure 3.5: Comparison of infiltration times between laboratory and PLAXIS analyses

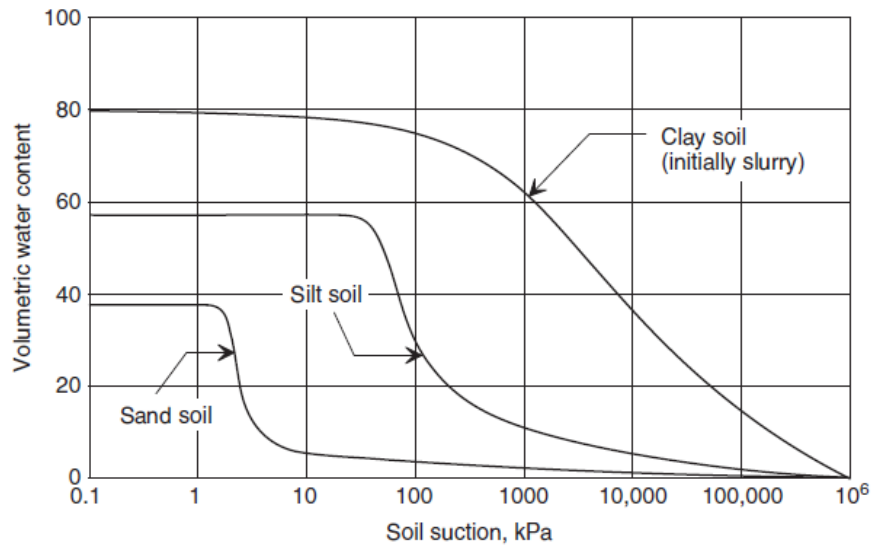


Figure 3.6: Typical SWCCs for sand, silt and clay material (Fredlund et al., 2012)

3.2.3 Discussion on Initial Testing

The SWCC depicted in Figure 3.4 shows the suction values in the desaturation zone of the SWCC range from approximately 0.1 kPa to 0.6 kPa over the VWC range of 5% to 43%. The range of suction values is small, and at very low suctions. This is relevant as the suction sensor ordered, discussed later in Section 3.4.2, had an operating range between suctions of 9 kPa to 100 kPa.

The operating range of the suction sensor did not extend low enough to be in the range of expected suction values in the sand and gravel material (0.1 kPa to 0.6 kPa), and would therefore have been unable to record changes in suction. As suction increases with fines content contained in a soil due to smaller capillary pores, it was decided to determine the amount of fine material required to be added to the sand to raise the range of expected suction values to within the sensor operating range. This was accomplished in PLAXIS, going back to using the standard hydraulic data sets from the USDA provided within the software.

3.3 Material Selection

Following the results of the initial testing, the original sand and gravel material required addition of finer grainsizes to increase the matric potential in the soil through reduction in overall pore size. However, increasing the fines content would also increase the time for infiltration to complete as the permeability of a sand is faster than for a silt or clay. In order to approximate the amount of fines to add to the initial material, reference was again made to the standard data sets in PLAXIS.

The USDA has split a ternary diagram into 12 regions classified as various soil types, on which SWCCs are based. The ternary diagram in Figure 3.7 shows the regions for each soil type outlined in Figure 3.8.

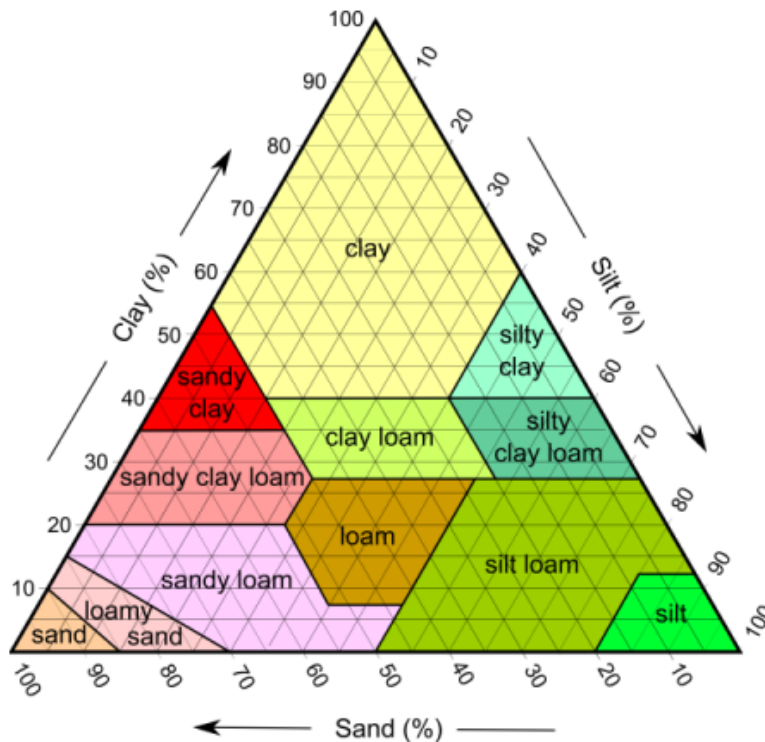


Figure 3.7: USDA soil types ([stackoverflow](#))

Each of the USDA SWCCs available in PLAXIS are shown in Figure 3.8. The lines are coloured the same as outlined in the ternary diagram for comparison. The sandier materials show lower air entry values and steeper transition zones, where more clayey soils exhibit more gradual transition zones and slightly higher air entry values.

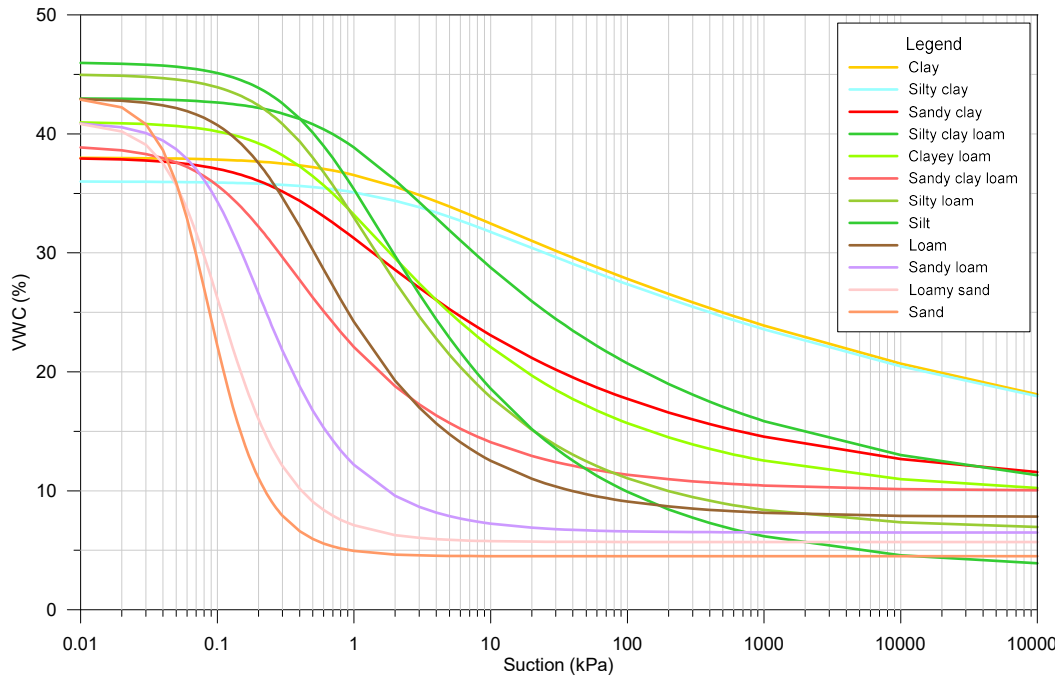


Figure 3.8: SWCCs from USDA dataset

From the SWCCs shown in Figure 3.8, the curves for loam, sandy clay loam, silty loam, silt and clayey loam were selected as options based on the range of suctions in the curves. In PLAXIS, using a model with soil height of 1 m, an infiltration analysis was run using each of these material types and 0.2 m of water head above the top of the soil column (i.e. hydraulic gradient of 1.2). The void ratio was set at 0.5 for analyses and the permeabilities were selected as the default for each data set since no actual testing could take place. The initial saturation for each soil type was set to slightly above the residual saturation for each data set as PLAXIS will not allow initial soil saturation levels below residual saturation. The infiltration times to the model base for each soil type are shown in Table 3.3, along with the grainsize fractions for each material.

Table 3.3: Infiltration time and grainsize distributions for selected USDA soil types

Material Type	Infiltration time [hours]	<2 μm	2 μm - 50 μm	50 μm - 2 mm
Loam	51	20	40	40
Sandy clay loam	58	28	12	60
Silty loam	109	14	65	21
Silt	15	6	87	7
Clayey loam	25	34	34	32

The silt material was eliminated due to the small amount of sand present in the sample, and the silty loam material eliminated due to the long period for infiltration to take place. The loam, sandy clay loam and clay loam all had acceptable infiltration times. These three materials are adjacent to each other in the ternary diagram, and if a central point were taken, the grainsize proportions would include 45% sand, 20% silt and 35% clay, compared to the initial material which comprised 70% sand and 30% gravel. The sand could be separated from the gravel, and mixed with other silt and clay materials to create a theoretically optimal material for testing.

Some silty material was available for use in the basement of NTNU for addition to the sand and gravel material. A hydrometer analysis was conducted to determine the GSD, but it was found that no combination of silt with the sand and gravel material could create a GSD close to the optimal proportions, as the silt contained mainly medium silt sizes, as shown in Figure 3.9. Additional fine silt and clay material was still required.

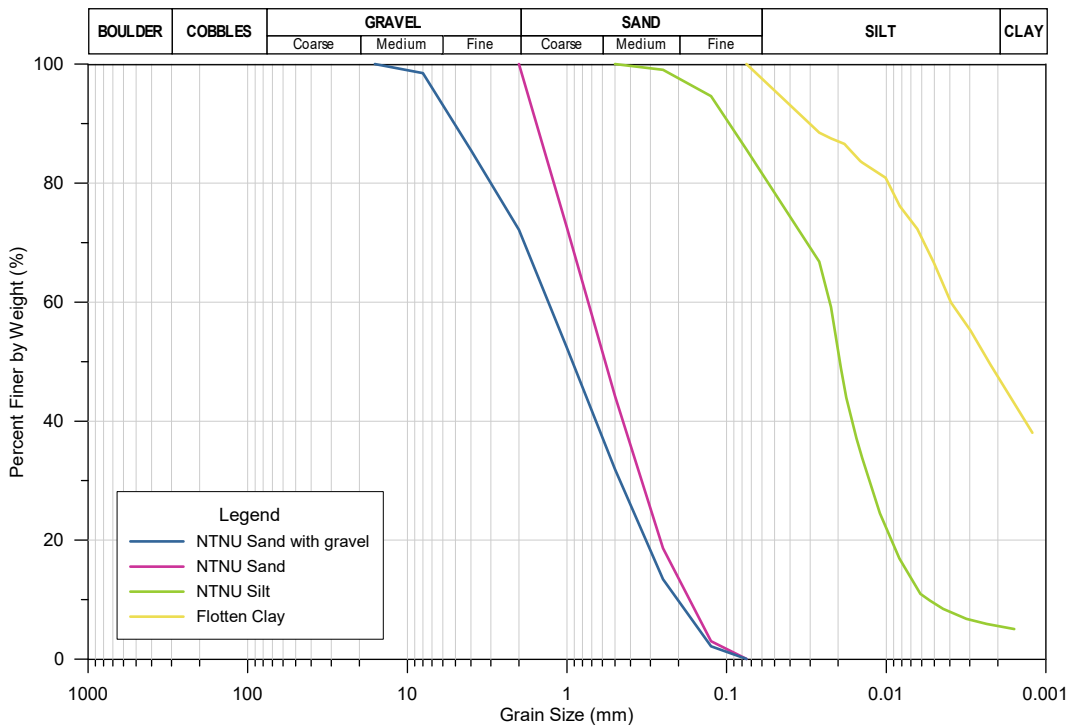


Figure 3.9: Grainsize distributions of sand and gravel, sand, silt and clay materials

The laboratory at NTNU had some extra fine grained material from sampling conducted at a Norwegian Geo-Test Site (NGTS) in Flotten, Tiller, approximately 10 km south of Trondheim. Based on previous hydrometer testing conducted in student laboratory courses, the high clay and fine silt content of the Flotten clay could serve well to increase the fines content of the test material. Some cuttings from other testing completed on Flotten clay were selected for use. The cuttings were oven dried and then pulverized using a Los Angeles Abrasion (LA Abrasion) machine from the roads department at NTNU. A sample of the crushed and dried clay was then

subjected to a hydrometer test. The results of the grainsize analyses from each of the individual materials are shown in Figure 3.9, with data from GSD analyses in Appendix B.

The three materials (NTNU sand, NTNU silt and Flotten clay) were combined to create a material close to the optimal proportions. Since the ternary diagram did not include any gravel portion, the gravel fraction was sieved from the sand and gravel sample before material combination. In Norway, a soil is classified as a clay if the clay fraction is greater than 15%. To avoid using a designated clay sample, the clay fraction was reduced to 10% and the silt fraction increased to 45%, designating the material a loam according to the USDA and a clayey sandy silt by Norwegian standards. The theoretical combined GSD is shown in Figure 3.10 along with grainsize analysis (sieve and hydrometer) conducted on a sample of the mixed material as a check on the theoretical combination. The data from GSD analysis can be found in Appendix B as the material used in test 1.

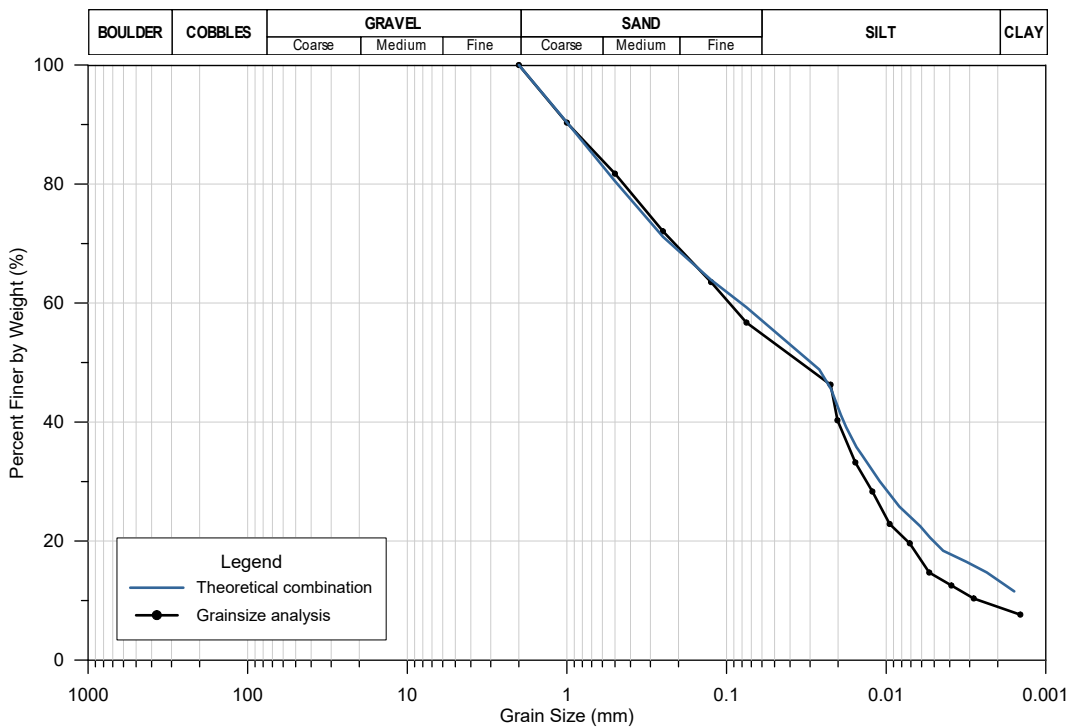


Figure 3.10: Combined grainsize distribution used in testing

The GSD from laboratory testing matched fairly well the theoretical combined material. The final material combination contained a mixture of the three materials. A mixture of 35% NTNU sand, 40% NTNU silt and 25% Flotten clay by weight theoretically resulted in a material with 43% sand, 43% silt and 14% clay, as shown in Table 3.4. The GSD determined from lab testing showed the material contained slightly less clay fraction and slightly more clay fraction.

Table 3.4: Material combination and final fractions used in testing

Fraction	Grainsize [mm]	Material Percentages			Final Mix [%]
		"NTNU Sand" [35%]	"NTNU Silt" [40%]	"Flotten Clay" [25%]	
Sand	2 - 0.06	100	18	2	43
Silt	0.06 - 0.002	0	76	50	43
Clay	<0.002	0	6	48	14

3.4 Selection of Instrumentation

The large-scale infiltration tests were intended to be monitored with sensors measuring moisture content and soil suction. A study was to be completed on the implementation of sensors, from installation to connection to datalogging and data interpretation, but also a study on the possibility of using sensors to monitor soil conditions in a field setting during rainfall infiltration. The sensors were procured with the intention of possible further use by NTNU or SINTEF in subsequent field studies.

Instruments were procured from METER Group, Inc. (METER) for use in measuring moisture content and soil suction in the infiltration column. The instruments were used in establishing the SWCC of the material and monitoring the wetting front progress during infiltration under constant head conditions. During initial testing the sensors were evaluated for reading accuracy and calibration, output stability and response time prior to installation into the large-scale column. Details about the instruments in use during infiltration column testing is discussed in Section 4.3.2.

3.4.1 Volumetric Water Content Sensors

Volumetric water content (VWC) sensors measure the moisture content in the soil in terms of volume of water compared to total soil volume. Conventional geotechnical engineering prefers the use of gravimetric moisture content, which eliminates the requirement of a volume measurement, however for in-situ applications volumetric moisture content is the only option. Conversion between volumetric and gravimetric moisture content is possible with knowledge of the dry bulk density of the material, by Equation 3.2.

$$\theta = w \cdot \frac{\rho_d}{\rho_w} \quad (3.2)$$

where:

θ = VWC

w = gravimetric moisture content

ρ_d = dry density of soil [kg/m³]

ρ_w = density of water [kg/m³]

The chosen VWC sensor was the ECH₂O EC-5 (EC-5) from METER, which has a small volume of influence and is suitable for laboratory testing. The sensor is shown in Figure 3.11 and was manufactured with a 5 m cable length with bare wire ends. The EC-5 sensor is an analog device which works on the basis of capacitance to measure the moisture content of the material.

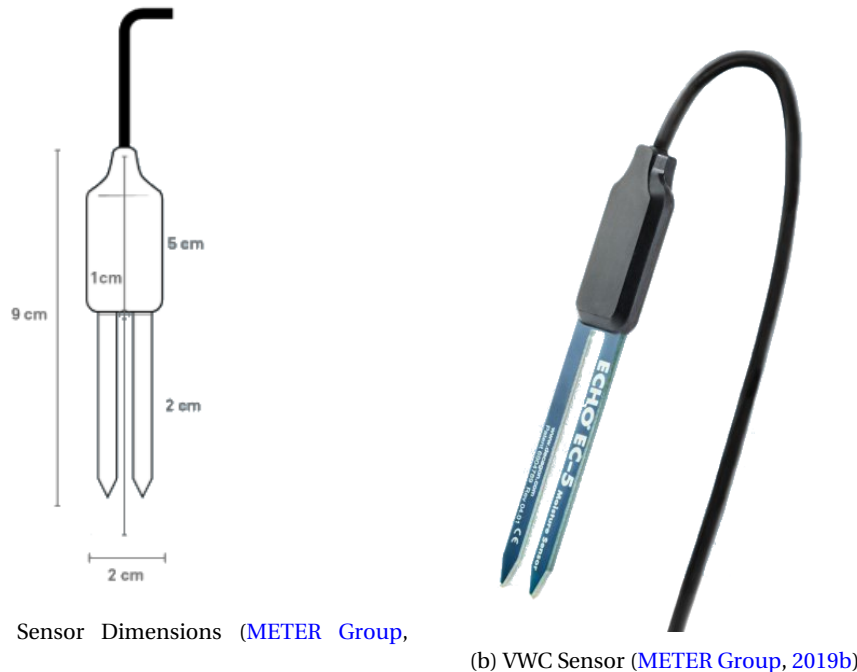


Figure 3.11: ECH₂O Sensor from METER Group, Inc.

Sensor operation

The capacitance of a material is based on the permittivity, or dielectric constant, of the material. In the case of soil, the permittivity is a function of the water, the air and the soil grain component proportions. The permittivity of water is 80, air is 1, and soil generally varies between 3 to 5 at room temperatures (Bittelli, 2011). Therefore, the capacitance of a soil medium is highly correlated to the amount of water in the soil, and the VWC of a soil can also be related to the capacitance.

Advantages of capacitance moisture sensors include lower cost and wide range of applicability, however disadvantages include necessity to calibrate sensors based on soil type and environment. Since capacitance based sensors operate below the frequency range of time domain sensors, the sensors have been criticized for increased sensitivity to factors including temperature, salinity, and electrical conductivity (Kizito et al., 2008).

Testing completed by Kizito et al. (2008) showed lesser sensitivities when the capacitance sensor was operated at a higher frequency, from 70 to 150 MHz, based on studies by others investigating

the effect of frequency. The EC-5 sensor operates at a frequency of 70 MHz. Capacitance moisture sensors have also shown dependence on soil density, with higher accuracy in denser soils (Matula et al., 2016). In this project, the effects of changing temperature, salinity or electrical conductivity were not considered.

Sensor calibration

Analog devices require a calibration curve to relate a measured parameter to the desired output, in this case moisture content. The EC-5 sensor returns a percentage of the excitation voltage, which can then be related to the dielectric permittivity of the soil based on equations such as the one from Topp, shown in Equation 3.3 (METER Group, 2019a), where mV is the sensor output voltage.

$$\epsilon_a = \frac{1}{(-3.3325 \times 10^{-9})(mV^3) + (7.0218 \times 10^{-6})(mV^2) - (5.11647 \times 10^{-3})(mV) + 1.30746} \quad (3.3)$$

METER provides calibration curves directly relating output voltage to volumetric moisture content for mineral soils and organic soils. The relationship from METER for mineral soils measured with non-METER dataloggers is shown in Equation 3.4, where mV is the voltage output of the sensor when excited at 2,500 mV (METER Group, 2019a).

$$\theta = (11.9 \times 10^{-4})(mV) - 0.401 \quad (3.4)$$

where:

$$\theta = \text{VWC}$$

$$mV = \text{sensor output voltage [mV]}$$

Prior to use in the infiltration column, trials were completed on moisture conditioned samples of the combined material to compare with the provided calibration curve. Fifteen samples of various moisture contents at known densities were prepared in the laboratory and the sensor was left inside the samples overnight to equalize. The samples were then oven dried and the gravimetric moisture content determined. The VWC was found from the gravimetric moisture content using Equation 3.2 and compared to the sensor output. The results of these trials are shown in Figure 3.12, with the METER provided calibration curve also shown for reference. There are two defined calibration curves for the initial testing. The curve for test 3 was used in future VWC determination, using equation 3.5, as there was an offset detected in the programming following tests 1 and 2. However, the relationship from tests 1 and 2 help to show the linear relationship between sensor output and VWC, therefore no additional testing was completed at the new calibration due to time constraints.

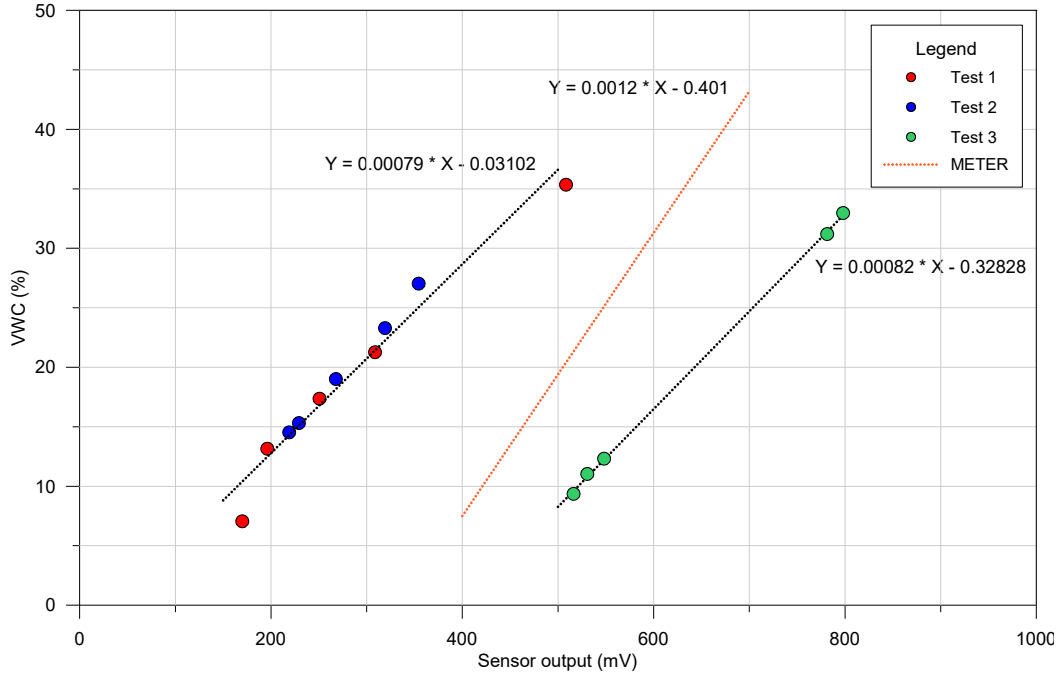


Figure 3.12: VWC calibration curves from laboratory testing and METER group

$$\theta = (8.2 \times 10^{-4})(mV) - 0.32828 \tag{3.5}$$

where:

θ = VWC

mV = sensor output voltage [mV]

As can be seen from Figure 3.12, the calibration curve from METER group does not match those determined in this thesis. This is because the relationship from METER is dependant on an input voltage of 2,500 mV, where in the calibration tests performed in this thesis, an input voltage of 3,200 mV was applied. For future use, it is important to note the voltage applied to the moisture sensor, as it will directly influence the validity of the calibration curve.

Sensor performance

The VWC sensors were left in the soil sample to record readings overnight, so it was possible to evaluate the sensor response and sensor reading stability. Figure 3.13 shows the results from one batch of initial testing, with one VWC sensor per moisture content sample.

The VWC sensor readings showed nice stability throughout the testing period within constant moisture content condition with no water flow. The datalogging of the sensors was started prior to sensor installation into the sample, so it is possible to see the reaction time of the sensor to

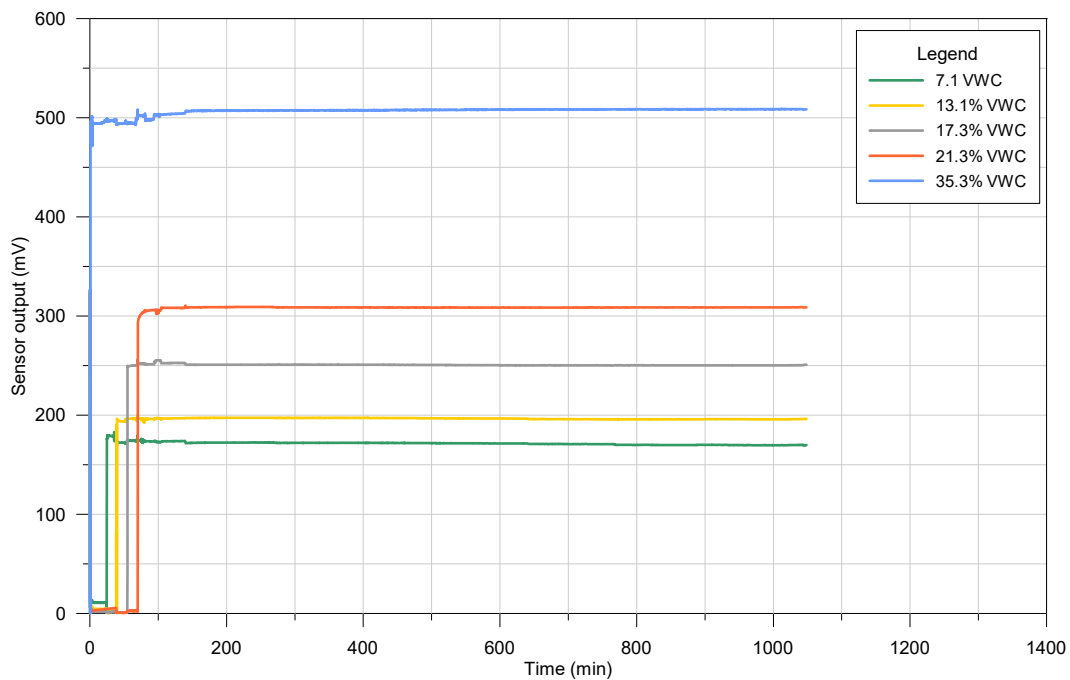


Figure 3.13: Performance of VWC sensors during initial testing

changing moisture content. It is obvious to see when the sensors were installed into the moistened soil due to the sharp reaction. The sensors were only initially tested in a stationary flow environment, where in the large-scale column test the sensors may perform differently when subjected to water infiltration conditions.

3.4.2 Suction Sensors

Suction sensors measure water potential, or negative pore water pressure in a material. In agricultural applications for example, the water potential provides important information regarding watering requirements as it gives information about water availability in a soil. With regard to slope stability, the negative pore water pressure or suction contributes to the shear strength of the material through influence on the effective stress, which can highly affect the stability or instability of a slope.

The suction sensors selected for this thesis were the TEROS 21 sensors from METER (Figure 3.14), which have a low maintenance requirement compared to other suction sensors. The sensors were manufactured with 5 m of cable length with a 3.5 mm stereo plug connection. Conventional tensiometers require a water filled reservoir attached to a piezoelectric pressure transducer which measures the difference in pressure due to suction compared to ambient air pressure. Once the suction in a conventional tensiometer exceeds the air entry value of the porous

ceramic filter, air bubbles begin to form and enter the water chamber, invalidating the results and de-saturating the tensiometer. These tensiometers require careful refilling to ensure no air bubbles are present and the ceramic tips are completely saturated, which can be challenging. The TEROS 21 sensor does not require any water chamber refilling since it measures the moisture content within the ceramic discs.

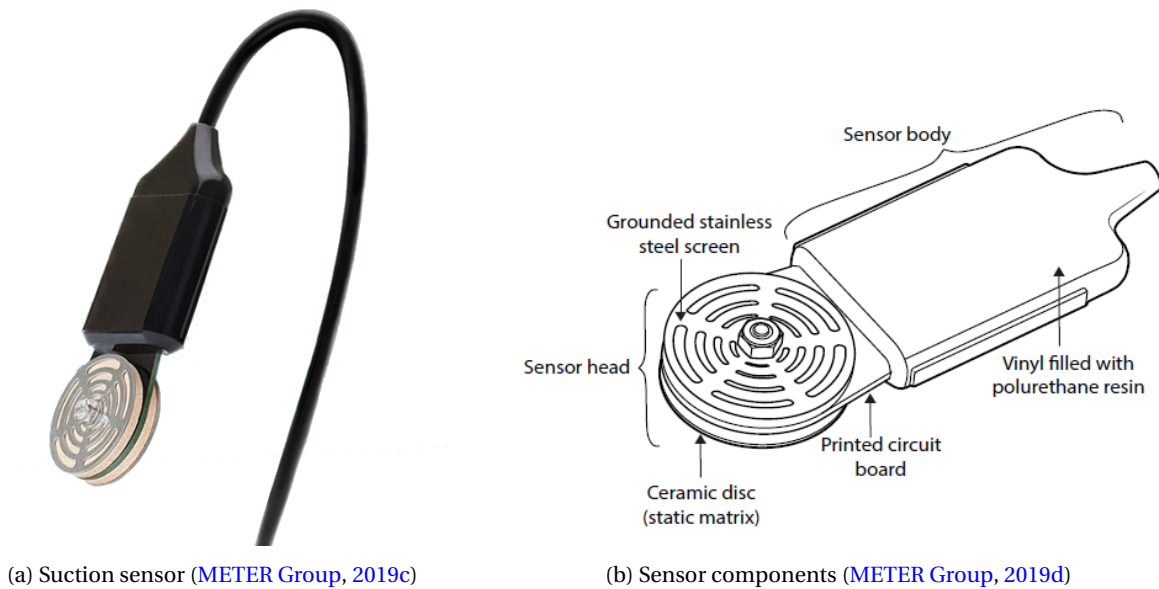


Figure 3.14: TEROS 21 suction sensor from METER Group, Inc.

A second advantage to the TEROS 21 suction sensors is they can be installed in dry or near-dry soil conditions. Conventional tensiometers have a limited supply of water to be pulled out through the ceramic filter due to high soil suction in dry soils and require high levels of maintenance for reservoir refilling. The TEROS 21 sensors can be installed into dry soils where the water will be removed from the ceramic discs, however upon soil saturation water will re-enter the disc pores and measurement accuracy will not be impacted. As infiltration testing beginning from a relatively dry state was conducted in this thesis, these sensors were more applicable than a conventional tensiometer.

Sensor operation

TEROS 21 sensors measure suction indirectly using the principle of solid matrix equalization (METER Group, 2019d). Two ceramic discs with known pore size distribution (and therefore SWCC) are placed into a medium and left to obtain hydraulic equilibrium by the second law of thermodynamics. The water potential in the ceramic discs, or suction, will equalize with that of the medium by water saturating some pores in the discs. The moisture content in the ceramic will be measured by the sensor through measurement of the dielectric permittivity of the discs

using the same principles as the VWC sensors discussed in Section 3.4.1. Since the SWCC of the ceramic discs is known, the suction in the discs can be found, which through thermodynamics is equal to the suction in the soil. The SWCC of the ceramic discs is shown in Figure 3.15, and is constant for each sensor, meaning no individual sensor calibrations are necessary.

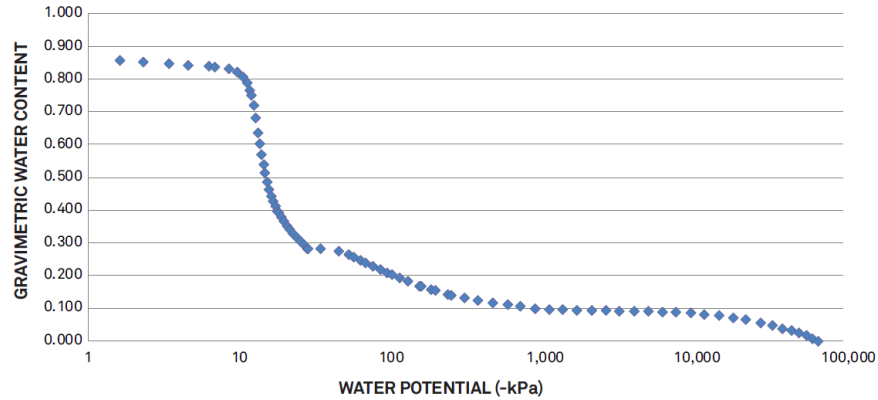


Figure 3.15: SWCC of porous discs in TEROS 21 suction sensors (METER Group, 2019d)

Conventional tensiometers can measure suction in the range of 0 to -100 kPa, and are limited on the negative end due to the bubbling pressure of water. The TEROS 21 sensor can measure suctions theoretically to dry soil (i.e. -100,000 kPa suction), however little calibration is completed below -100 kPa and so the accuracy is reduced at high suctions (METER Group, 2019d). METER also notes acceptable accuracy and good correlation between sensors up to -1,500 kPa in laboratory settings.

The output from the sensor is total suction, which is composed of several components: pressure, gravitational, osmotic and matric suctions (Figure 3.6).

$$\psi = \psi_p + \psi_g + \psi_o + \psi_m \quad (3.6)$$

where:

ψ = total suction [kPa]

ψ_p = pressure suction [kPa]

ψ_g = gravitational suction [kPa]

ψ_o = osmotic suction [kPa]

ψ_m = matric suction [kPa]

According to METER Group (2019d), ψ_p and ψ_g are normally small and not considered in most applications. Osmotic suction arises from salt content in pore fluid. The TEROS 21 sensor reacts to matric suction, or the difference in pore air and pore water pressure. The TEROS 21 sensor is not recommended for use in saline soils when the electrical conductivity exceeds 10 dS/m, as the permittivity measurements on the ceramic discs may be impacted.

Sensor calibration

The TEROS 21 sensor did not undergo any calibrations as there was no available method to independently measure the output suction values. The moisture content change of the porous discs was also not measured to check the calibration curve provided by METER.

Sensor performance

As with the VWC sensors, the suction sensors were left in moistened soil samples overnight and left to equalize. The suction measurements with time are plotted in Figure 3.16 for the same batch of initial testing as for the VWC sensors. As the range of suction values is large, the suction axis was broken from -9,000 kPa to -20,000 kPa.

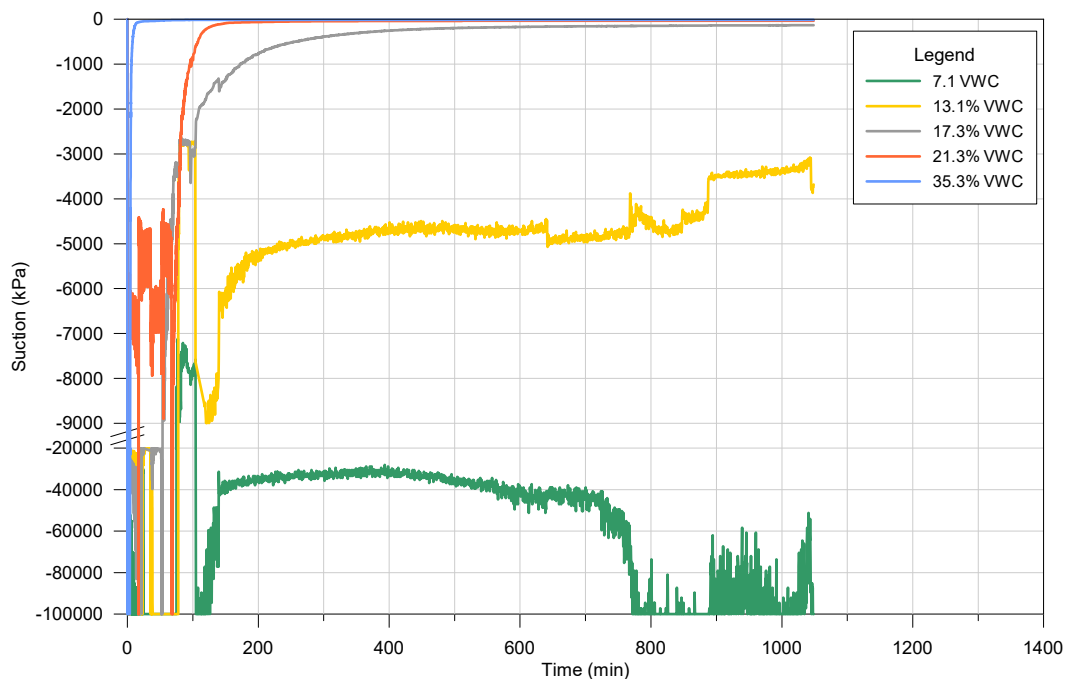


Figure 3.16: Performance of suction sensors during initial testing

Per the [METER Group](#) manual, sensors in air are expected to have readings fluctuating between -50,000 kPa and -100,000 kPa, however once installed, even in dry soil, become more stable. This was observed during initial testing before the sensors were installed into the respective soils, so the noise was filtered out for graph clarity.

The sensors installed into wetter soils showed a quicker reaction time than those in drier soils. It should be noted, however, that the sensors in the wettest samples stopped recording suction values lower than -12.9 kPa, which is close to the lower limit of the sensor. METER notes

the laboratory accuracy and sensor to sensor variability is acceptable until about -1,500 kPa for TEROS 21 sensors, or the upper limit of matric suction measurements (Fredlund et al., 2012).

The two sensors tested in the driest conditions had some problems with stable readings through the testing period. The sensor output at 13.1% VWC varied from around -3,200 kPa to -5,000 kPa. The accuracy of the sensor is $10\% \pm 2$ kPa in the range of -9 to -100 kPa. Since 10% of 5,000 kPa is only 500 kPa, the accuracy of the sensor below -100 kPa seems to decrease. There were several points in time where the sensor reading abruptly changed, but it was not possible to verify if this was caused by external influence. The sensor at 7.0% VWC stabilized around -30,000 kPa, however around 7,700 minutes, an abrupt change in suction reading occurred in the 7.0% VWC sensor and in the 13.1% VWC sensor. In the case of the 7.0% VWC sensor, the readings dropped to -100,000 kPa, or the maximum possible sensor output and remained there for the duration of the test.

Based on the initial testing from all three batches of various moisture contents, the suction sensors can take some time to equalize, particularly in drier soils. Additionally, in high suction ranges the sensor accuracy may not be within the limits stated for suctions between -9 kPa to -100 kPa. High moisture contents may result in suction levels beyond the sensor limit.

3.5 Soil Water Characteristic Curve from Initial Testing

The SWCC was determined in the laboratory outside of the large-scale column prior to testing using the sensor output results from the 15 samples prepared for initial sensor evaluation. The moisture content and suction reading pairs for each sample were plotted in Figure 3.17.

The points in grey in Figure 3.17 were excluded from SWCC fitting as they were determined to fall beyond the measuring range of the suction sensors. The black points were considered acceptable to fit the SWCC. Using the Microsoft Excel Solver tool, a van Genuchten-Mualem curve was fit to the data by adjusting the curve fitting parameters " a " and " n " and the residual VWC to maximize R^2 . The saturated VWC was taken as the average porosity of the valid points, since the sample density was not constant across all tests. The resulting SWCC is shown in Figure 3.17 with the curve fitting parameters shown in Table 3.5.

Table 3.5: SWCC parameters for initial testing fitting equations

van Genuchten-Mualem		van Genuchten (full)		Fredlund-Xing	
Parameter	Value	Parameter	Value	Parameter	Value
θ_r	0.115	θ_r	0.116	ψ_r	2136
θ_s	0.520	θ_s	0.520	θ_s	0.520
a [1/kPa]	0.3723	a [1/kPa]	0.3280	a_f [kPa]	5.658
n	1.570	n	1.257	n_f	5.922
$m = 1 - \frac{1}{n}$	0.363	m	0.204	m_f	0.390
R^2	0.96	R^2	0.96	R^2	0.95

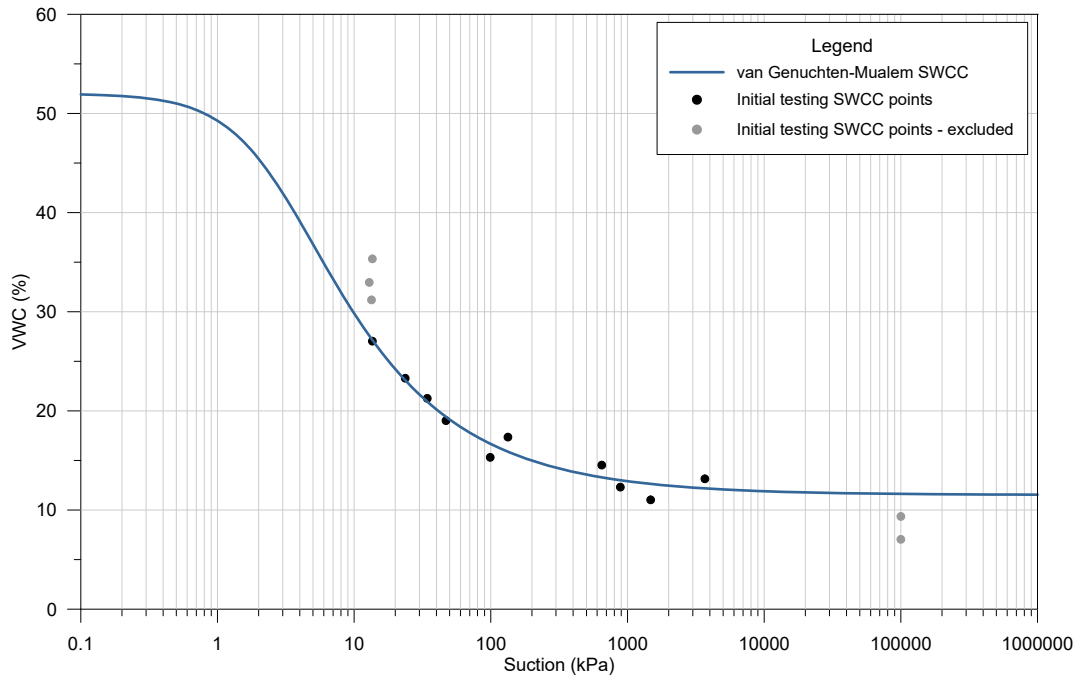


Figure 3.17: Initial testing points for SWCC with van Genuchten-Mualem fit

The fitted van Genuchten-Mualem curve gave a R^2 value of 0.96 with the parameters in Table 3.5. For comparison, SWCCs were fit using the 3-parameter van Genuchten equation and the Fredlund-Xing equations. Figure 3.18 shows the comparison between the three fitted SWCCs.

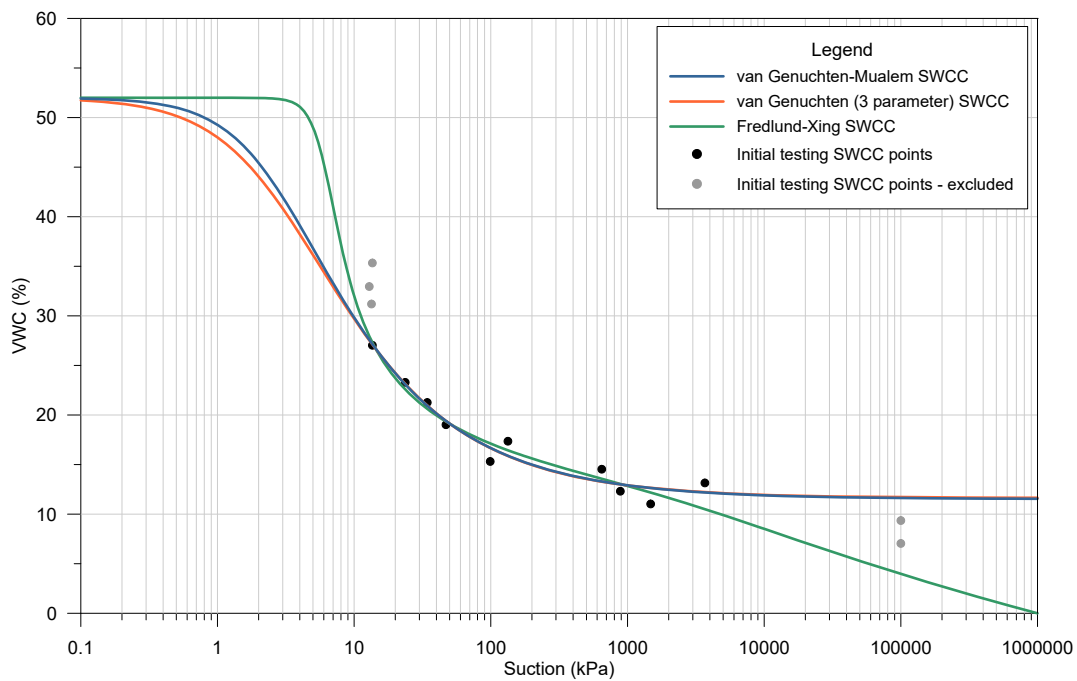


Figure 3.18: Fitted SWCCs comparison

Adding the third fitting parameter to the van Genuchten equation does not have a large effect on the shape of the SWCC, except by slightly decreasing the air entry value. The Fredlund-Xing equation has a significantly different shape in the dry and wet ranges of the SWCC than the van Genuchten style equations. The air entry value is higher than for the van Genuchten equations and the steepness of the curve increases. In the dry portion of the curve the Fredlund-Xing correction factor was applied such that the VWC reaches 0% at 1,000,000 kPa of suction, instead of asymptotically extending from the residual VWC.

Since the measurement range of the suction sensors does not cover the extreme high end of suctions it is impossible to verify the curve in the high suction range. Additionally, the air entry value by all three equations is less than the lower limit of the suction sensor, meaning the air entry value can only be estimated and not confirmed. However, all three equations fit the curve similarly in the initial testing measurement range.

Chapter 4

Large-Scale Infiltration Column Testing

A large-scale infiltration column was designed and constructed to study infiltration through an unsaturated soil using instrumentation and visual interpretation. Three constant head infiltration tests were conducted and the collected instrument readings evaluated and then used to create an updated SWCC for the material. Several methods were employed to create an unsaturated SPF for the material and the results compared. The infiltration process was finally compared to a common infiltration model.

4.1 Design of Infiltration Column

Technical drawings of the column can be found in Appendix A. The constructed infiltration column filled with soil and ready for testing is shown in Figure 4.1, with VWC and suction sensors installed at various points along the column depth.

The column was designed with reference to ASTM D7664—10: Standard Test Methods for Measurement of Hydraulic Conductivity of Unsaturated Soils (ASTM International, 2010), and previously conducted column testing by Duong et al. (2013), Li et al. (2009) and McCartney et al. (1981). The column stands 1300 mm tall, of which 1000 mm is filled with soil and 300 mm remains for constant water head above the soil. The column is made of acrylic plexiglass, has an outer diameter of 250 mm and inner diameter of 240 mm.

The column slides onto the base assembly around an o-ring to prevent water leakage out of the base. Above the column base is a filter system composed of geotextile (Figure 4.2a) overlying a stainless steel perforated plate (Figure 4.2b) to minimize fines migration and support the soil column. On the underside of the filter, drainage paths are etched into the polyoxymethylene (POM) base which drain to a closeable ball valve (Figure 4.2c). Depending on the testing requirements, the valve can be opened to allow water drainage, or closed to hold a water table in the soil column. A stainless steel perforated plate and filter cloth are also placed at the top of the

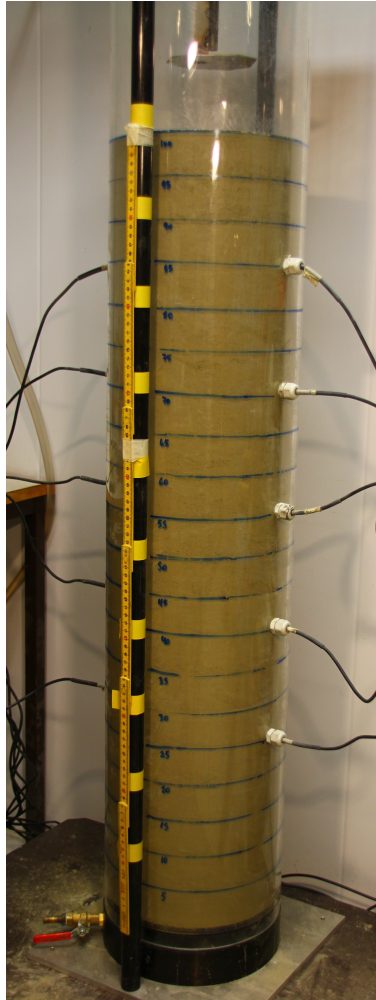
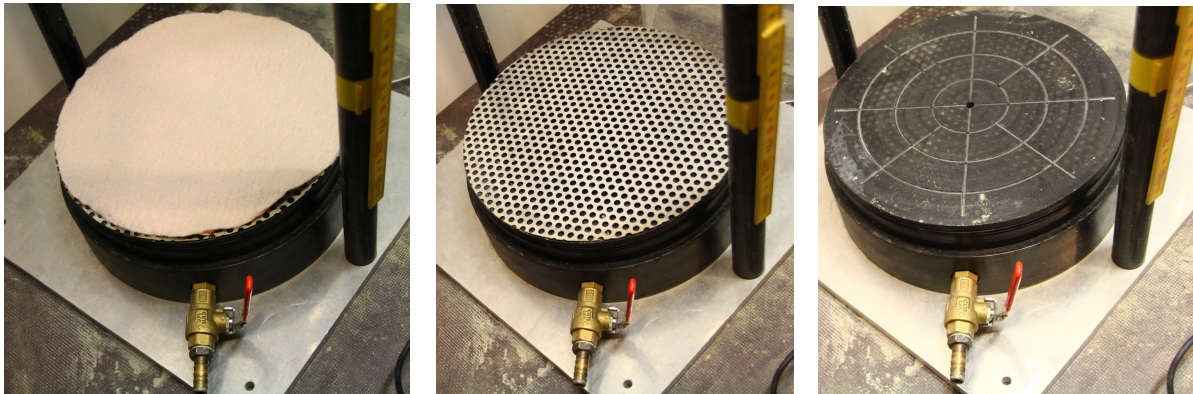


Figure 4.1: Instrumented column used for infiltration testing

soil column to minimise disturbance to the soil surface due to water filling. The column base is bolted to a stainless steel base plate, which is attached through POM dowels to another stainless steel plate on top of the column to hold the entire system together. The sensors are installed through the wall of the column using cable glands, which seal around the wire to prevent any water leakage. The entire column setup can be bolted to a pallet for easy transport with a pallet jack, or disassembled and relocated by hand.

To provide a constant head of water to the top of the soil column, a water supply system was designed by NTNU (shown in Appendix A drawings and later in Figure 4.8). The water tank can contain approximately 28.5 L of water and is airtight. The outlet at the base of the water tank goes through a pipe to the top of the soil column and can be placed at the desired height above the soil column. When the water level is the appropriate height, air is unable to enter the supply tank from the pipe outlet and the water level remains constant. Over time, due to infiltration, the water head level will drop and allow air to enter the pipe to the supply tank, which will then allow water out of the tank and raise the water head above the soil back to the desired level.



(a) Filter fabric on top of wire mesh to minimize fines migration (b) Wire mesh on top of column base (c) Base of column with drainage channels towards the center drain

Figure 4.2: Components of the column base

4.2 Experiment Preparation

Preparation of the test setup for use involved a series of steps which are detailed below. The time beginning from sample conditioning to placement into the column with the instruments to starting the infiltration required a minimum of 5-6 hours, however decreased with each test.

4.2.1 Sample Preparation

The soil sample to be tested required mixing and conditioning prior to placement into the column. As described in Section 3.3, the material was created from a combination of three soils. The sand fraction was collected from a sand and gravel mixture by taking the material passing a 2 mm sieve. The silt fraction was available material in dry form from the NTNU basement, but required some manual effort to break apart dry lumps. The Flotten clay material came from a NGTS near Trondheim, collected from cuttings leftover from index testing by others. The Flotten clay cuttings were oven dried and then placed into an Los Angeles (LA) Abrasion machine with steel balls to break up the dried lumps. The LA Abrasion machine is a large, 711 mm diameter drum with one internal paddle which rotates for a set number of revolutions. Once the revolutions were completed the clay was placed through a 1.6 mm sieve to remove the larger lumps for another set of revolutions. A smaller sieve size was not used as the dried clay would plug the sieve openings. The individual materials were mixed together in the proportions outlined in Table 3.4 using a mixing machine, shown in Figure 4.3. The mixer contained 4 paddles at various positions in the drum to thoroughly combine the materials.

In all three column tests, the material was prepared at an initial gravimetric moisture content of 7%, by adding water to the combined material in the mixer. The mixer was not optimal for evenly distributing the moisture in the material as many small lumps formed once the water



Figure 4.3: Machine used for mixing and conditioning material

was added. The lumps were broken apart by hand until the colour inside the lumps was the same as the surrounding material, and then it was considered evenly moistened, however small lumps still remained. The sample was then ready for placement into the column.

4.2.2 Instrumentation Setup

Prior to soil placement into the column, the instruments were installed through cable glands at various depths in the column wall. Since the instrument heads were too large to fit through the cable gland, the instrument cables were fed from the inside and pulled through until the instrument could hang out the top of the column as shown in Figure 4.4. This was done during soil placement to avoid damaging the sensors while compacting each soil lift.

The cable leads were connected to dataloggers which transferred data from the sensors to a computer. The VWC sensors were connected to a National Instruments datalogger which was modified by NTNU staff to provide the correct input voltage according to the manufacturer recommendations. The suction sensors were connected to a datalogger designed and constructed by NTNU staff to accept data through 3.5 mm stereo plugs and output to RS232 serial cables. The serial cables were connected to an 8 port Startech USB serial hub, which output the data to the computer by a USB cable. The software program LabView (Version 18.0.1f2, 64-bit) was used to record readings from the instruments which were saved to a .txt file. The program was written by NTNU staff to record readings at set intervals, typically set to 10 seconds.

A Canon EOS 60D SLR camera was mounted onto a tripod and programmed through the computer to take photographs of the test setup every 1-2 minutes throughout the test duration. The software used to control the camera was Canon EOS Utility, version 0.1.18.0. Due to battery life and required recharge time the entire test durations could not be monitored, however efforts were made to have photographs of the setup for as much of the test as possible. The

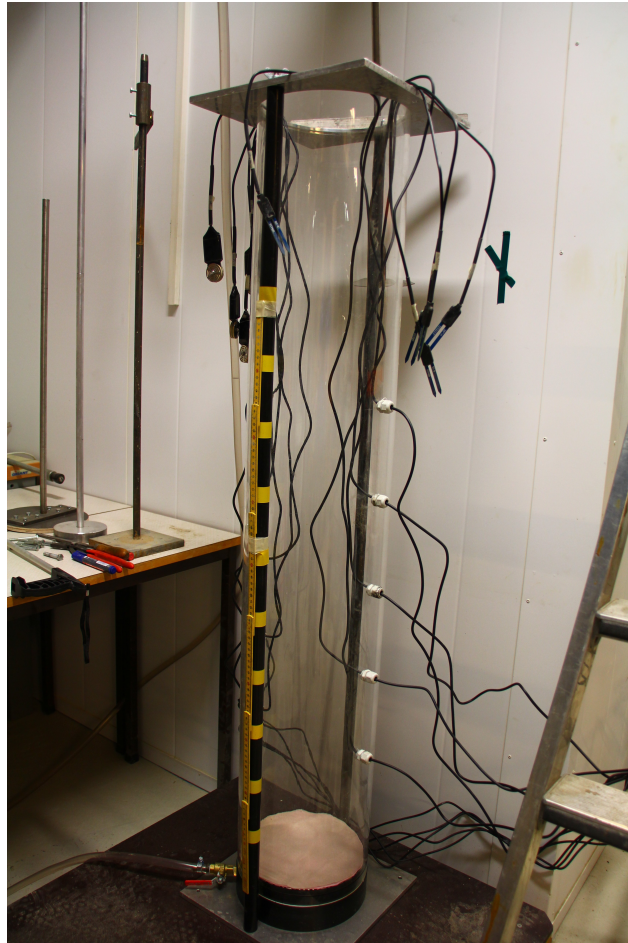


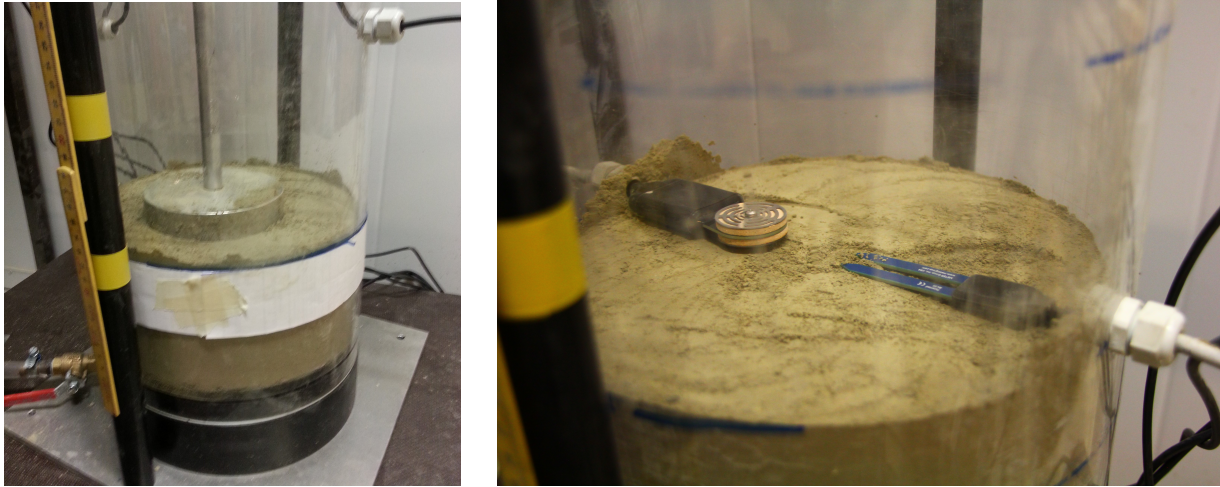
Figure 4.4: Instrument arrangement during soil placement and compaction

photographs were used to track the wetting front advance as well as monitor the water head level above the soil to ensure the water filling system performed as intended. Examples of photographs are provided for test 2 in Appendix C.

4.2.3 Compaction into Column

The material was placed into the column in 50 mm lifts and compacted to the same density throughout the column height. Lines were drawn on the column every 50 mm and the same mass of moistened soil was placed into the column and levelled, then compacted down to the proper height using a 120 mm diameter aluminium plate attached to a handle, as shown in Figure 4.5a. The handle separated into two pieces so as the soil height increased in the column the handle could be shortened. As the soil height reached each level of instruments, the sensors were placed on the previously compacted lift as shown in Figure 4.5b. The sensors were placed so a small amount of cable was inside the column but not so close the tips of the sensors were touching. The subsequent lift was placed gently on top of the sensors to full height, and

compaction took place as normal.



(a) Compaction of soil into column

(b) Placement of instruments

Figure 4.5: Compaction of soil lifts and placement of instruments in column

The dry density of the soil in each column test was 1415 kg/m^3 . In the first test a density estimate was used to determine the mass of soil to be placed in 50 mm height, however it was not possible to compact the material to that density. The density of that larger lift was calculated to be 1415 kg/m^3 , and used for the remainder of the column height.

4.2.4 Test Initiation

The water tank above the soil column was filled with water (approximately 28.5 L) prior to test initiation with the inlet and air vent valves open, and the outlet valve closed. The pipe outlet from the water tank was placed at the desired head height above the soil column. Since the tank volume was limited, the initial head of water atop of the soil column was hand filled and not from the water tank. The water was filled to the pipe outlet and then the valves on the water tank all reversed such that the inlet and air vent valves were closed and the outlet was opened.

The program developed to record instrument readings, as well as the program for the camera photo frequency, were started just prior to filling the water head above the soil.

4.2.5 Test Completion

After the test was completed, including permeability measurements, the program reading the sensors was terminated. The water head on top of the soil was removed using a scoop and bucket, and the remaining water atop the filter system absorbed with a sponge. The soil was removed using a small scoop, using care around the sensor heads. It was possible to remove the soil down to the level of the third row of sensors, or approximately 50 cm above the column

base before the soil became too low to reach. At this point the column was tilted to a horizontal position on top of pallets, as shown in Figure 4.6. Care was taken to prevent the soil from sliding up or down in the column as this could cause damage to the sensor cables from stretching. Blocks were placed on either side of the column to prevent it from moving, and the base of the column was removed.

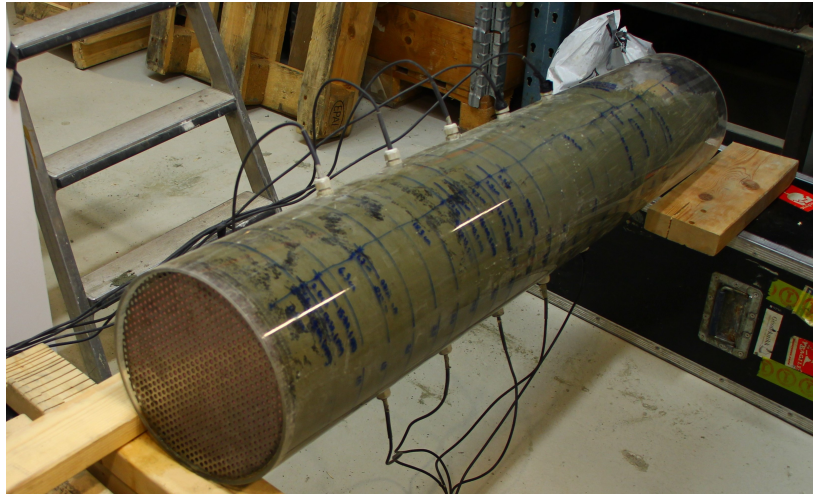


Figure 4.6: Column tilted for soil removal from base

In this position it was possible to remove all the material from the bottom half of the column using the scoop. A spatula was also used to scrape some material from the side of the column, particularly between the sensors. In tests 2 and 3, moisture content samples were taken to represent every 10 cm of the column depth and placed into the oven. The remainder of the removed soil was placed into oven-proof containers and placed into ovens set to 110°C to dry. The column and base were rinsed in the nearby sink with a hose, shown in Figure 4.7. The instruments were also rinsed gently with the stream of water from the hose while remaining inside the column.

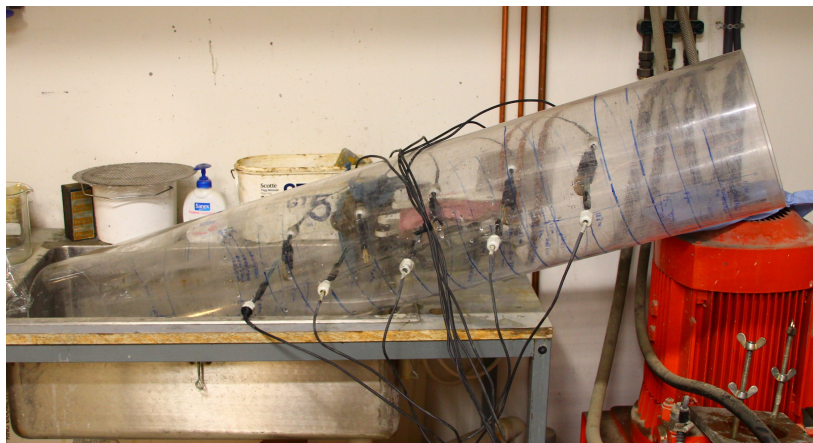


Figure 4.7: Rinsing the column in the sink

After test 1, the soil was dried in the oven, then re-crushed and re-used for test 2. The material was broken apart manually using a drop-weight. After test 2 the material was again placed into the oven to dry for future testing, however the material in test 3 was freshly mixed instead.

4.3 Large-scale Column Test Results and Discussion

Three large-scale infiltration column experiments were conducted in the test setup. The entire test setup is shown in Figure 4.8, showing the soil column full of soil, water tank and monitoring station at the start of test 1.

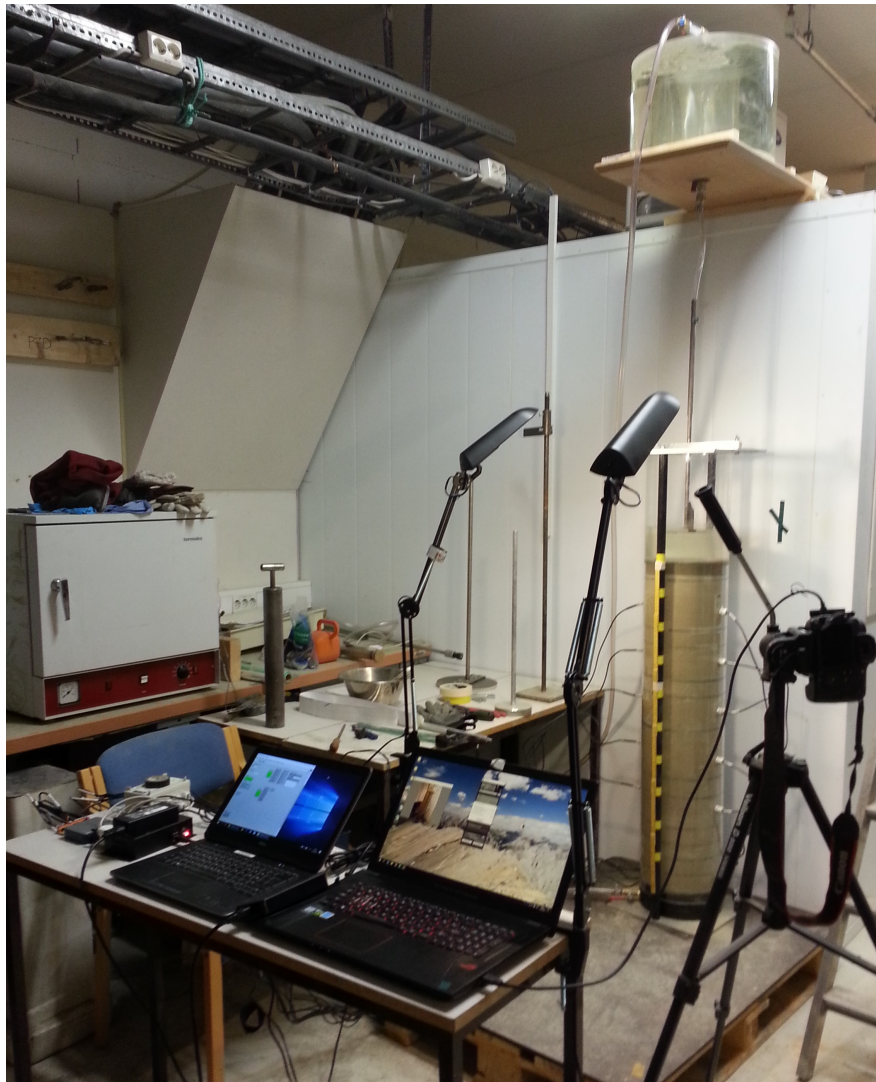


Figure 4.8: Experiment setup

The two lights pointed towards the column were necessary for the camera photos as the overhead lights in that area of the university basement operate on motion sensors and would shut off automatically. Two computers are also pictured as the main laptop for recording sensor data

only contained three USB ports, and the camera required a fourth port. In subsequent tests a computer monitor was used as a USB hub to add additional USB ports for connecting the camera to the main laptop.

The following sections present the testing conditions, results from testing and comments on the performance of each test.

4.3.1 Testing conditions

Table 4.1 outlines the variables for each test. All tests were prepared in the column identically to each other, except test 2 re-used material from test 1, and test 3 had double the water head above the soil.

Table 4.1: Variables for large-scale column tests

Variable	Test 1	Test 2	Test 3
Soil source	Fresh	From Test 1	Fresh
Dry density [kg/m ³]	1415	1415	1415
Gravimetric moisture [%]	7	7	7
Volumetric moisture [%]	9.91	9.91	9.91
Initial soil height [cm]	100	100	100
Water head above soil [cm]	10	10	20

The GSDs for each test are presented in Figure 4.9, with full testing sheets included in Appendix C. The GSD for tests 1 and 3 were completed prior to testing and the GSD for test 2 was completed following testing.

4.3.2 Instrument Readings

As the initial testing was completed with stationary hydraulic conditions, test 1 was the first chance to evaluate the sensor response to an approaching wetting front. The instrument readings from test 1 are shown in Figure 4.10 with time, normalized to the maximum reading from each sensor, which was maximum output voltage for the VWC sensor and minimum suction output for the suction sensor.

The VWC and suction sensors both had a sharp response to the wetting front approach, and appeared to react to the wetting front at the same time. Using the photographs taken through the testing period it was possible to visually identify when the wetting front arrived at each cluster of sensors. The black vertical lines in Figure 4.10 show the visual interpretation of the wetting front at each sensor location, and match relatively well with the sensor response. The visual interpretation is slightly behind the sensor measurements, indicating the sensors are able to detect moisture some distance away. This distance was measured to be around 2-3 cm, which agrees with the specifications listed by METER for the sensing range of the EC-5 VWC sensor. No specifications were given for the suction sensor for comparison.

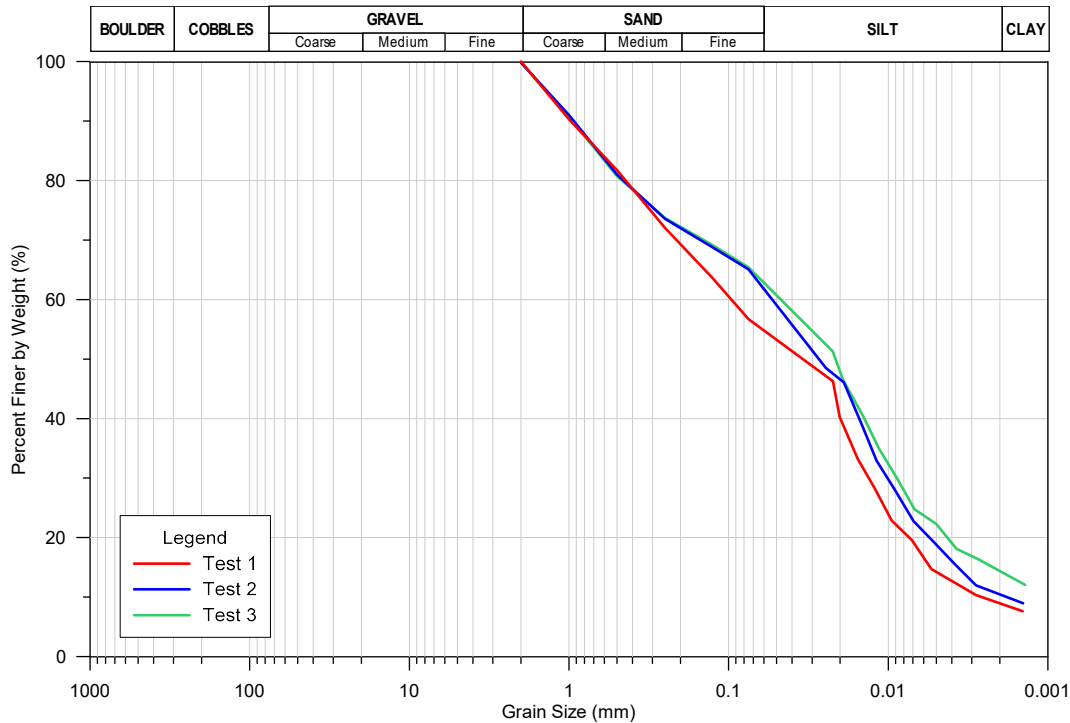


Figure 4.9: Grainsize distributions for large-scale column testing

Before wetting front arrival the VWC sensors showed stable readings, consistent with performance during initial testing. On wetting front arrival, the VWC sensors showed a quick response by a sharp increase in moisture content. However, once the wetting front passed by, the soil appeared to saturate slowly due to a slow increase in VWC with time. In all cases the maximum VWC reading was taken at the last time increment, indicating the soil continued to saturate further despite infiltration already reaching the base of the column. The sensors also showed VWC fluctuation as the test progressed, which may have been due to air becoming trapped in the sample as the soil consolidated. This is further explained in Section 4.3.4.

The instruments were not given time to equilibrate with the surrounding soil prior to commencing each test. During initial testing the suction sensors were found to require significant equalization time in drier soils, and since the tested material was moisture conditioned in a damp state, the suction sensors in the upper part of the soil column did not have sufficient time to equalize before the wetting front arrived. The sensors installed deeper in the soil column had more time to stabilize before the wetting front arrived, so the suction readings for those sensors are more reliable for determining the initial soil suction. Upon wetting front arrival the suction sensors recorded a very sharp response, and quickly passed the lower bound of the sensor measurement range. Once the sensors reached the minimum suction measurement, no variation was observed for the duration of the test.

The instrument readings from test 2 are shown in Figure 4.11, with similar performance to test 1.

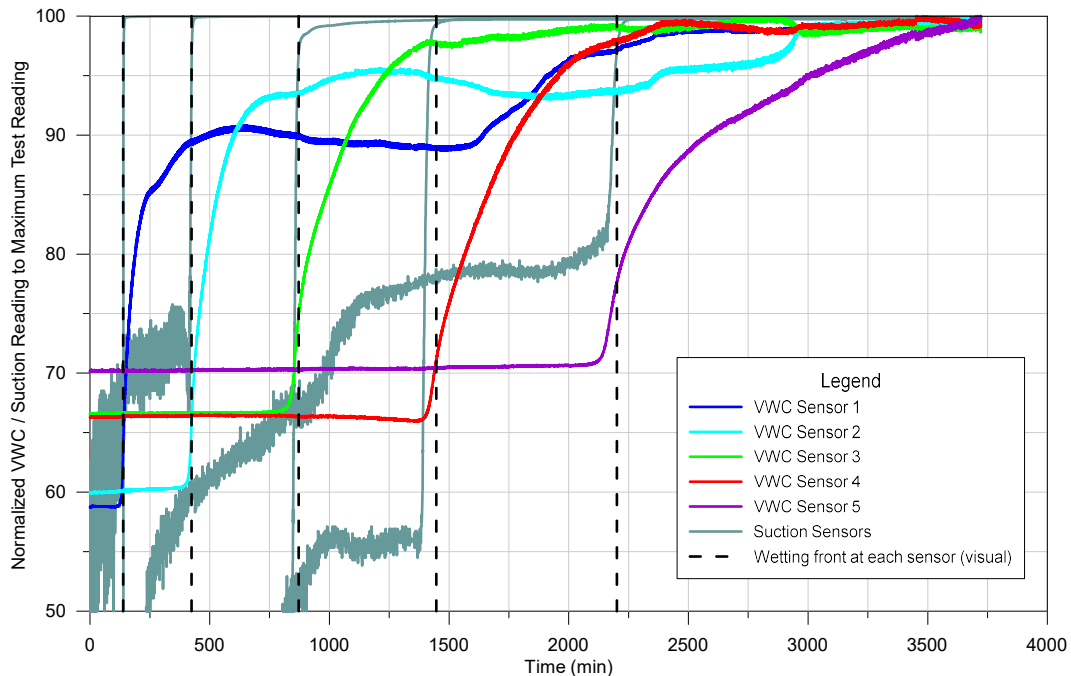


Figure 4.10: Instrument readings from column test 1

The reaction of the sensors in test 2 to the approaching wetting front was sharp initially and at similar times for both sensor types. The visual interpretation of wetting front arrival at the sensor locations agreed well with the sensor readings. Once the suction sensors became saturated there was no variation in output, however the VWC sensors showed a similar trend as for test 1, where as the test progressed there was some variation in the readings with time.

The instrument readings from Test 3 are shown in Figure 4.12. The suction sensor readings for test 3 are as expected from tests 1 and 2. The VWC sensors showed some interesting readings with larger variations in moisture content as the test progressed. At a testing time of around 2800 minutes most of the VWC sensors experienced a sharp jump in reading magnitude. It is not known what caused this disturbance at this time.

During the test it was not possible to retrieve samples from the column for moisture content determination to check the output of the VWC sensors. The only chance to check the readings was at test completion, when a final sensor reading could take place before the soil was removed from the column. In tests 2 and 3, 10 moisture content samples were retrieved during soil removal, each representing 10 cm of depth in the column. The samples were oven dried and the VWC computed using the calculated final density of the soil.

When the wetting front reached the base of the column, prior to permeability measurements, the amount of water which had entered the soil was calculated based on the remaining water in the water tank, the level of water above the soil and any water in the hose between the water

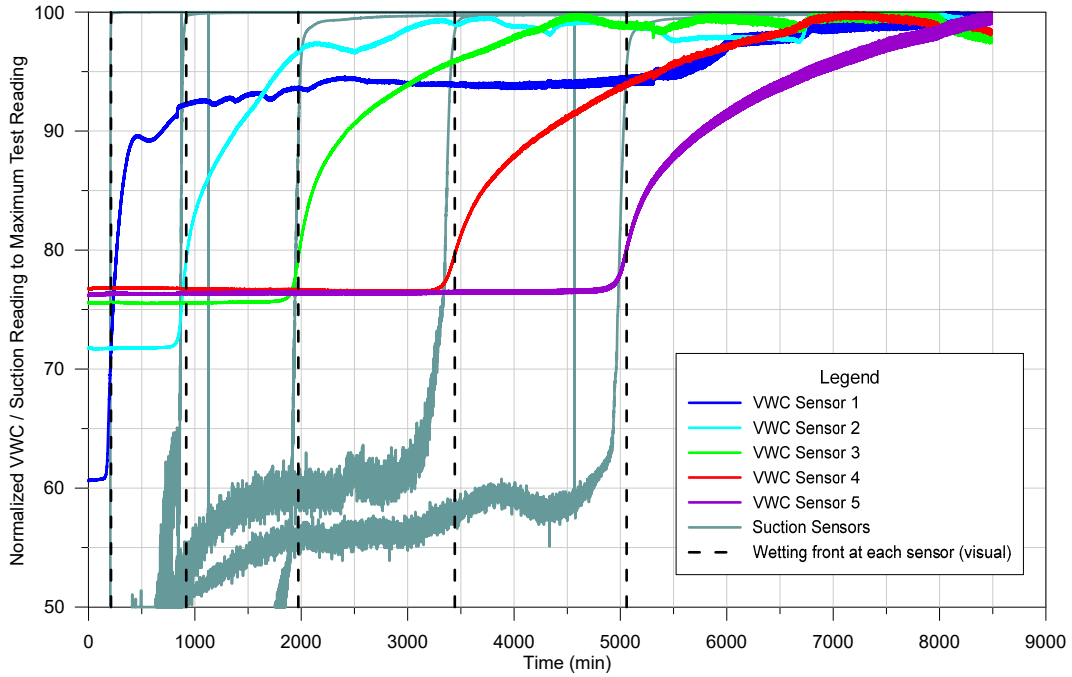


Figure 4.11: Instrument readings from column test 2

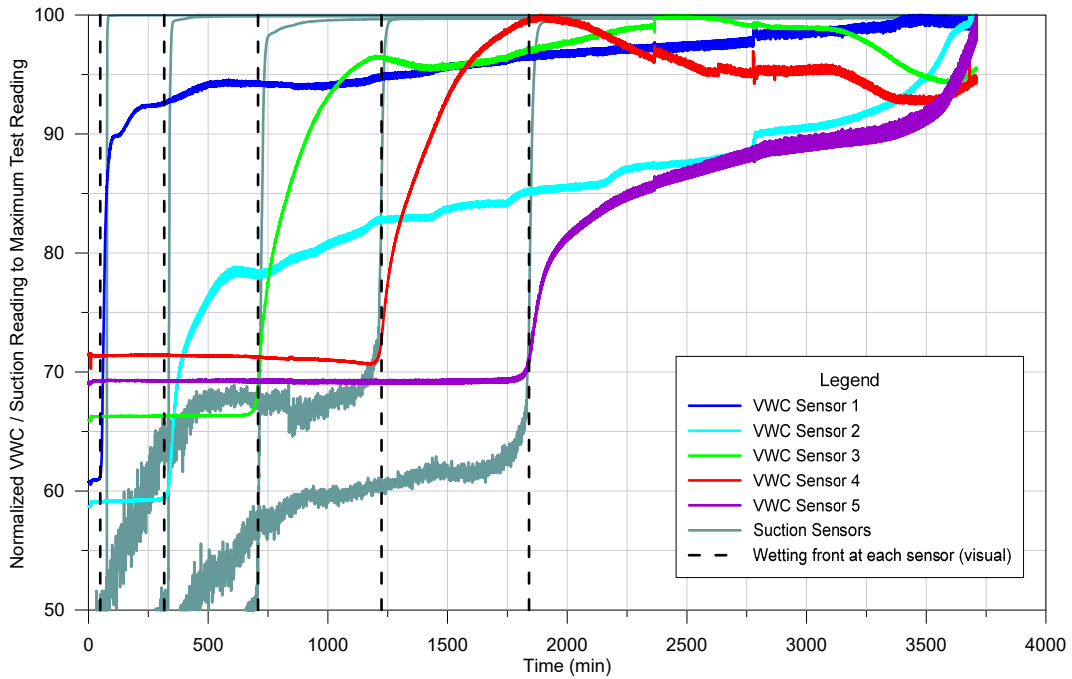


Figure 4.12: Instrument readings from column test 3

tank and the column. The change from initial water in these locations to final water was taken as the amount of water which entered the soil, and the final VWC could be calculated. Figure 4.13 shows the final VWC of the soil from the three different methods against column depth.

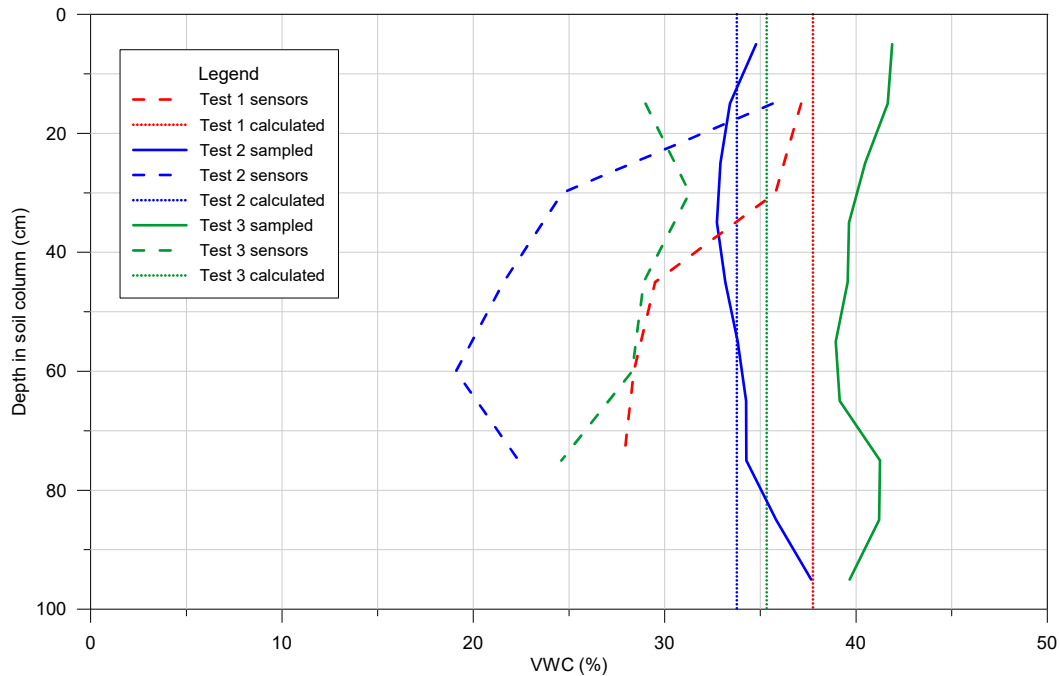


Figure 4.13: Comparison of VWCs with depth

After test 2, no samples were taken during soil removal. After test 3, the sensor readings were terminated and the soil water volume change computed several days prior to soil removal, and no more readings were collected directly before soil removal. The test 3 sampled moisture contents are therefore likely higher than they were when the final instrument readings were collected and the water volume change in the soil calculated. The VWCs from samples and from calculations of water volume change in the soil showed similar results in test 2, however due to late removal of soil in test 3, the sampled VWC is higher than the calculated and sensor measured VWC.

In all tests the sensors recorded lower VWCs than expected, possibly due to voids which were formed around the sensor heads during consolidation in the column throughout testing, discussed in Section 4.3.4. All tests also showed higher moisture contents in the upper column than the lower column, which could be explained by voids nearby the sensors becoming filled with water instead of air, since according to the samples there was not a significant difference in VWC with depth in the column. The lower sensors may show a lower VWC due to the voids adjacent to those sensors being air filled instead of water filled. Although there is a difference in VWC from all three methods, each method shows the same trend in that test 1 was the most saturated and test 2 the least.

4.3.3 Saturated Permeability Measurements

At the completion of each test the saturated permeability was found by performing a constant head permeability test through the infiltration column. Measurements of water volume from the base of the column were taken at set intervals and continued until the volume of water expelled stabilized for the same time increment. The hydraulic gradient was calculated to be the height of water head above the soil column plus the height of the soil column plus the drop from the base of the soil column to the outlet of the hose divided by the final height of the soil in the column. Table 4.2 shows the hydraulic gradients and calculated saturated permeabilities for each test.

Table 4.2: Saturated permeabilities from column testing

Test	Hydraulic gradient	Saturated Permeability [m/s]
1	1.24	3.71E-07
2	1.28	2.26E-07
3	1.35	3.57E-07

Test 2, which had the longest infiltration time, also showed the lowest permeability. Tests 1 and 3 showed similar permeabilities and also had similar infiltration times. This magnitude of permeability matches well with the expected permeability for a silt loess or silty sand material (Dingman, 2015), however these permeabilities are likely lower than the true saturated permeability as at completion of infiltration the soil was not fully saturated. Table 4.3 shows the initial and final moisture content and saturation levels of the three column tests.

Table 4.3: Saturation levels in soil columns after infiltration completion

Test	Initial VWC [%]	Final Calculated VWC [%]	Final Saturation [%]
1	9.91	37.7	80.6
2	9.91	33.8	72.2
3	9.91	35.3	75.5

The levels of saturation vary between 72% and 80%, meaning a significant amount of trapped air remains within the soil. The permeability of a soil is dependant on available flow channels within a soil column, and trapped air within a sample reduces the number of continuous flow channels (Fredlund et al., 2012). Therefore, the measured permeabilites are within the typical range for the soil type, but may be underestimated due to undersaturation during measurement.

4.3.4 Physical Observations

As the soil saturated, consolidation took place in the wetted soil and reduced the overall height of the soil column. No markers were placed in the soil column to mark the settlement with depth, so the only measurements taken were at the soil surface. The surface displacement readings with time are shown in Figure 4.14 for all three tests. It is also possible see the surface settlement in the photos of test 2 in Appendix C.

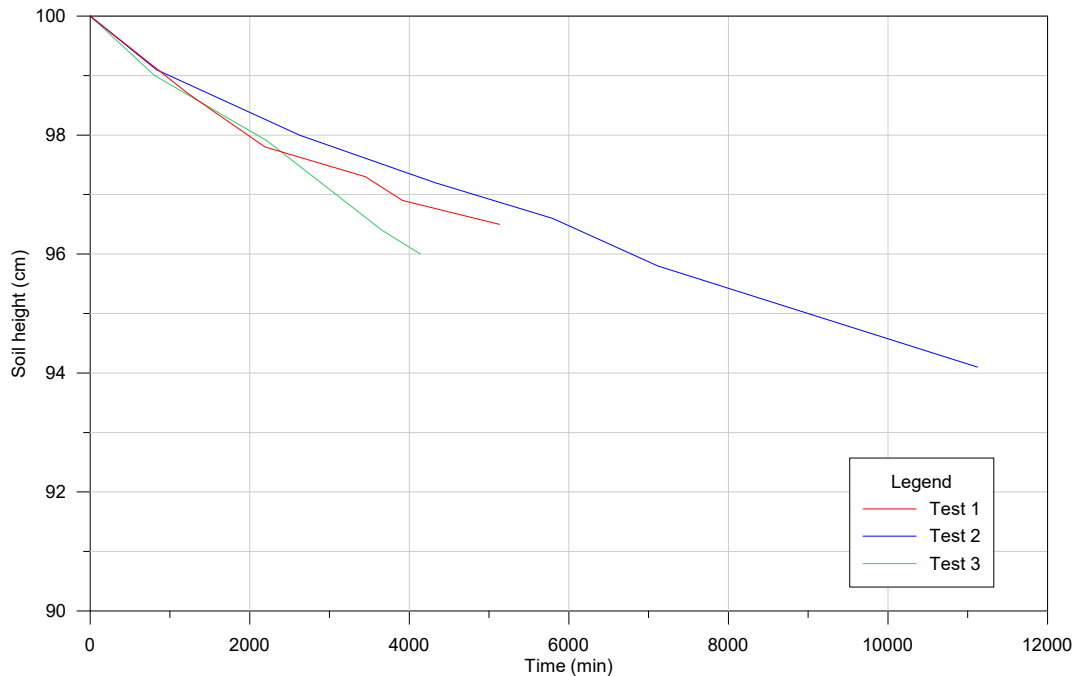


Figure 4.14: Surface settlement with time during column tests

Voids developed beneath the cable glands where the instrument cables passed through the column wall as the soil column settled (Figure 4.15a). These were not measured, however it was observed that the higher sensor ports had larger voids traveling further beneath the cable gland, indicating greater settlement at the top of the column than the bottom. The voids beneath the sensors may have impacted the readings of the VWC sensors as they showed some fluctuation in VWC as the test progressed. The suction sensors did not show any reaction to the consolidation, likely because any change in moisture content was not significant enough to raise the suction into the sensor operating range. While removing the soil from the column of test 2 after testing was completed, careful excavation was performed on the top row of sensors to see the final position of the sensor tips. Figure 4.15b shows the imprint of one suction sensor during removal and a small line on the edge of the column showing the downward movement of soil around the instrument. The ceramic disc was fully contacting the soil as it was able to move downward with the soil, however since the cable from the sensor head was fixed as it went through the cable gland, the sensor ended up angled upwards towards the column edge, creating the void below the sensor head. The VWC sensors ended up in a similar position to the suction sensors.

The water filling system performed as intended for the majority of testing. During the first 12 hours of test 2, which began in the early evening, the water filling system did not refill the head of water atop the soil column, resulting in a falling-head type infiltration for this time period, where the head of water decreased from 10 cm to 6 cm. Once this was recognized, the water was refilled to the appropriate head of 10 cm and the filling system performed as expected for the

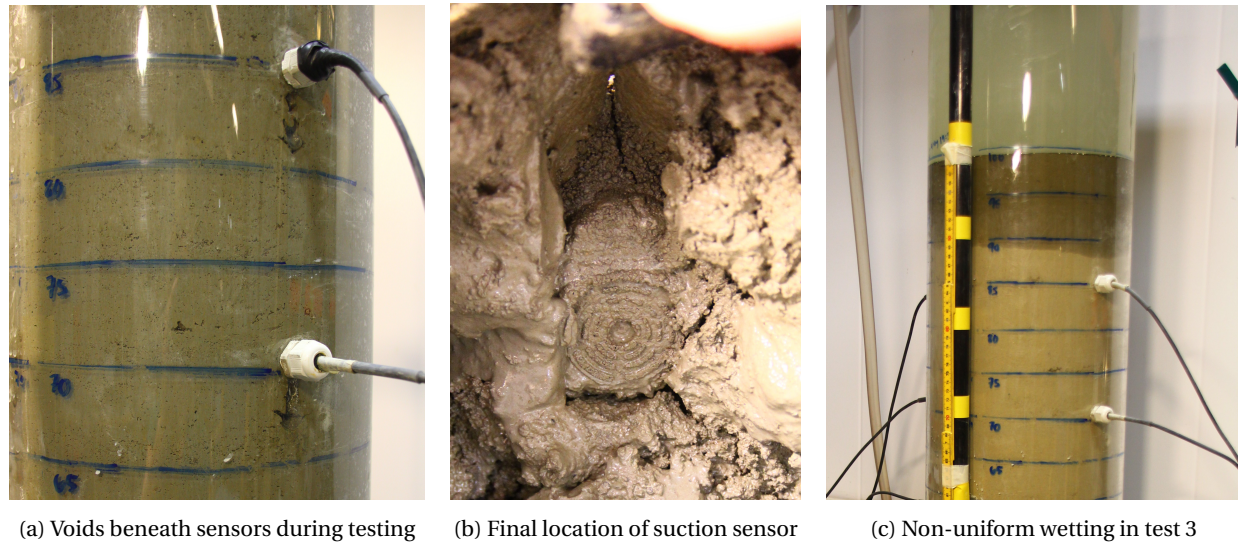


Figure 4.15: Movement of soil, sensors and wetting front during testing

remainder of the test.

The water filling system did not keep the water head exactly constant throughout the test. Due to the method of water refilling, the system would often overflow the head of water by around 2 cm. From surface tension, air would not be able to enter the pipe outlet to the water tank until the water head was approximately 0.5 cm below the pipe outlet. Therefore, the head of water on top of the soil column was not completely constant, but variable with time.

Test 3 was prepared using two different soil placement techniques. In tests 1 and 2 the material was placed into the column using a scoop to pour small portions of soil equally around the inside of the column, where in test 3 the entire mass for each lift was poured into the column from the measuring bowl at once. In both cases the loose soil was level prior to compaction, however it was noticed in test 3 that some of the lifts could be delineated through the column walls due to particle sorting. The lumps which formed during conditioning of the soil concentrated in one area of the poured in soil, and when compacted formed small but visible voids along the bottom boundary of the lift. At some points during infiltration, particularly at the beginning of the test, this caused a non-uniform and non-horizontal layer of downward infiltration, particularly in the early stages of the test as shown in Figure 4.15c.

Despite all three tests having the same initial conditions, the infiltration times varied. Tests 1 and 3 were both started from freshly combined material where test 2 reused material from test 1 which had been oven dried and re-pulverized. Figure 4.9 shows little difference between the GSD in tests 1 and 2, indicating the breaking apart of the oven dried material did not result in a finer grained material. Test 3 was run with another batch of freshly combined material, however with an increased head of water, so the infiltration time was slightly faster than that of test 1. There is a possibility that wetting of the combined material caused some reaction in the

material that reduced the permeability for test 2, but this has not been confirmed. Since tests 1 and 3 were both conducted on freshly mixed material and provided similar infiltration times, the test is thought to be repeatable.

4.4 Derivations from Results and Discussion

The column testing data and results presented in Section 4.3 were used to finalize the SWCC for this material, construct unsaturated SPFs and were compared with the Green-Ampt infiltration model, all introduced in Section 2.

4.4.1 Soil Water Characteristic Curve from Column Testing

The moisture content and suction sensor readings from each test were plotted against each other along with the initial testing points in the form of a SWCC, shown in Figure 4.16.

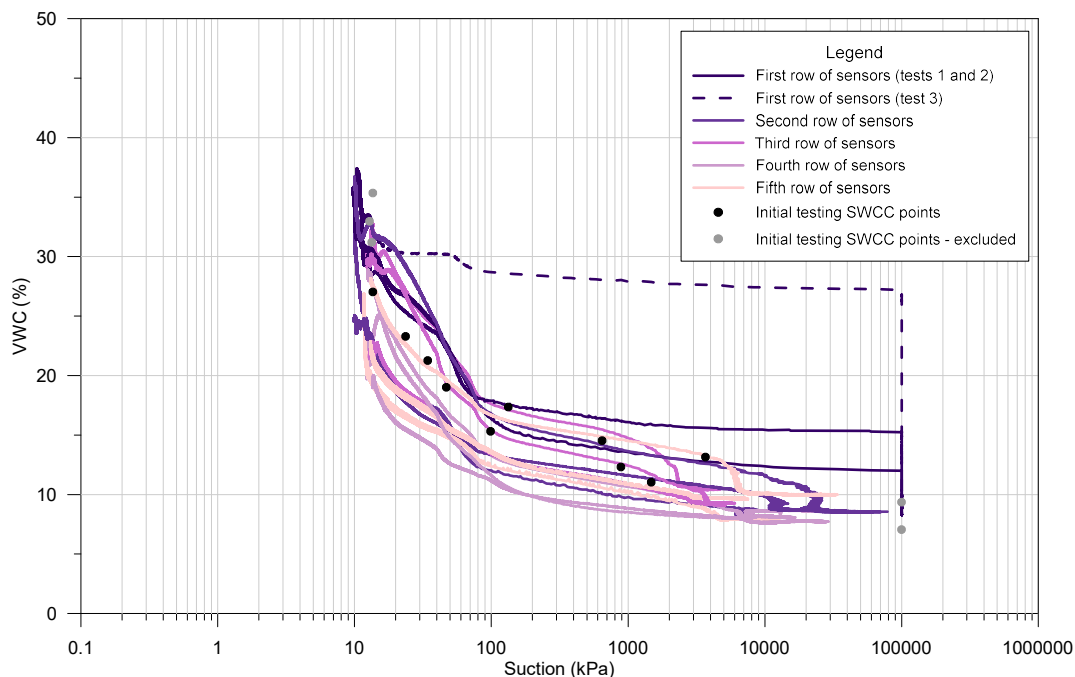


Figure 4.16: SWCCs plotted from large-scale test data

All the curves follow a similar trend, despite deviation between instrument pairs. The first row of sensors (top row) from test 3 followed a different curve than the rest, illustrated by the dotted curve in Figure 4.16, however this was attributed to the wetting front passing by this sensor pair quite quickly. The suction sensor was not able to react at the same rate as the moisture sensor, and therefore the moisture sensor recorded the saturated state more quickly than the suction sensor, resulting in high moisture readings throughout the curve.

There is a trend within the sensor readings where the sensors higher in the soil column generally plot with a higher VWC for the same suction value. This is the most evident with the top sensors in test 3 as mentioned above, however this seems to be the general trend for all the sensor data. In Figure 4.16 the darker coloured curves represent the highest sensor pairs and the lightest colours represent the lowest sensor pairs. The lighter coloured curves generally cluster towards the lower VWC values and the darker curves generally higher. In the upper part of the soil column the wetting front is moving faster than the lower portion, indicating the speed of wetting front travel may influence the SWCC trend based on response time of the sensors.

In the transition zone of the SWCCs there is nearly one log cycle of difference (i.e. one order of magnitude) between the suction values in the highest and lowest curves. In a study by Fredlund et al. (2011) on the shift of a SWCC between the wetting and drying curves due to hysteresis, they found silt and loam soils could laterally shift between 35% to 60% of a log cycle and clay soils could shift up to 100% of a log cycle. All of the curves developed from infiltration testing were on a wetting path, so the range of deviation between sensor pairs is quite high considering the deviation in the full-scale column test data in the transition zone is in the range of 50% to 90% of a log cycle for all tests on a wetting path only. The sensor accuracy could only account for a small portion of the data scatter, so other factors such as sensor response time must have contributed.

The equations from Brooks and Corey, van Genuchten-Mualem and Fredlund-Xing were used to fit the column testing data and initial testing points to generate an average SWCC from all testing data. All equations were optimized by maximizing R^2 using the Excel Solver tool. The van Genuchten-Mualem and Fredlund-Xing equations were optimized directly, and the Brooks and Corey equation was optimized to find the pore size distribution index, λ_{bc} , and the air entry value, ψ_{aev} as described in Section 2.2.3 (Figure 4.17).

Prior to curve fitting, the SWCCs shown in Figure 4.16 were clipped so readings outside of the suction sensor reading range were eliminated. The fitted curves are shown in Figure 4.18 with the SWCCs and points used to fit the data shown greyed out behind. The curve fitting parameters for each equation are shown in Table 4.4.

Table 4.4: SWCC fitting equation parameters from column testing data

Brooks and Corey		van Genuchten-Mualem		Fredlund-Xing	
Parameter	Value	Parameter	Value	Parameter	Value
θ_r	0.0909	θ_r	0.0909	ψ_r	19.2
θ_s	0.468	θ_s	0.468	θ_s	0.468
λ_{bc}	0.546	a [1/kPa]	0.1796	a_f [kPa]	6.586
ψ_{aev} [kPa]	4.427	n	1.600	n_f	19.99
				m_f	0.1944

The SWCCs plot generally in the middle of all the sensor data, and particularly in the transitional zone. The air entry value is not clearly defined since all curve fitting methods produce

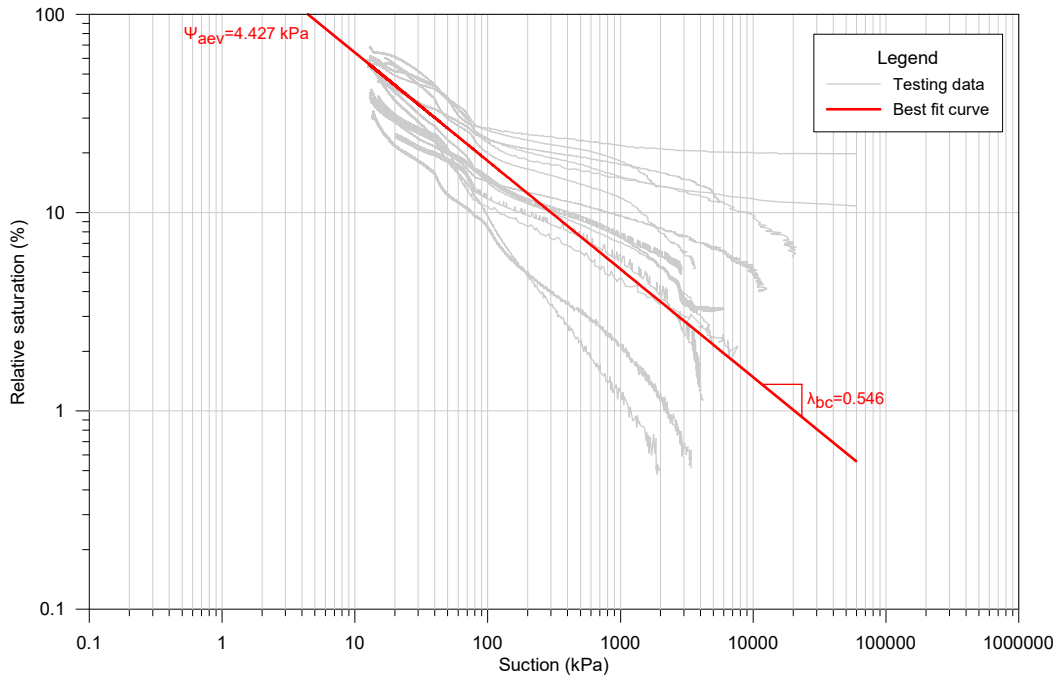


Figure 4.17: Optimization to find Brooks and Corey pore size distribution index and air entry value

a different curve at the boundary of the capillary and transitional zones and there is no sensor data to confirm which curve produces the best fit. In the residual zone the Brooks and Corey and van Genuchten-Mualem models both asymptote slightly below the residual saturation, and the Fredlund-Xing equation reaches a dry state at maximum suction due to the correction factor. There is also no sensor data in the high suction range to confirm whether the theory of dry conditions at maximum suction holds true for this soil.

Upper and lower bound curves were fit to the uppermost and lowermost testing data for later use in permeability function determination and to show the range of SWCCs possible from the scatter in the testing data. The upper and lower bounds are shown with the van Genuchten-Mualem formulation in Figure 4.19.

The upper and lower bounds were fit by maximizing the R^2 value on the uppermost and lowermost two SWCCs from the testing data. For these bounding curves the saturated VWC remained at the initial porosity of the soil, however the residual saturation was allowed to change, along with the curve fitting parameters " m " and " n ".

The average van Genuchten-Mualem model was further used in numerical modeling, discussed in Section 5.1.

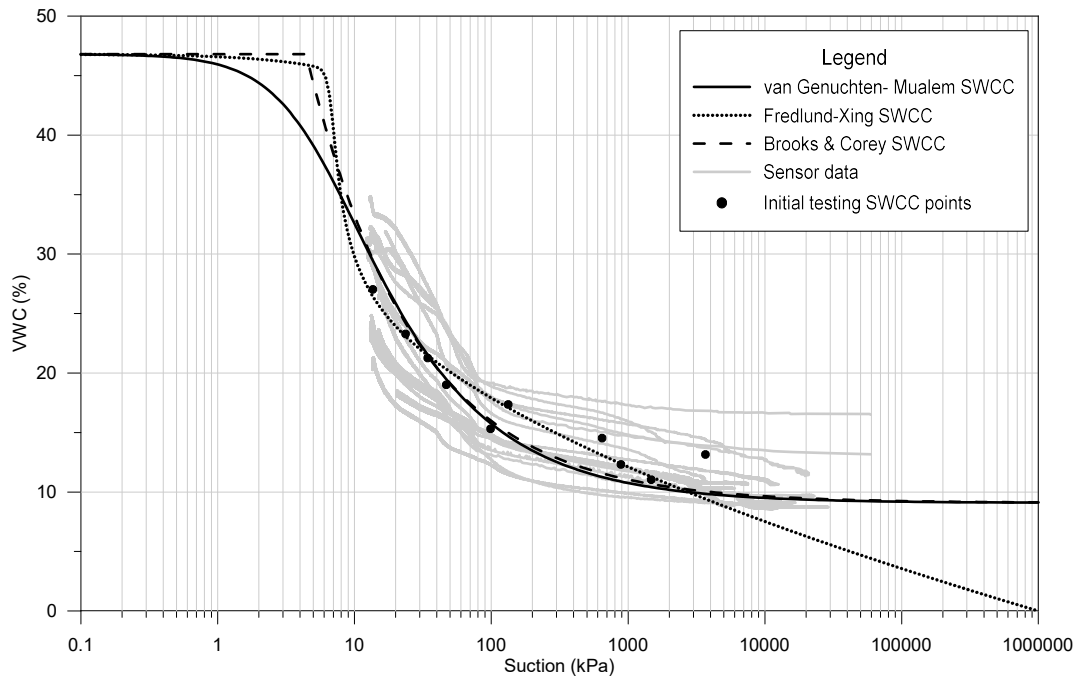


Figure 4.18: Fitted SWCCs using column testing data

4.4.2 Unsaturated Soil Permeability Function

The SPF for the tested material was estimated using three methods as described in Section 2.4. With the instrumentation data, the instantaneous profile method and the wetting front advance method were used to generate two SPFs, and the average SWCC shown in Section 4.4.1 using the van Genuchten-Mualem model was used to generate the third SPF. Figure 4.20 shows the estimated SPFs using each method.

Only the van Genuchten-Mualem approximated SPF is given as a continuous curve. The instantaneous profile and wetting front advance methods show calculated permeability points at average suction value used in finding the permeability. These two methods rely on laboratory measurements, but data could only be collected in the measurement range of the suction sensor. At the bounds of the measurement range large data scatter was observed, therefore the points in Figure 4.20 were clipped to suctions between 14 kPa and 1000 kPa to avoid excessive data scatter beyond this range.

Each of the three methods produced a different trend for the SPF, however within each method the SPF followed a similar trend between column tests. The difference in permeability for a given suction is in the range of several orders of magnitude, however the data directly from sensor measurements seems to agree relatively well. Some of the differences are explained in the paragraphs below. Test 2, shown in blue, shows the lowest permeability for the same suction compared to tests 1 and 3. This agrees with the laboratory results, where test 2 had the slowest

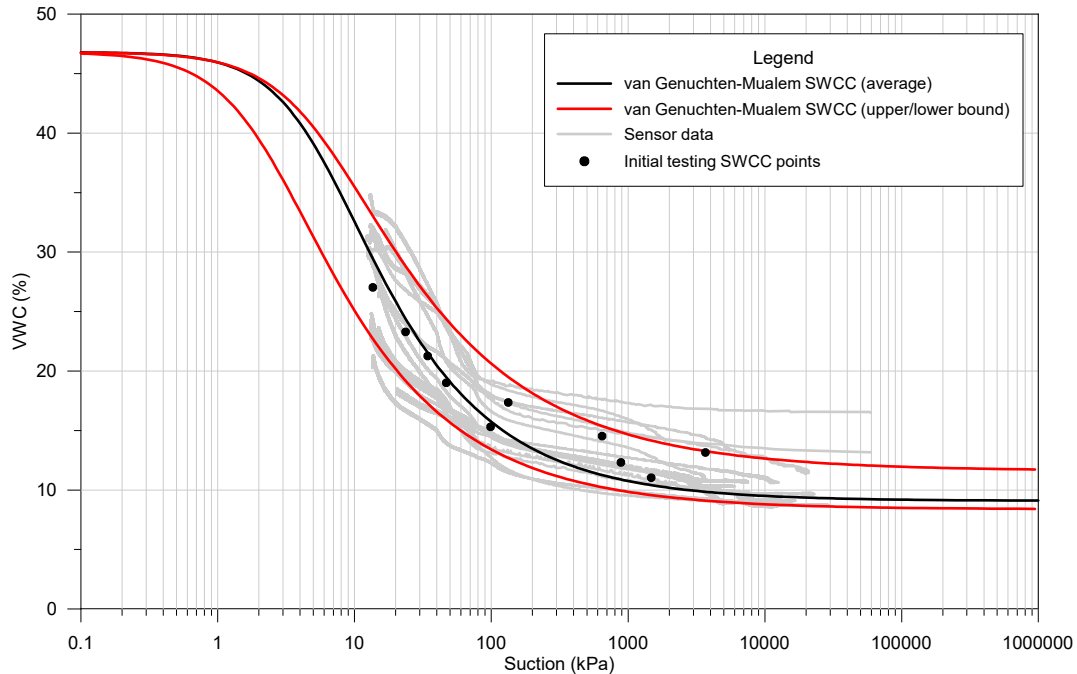


Figure 4.19: Upper and lower bound of van Genuchten-Mualem SWCCs from testing data

infiltration time and tests 1 and 3 similar infiltration times.

Discussion on Direct Measurements

The instantaneous profile method introduces error when calculating the hydraulic gradient at the measurement points due to averaging of suction readings. To calculate the hydraulic gradient at a sensor measuring location, the suction measurements from the two adjacent sensor clusters were averaged over the separation distance to find the rate of change of suction at the middle measuring point. To find the rate of change at sensor cluster 2 for example, the suctions at sensor clusters 1 and 3 were used over the separation distance of 300 mm. When the wetting front was in between sensor cluster 1 and 3, the suction difference between the two sensors could be as large as 13 kPa for the wet portion and 100,000 kPa for the unsaturated portion, as shown in Figure 4.21a. Typically the wetter sensor had a suction at the lower limit of the sensor, around 13 kPa, and the drier sensor reduced in suction as the wetting front approached, resulting in decreasing yet overestimated average suctions due to the averaging between a wet and dry sensor.

Figure 4.21 shows the WVC and suction measurements at the time "instants" selected for calculating the instantaneous permeability in test 3. The time increments were chosen to try and capture the moments when the wetting front passed each set of sensors. [McCartney et al. \(1981\)](#) note that using suction sensors for use in determining hydraulic conductivity may lead to errors

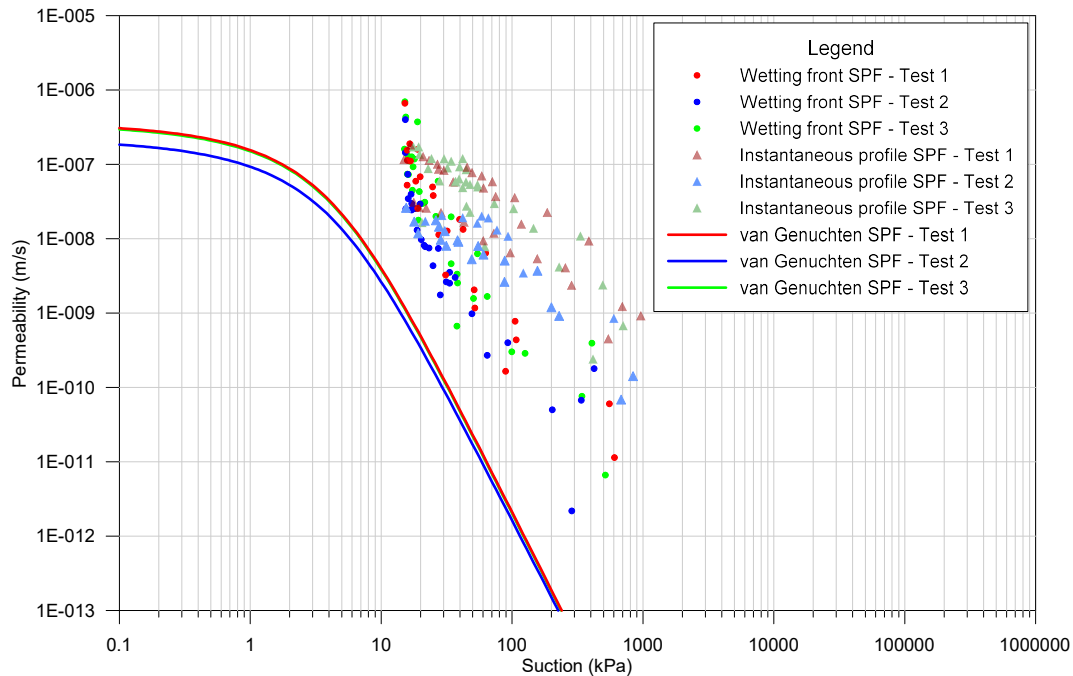


Figure 4.20: SPFs generated using three different methods from column test data

resulting from lag time in sensor response to wetting. They recommend using only moisture sensors and using a previously determined SWCC to find the corresponding soil suction at each moisture condition.

Li et al. (2009), in their proposal of the wetting front advance method, note the large spacing between measurement sections introduced more scatter into the SPF points. As can be seen in Figure 4.20, the permeability functions estimated using the instantaneous profile method plot the same permeability at a highest suction between the three methods in most cases.

The wetting front advance method is based on a combination of instrument readings and visual observations of the wetting front. The interpretation of the wetting front location is based upon discerning the colour change in the soil as it changes from initial conditions to saturated conditions and could have been misinterpreted in some locations. However, photo quality was generally good and compared well with observations taken at the column itself, so errors in visual interpretation were considered to be small. Some examples of wetting front observations every 50 mm are included in Appendix C from test 2.

The suction values used for plotting the permeability in the wetting front advance method were the average suction values between the two time steps used to calculate the wetting front advance rate. This also overestimated the suction value that should be used for plotting as the time steps were long enough for the suction values to decrease significantly in some cases. This could be improved by using finer time increments of wetting front advance, however due to the

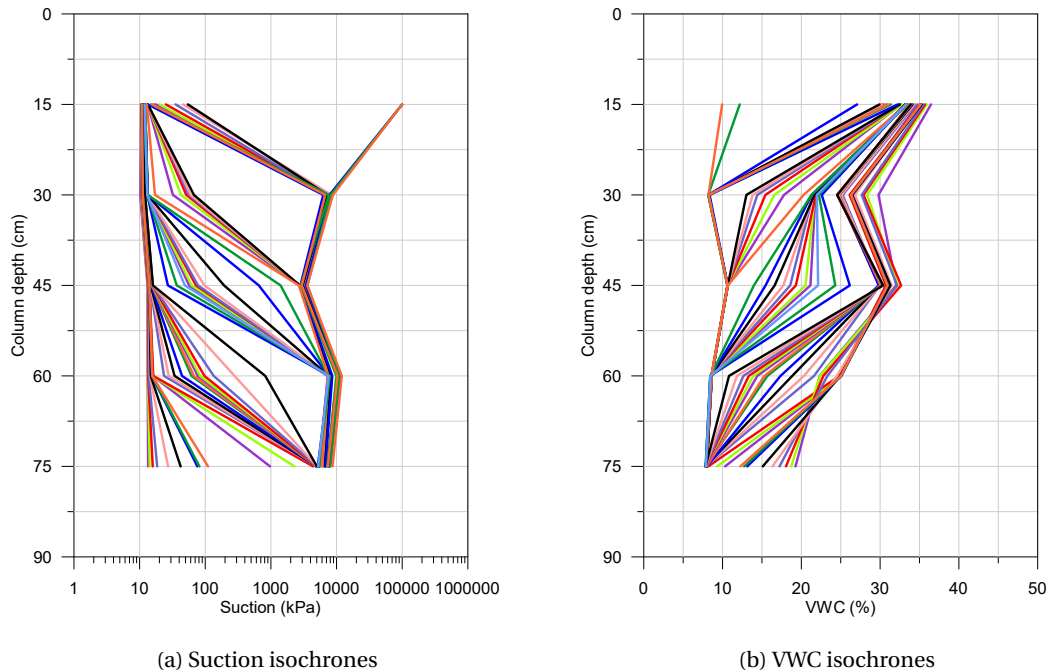


Figure 4.21: VWC and suction measurements with depth at instantaneous profile method time increments

slow wetting front advance rate it was difficult to discern small changes in wetting front advance to a lesser degree than already accomplished.

The instantaneous profile method averages suction measurements between different sensor locations at the same time, where the wetting front advance method averages suction measurements at the same sensor location but at two points in time. The error in suction measurements in the wetting front method is considered to be less than that for the instantaneous profile method as the suction measurements were taken as the sensors were wetting, so no dry end measurements were averaged with wet end measurements. Despite both the instantaneous profile method and wetting front advance method overestimating suction values, the permeabilities agree relatively well.

Discussion on Indirect Development

The van Genuchten-Mualem SPF formulation is based on a statistical interpretation of the SWCC. The SWCC definition itself was challenging due to large variation in the results and lack of information in the low and high suction ranges, so upper and lower bounds were fit to the extreme data values. Figure 4.22 shows the range of possible SPFs, taking the saturated permeability from test 3. The instantaneous profile data and wetting front data are plotted in greyscale behind for comparison.

The bounding curves on the SPF do not move in the direction of the estimated SPFs using the

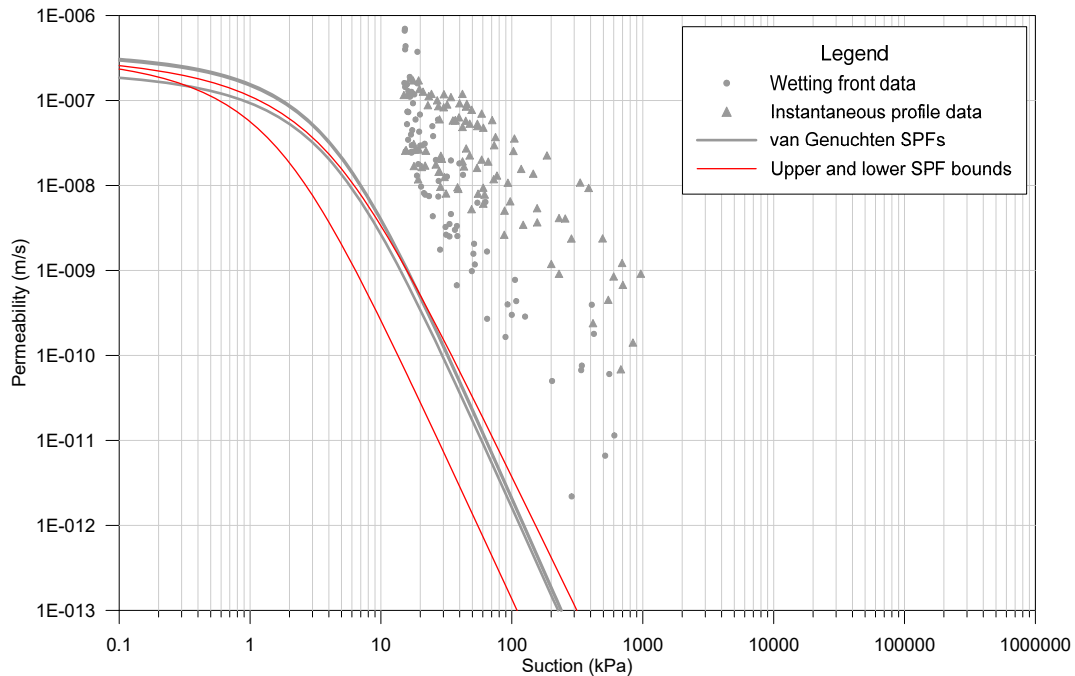


Figure 4.22: Range of SPFs based on van Genuchten-Mualem formulation of the SWCC

instantaneous profile method or the wetting front advance method, indicating the bounds likely do not improve upon the average SWCC in representing the soil behaviour. However, if the saturated permeability found in the soil column was too low by one order of magnitude (i.e. the true permeabilities were in the 1×10^{-6} range) due to air filled pore channels during permeability measurements, the SPFs estimated by van Genuchten would translate closer to the instantaneous profile and wetting front permeabilities.

All three methods have one source of error in common: the suction sensor. Measurements from this sensor were used to generate the average SWCC and subsequent SPF, and were used in both the SPF direct determination methods. It is recommended to obtain a suction sensor which can measure in lower suction ranges to be able to define the air entry value in the SWCC. Additionally, a suction sensor which has a quicker response time would be better suited for measurements in infiltration testing where accurate measurements of suction with time are crucial.

4.4.3 Infiltration Model Comparison

The infiltration process during large-scale column testing was compared with the Green-Ampt model. The Green-Ampt model is typically used to find the time at which the wetting front will reach a certain depth below ground surface, and when ponding will begin based on the water supply rate. In column testing the time to ponding was set at zero as testing was completed under constant head conditions. During column testing the wetting front depth was monitored

visually with time, so the only unknown in Equation 2.16 was the wetting front suction.

The wetting front suction was found using the trial and error technique to match the Green-Ampt wetting front advance prediction to the column testing wetting front advance. The comparison between predictions and reality for each column test are shown in Figure 4.23. The wetting front suction was calculated to be between 100 kPa and 180 kPa for all three tests using the trial and error technique to match the curves shown in Figure 4.23. These values correspond to suctions slightly above the residual saturation level of 9.09% for the average van Genuchten-Mualem SWCC, between VWCs of 14% to 16%.

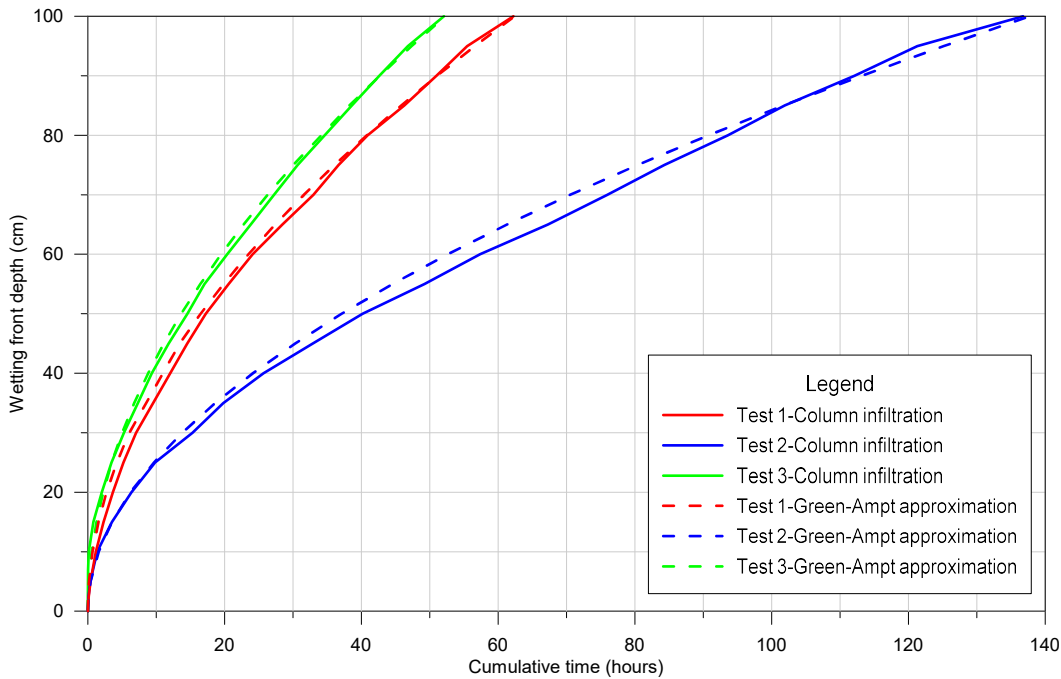


Figure 4.23: Comparison of Green-Ampt model with column testing infiltration

For in-situ installations it is generally not possible to measure the wetting front depth at different times and back-calculate the wetting front suction, so two methods were used to estimate the wetting front suction for comparison to the back calculated values. Rawls et al. (1983) produced Figure 4.24 which estimates the wetting front suction based on the proportion of sand and clay in a sample. The material used in column testing contained 45% sand and 10% clay, which according to the figure corresponds to approximately 17 cm, or 1.7 kPa, of wetting front suction.

Mein and Larson (1973) suggested integrating the suction across the range of relative permeabilities from 0 to 1. For this purpose the generated SPF from the van Genuchten-Mualem formulation was used, and the saturated permeability found in each column test. The wetting front suction was found to be 14.9 cm, or 1.49 kPa for all three column tests. This agrees with the wetting front suction proposed by Rawls et al. (1983) shown above, but again not with the back-calculated values. These small amounts of suction are likely below the air entry value of

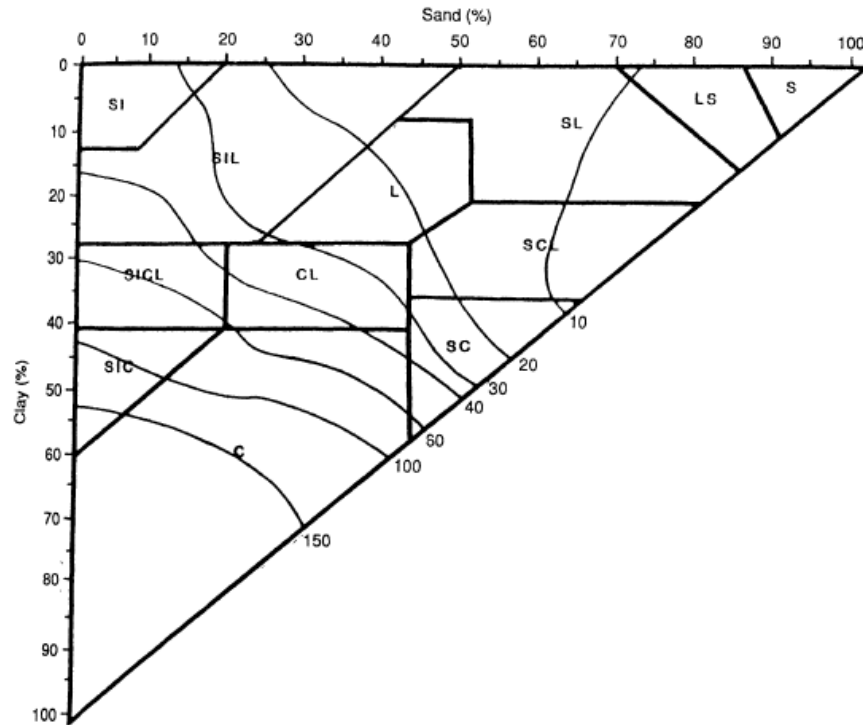


Figure 4.24: Wetting front suction based on soil fractions (from [Dingman \(2015\)](#) after [Rawls et al. \(1983\)](#))

the average van Genuchten-Mualem SWCC, and close to full saturation, which coincides with the Green-Ampt model assuming a sharp wetting front. The sharp wetting front assumption is more applicable for sand material than clay material as clays generally have a less distinct wetting front ([Dingman, 2015](#)). The wetting front in the column test may have been too gradual for the Green-Ampt model.

The Green-Ampt infiltration model is highly dependant on the accurate measurement of saturated permeability. As mentioned earlier, the saturated permeability determined is likely low due to lack of complete saturation during permeability measurements. If the saturated permeability of the material was one order of magnitude higher than what was measured, the back-calculated wetting front suctions would be in the range of 50 cm, which is closer to the suggestions by [Rawls et al. \(1983\)](#) and [Mein and Larson \(1973\)](#).

Despite the wetting front suction differing from typical values, the infiltration process follows the trend of decreasing infiltration rate with time, following a power type equation based on trendlines fitted to the experimental data. Over time as the wetting front advances, the gradient of wetting front suction over cumulative infiltration depth decreases, reducing the infiltration rate ([Dingman, 2015](#)).

Chapter 5

Numerical Infiltration Study

An initial attempt was made to model the column infiltration with the finite element software PLAXIS 2D, using the average SWCC and measured saturated permeabilities from laboratory testing. Comparisons were made between the laboratory infiltration times and the PLAXIS infiltration times, and discussions are made on the differences through a sensitivity analysis. A back-analysis was then conducted on the SWCC fitting parameters to find a parameter set matching the infiltration time in PLAXIS to the column infiltration time.

5.1 Model Description

The PLAXIS model used in initial testing, described in Section 3.2, was modified for comparison with large-scale column testing results. The model remained axisymmetric, however the radius was increased to 0.12 m and the soil height increased to 1.0 m. The mesh size was set to medium, with a soil polygon coarseness factor of 0.35 as shown in Figure 5.1a. Nodes were selected along the centerline of the model at surface, at each instrument cluster depth and at the base of the column, shown in Figure 5.1b. The calculation mode flow only was selected in the initial phase, with transient flow conditions in subsequent phases.

The material parameters selected were based on the results of column testing. Since a flow only analysis was used, only hydraulic properties were required as inputs, as stress computations are not performed in a flow only analysis. The initial void ratio for all column tests was 0.98, as was calculated based on the compaction level of the tested material in the column. The saturated permeability was computed for each column test separately. The van Genuchten-Mualem SWCC model was employed with user-defined parameters shown in Table 5.1, found during final SWCC determination explained in Section 4.4.1.

In the initial phase, soil water conditions were set to unsaturated, using the initial saturation level from the large-scale column tests. The porosity of the column tests was 46.8%, which was

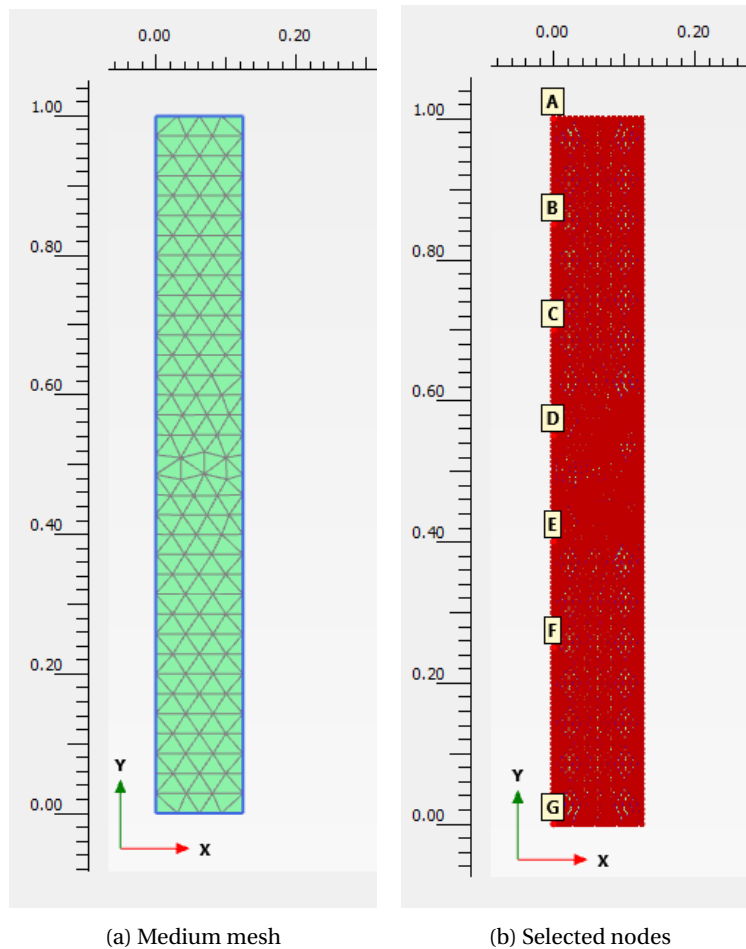


Figure 5.1: PLAXIS large-scale column test model

taken to represent the VWC at 100% saturation. Therefore, the initial soil VWC of 9.91% corresponded to a saturation of 21.1%. The " a " parameter is listed in units of [1/kPa], however in PLAXIS the units are [1/m] so the input was 1.796 1/m instead of 0.1796 1/kPa.

Table 5.1: van Genuchten-Mualem SWCC parameters used in PLAXIS model

Parameter	Value in Average SWCC
S_{res}	0.2114
S_{sat}	1
a [1/kPa]	0.1796
n	1.600
l	0.5

The vertical and bottom boundaries were set to closed, and the upper boundary set to seepage. The bottom boundary was set to closed, or a no flow boundary, so that water would not drain from the sample. Seepage boundaries allow water flow and since the soil was above the groundwater table having a seepage boundary at the base of the model could affect the initial pore pressure calculation. Since the initial soil water conditions were set to unsaturated, the phreatic option for pore pressure calculation was selected, as the steady-state option does not

consider unsaturated soils.

In the second phase, the boundary condition at the surface was changed to a head height linearly increasing from 1 m to 1.1 m or 1.2 m in 2 minutes time, depending which of the column tests was being analyzed. This was to simulate the time it took to fill the water head height above the soil at the beginning of the column tests. The soil polygon water conditions were also set to total head in the same manner as the top boundary. The pore-pressure calculation was set to transient groundwater flow with a total phase time of 2 minutes.

The final phases were run for sufficient time to allow saturation to the base of the column, which varied between tests. All boundary conditions were the same as in the second phase, however the head on the top boundary of the soil column remained constant at 0.1 or 0.2 m. Due to numerical uncertainty when finding infiltration times, multiple phases were used with the full head height to obtain stable results.

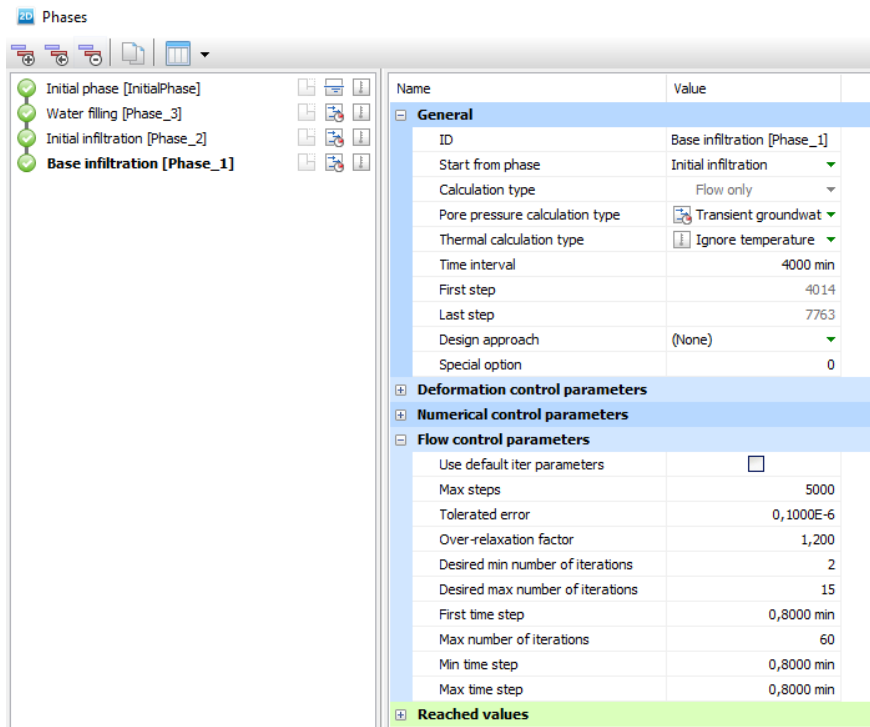
5.2 Numerical Control Parameters

PLAXIS uses a load stepping procedure where the portion of the total load applied in each step varies depending if the solution converges between a minimum and maximum number of iterations. If the load increment is too large, the solution will converge higher than the maximum number of iterations, and vice versa for a small load increment. If the applied load increment is between the desired iterations, the load increment will increase on the next load step. By this method, the load increment could continue increasing until the end of the desired time step.

In these PLAXIS simulations the information required was the time to reach full saturation at the base of the model, which is towards the end of the phase time increment, where the load increment application is likely the largest. As a result, highly non-linear parameters may cause different load stepping to occur, resulting in differing numbers of load steps to complete the analysis, which gives different infiltration times. This was found to be the case during large-scale infiltration analysis, where multiple simulations would be run on multiple computers, all with the same input parameters, but obtain different infiltration results with each simulation. As a result, the flow control parameters in the phase explorer were modified to find a time step increment which gave stable and consistent results.

The final modifications were made to the first step size, minimum and maximum step sizes, and the tolerance level. It was found that a constant step increment of 2 minutes with a tolerance of 1×10^{-7} provided nearly the same accuracy as a smaller step size. Decreasing the step size from 2 minutes to 0.8 minutes per step changed the infiltration time by 1 to 2 minutes, and further to 0.3 minutes per step did not give different results. Decreasing the tolerance did not improve results so was left constant at 1×10^{-7} . Increasing the step size to 5 minutes significantly reduced the accuracy of the infiltration times, as did increasing the tolerance to 1×10^{-6} or higher.

The maximum number of steps available per phase is 10,000, so in order to obtain a step size of 0.8 minutes per step when infiltration reached the base of the model, the third phase was split into two phases. The first phase was set to a time increment of 2 minutes per step for some time less than the expected infiltration time. The second phase was set to a time increment of 0.8 minutes per step to a time past when infiltration was expected to reach the column base. In this way the time for full saturation at the base could be more accurately determined with smaller step sizes while maintaining a good level of accuracy in the upper parts of the column. Each simulation was run a minimum of twice, to ensure at least two simulations gave the same infiltration time. The control parameters are shown in Figure 5.2 for the final phase, with a time step of 0.8 minutes. In this simulation the expected infiltration time was between 8000 and 12000 minutes, so the last phase lasted 4000 minutes. The previous phase was set to 8000 minutes with a step time of 2 minutes.



The screenshot shows the 'Phases' window with a list of phases on the left and a detailed parameter table on the right. The 'Base infiltration [Phase_1]' phase is selected. The parameter table is as follows:

Name	Value
General	
ID	Base infiltration [Phase_1]
Start from phase	Initial infiltration
Calculation type	Flow only
Pore pressure calculation type	Transient groundwat
Thermal calculation type	Ignore temperature
Time interval	4000 min
First step	4014
Last step	7763
Design approach	(None)
Special option	0
Deformation control parameters	
Numerical control parameters	
Flow control parameters	
Use default iter parameters	<input type="checkbox"/>
Max steps	5000
Tolerated error	0,1000E-6
Over-relaxation factor	1,200
Desired min number of iterations	2
Desired max number of iterations	15
First time step	0,8000 min
Max number of iterations	60
Min time step	0,8000 min
Max time step	0,8000 min
Reached values	

Figure 5.2: Numerical control parameters giving stable infiltration times

5.3 Model Results and Discussion

Numerical simulation was performed with each of the three column test input parameters using the same SWCC, but updating the saturated permeability. The suction and saturation profiles, and water flow vectors are shown in Figure 5.3 after 2 minutes of infiltration in test 2. The suction profile shows decreasing suction at the surface where infiltration has increased the VWC of the soil. The saturation of the soil shows moderate increase directly at surface but has not

reached saturation anywhere in the soil profile. This shows the large influence small VWC changes have on the suction in the soil around the residual saturation range, especially with the van Genuchten-Mualem SWCC which asymptotes past the residual suction value. The flow vectors show higher flow closer to surface where the saturation level is higher and low to no flow deeper into the soil column where permeability and moisture content are low. Also shown in the figure is the level of the water head above the soil, set to 0.1 m.

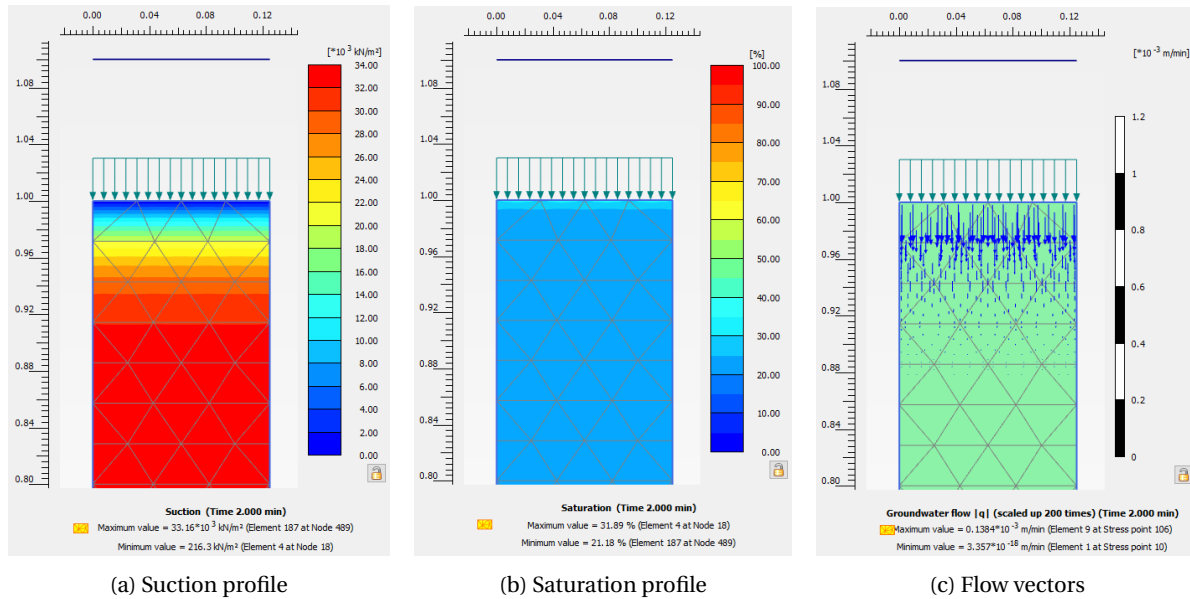


Figure 5.3: Suction and saturation profiles, and flow vectors after 2 minutes of infiltration during Test 2

The time for infiltration to the base of the column for each test is listed in Table 5.2 along with the infiltration time from column testing.

Table 5.2: Comparison of infiltration times between PLAXIS model and large-scale column testing

Test	PLAXIS Infiltration [min]	Column Infiltration [min]
1	13464	3735
2	21935	8207
3	12672	3124

The infiltration results using PLAXIS overestimated the infiltration time significantly in all three tests. The PLAXIS infiltration time was between 2.7 to 4 times longer than the column infiltration test, and showed the least agreement with test 3.

5.4 Sensitivity Analysis

A sensitivity analysis was run on the van Genuchten-Mualem SWCC fitting parameters to determine the influence of each parameter on the infiltration time. First, the "a" and "n" parameters were modified individually to see the effect on the shape of the SWCC. Next, the infiltration

times were computed using PLAXIS with different combinations of " a " and " n " to back-analyze the combination giving a similar infiltration time to the laboratory test.

5.4.1 Curve Fitting Parameter Modification

The van Genuchten-Mualem " a " and " n " parameters were varied individually to see the effect on the shape of the SWCCs and SPFs. The saturated and residual VWCs were kept the same as the average SWCC determined from column testing data (Table 5.1), and the permeability was taken from the test 3 sample.

The " a " parameter is related to the air-entry value of the SWCC, and shifts the curve higher and lower on the suction axis while maintaining the slope of the curve, as shown in Figure 5.4. In this analysis the " n " parameter was held constant at 2.7. The " n " parameter is related to the distribution of pore sizes in a sample and adjusts the slope of the transition zone of the SWCC, as shown in Figure 5.5. In this plot the original " a " value from the average SWCC is held constant where the " n " value is varied. The van Genuchten-Mualem " m " parameter is dependant on the value of " n " but is related to the asymmetry of the model. This value was calculated with the Mualem approximation where $m = 1 - \frac{1}{n}$.

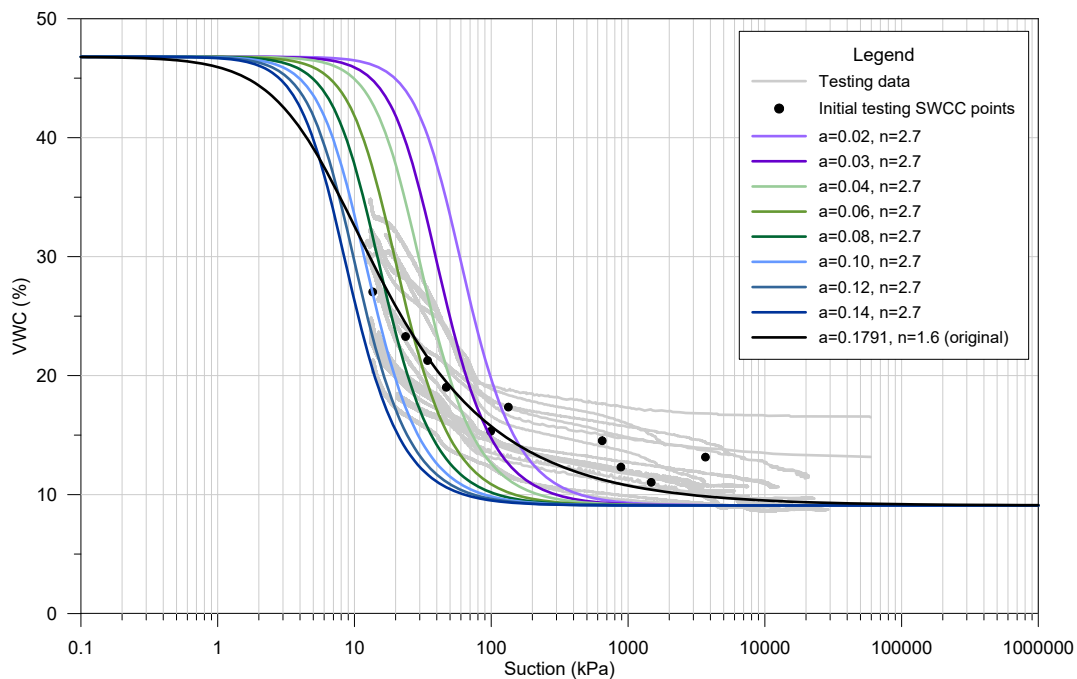


Figure 5.4: Sensitivity of SWCC due to variation in van Genuchten-Mualem " a " parameter

Figures 5.6 and 5.7 show the change in SPF with modification of the " a " and " n " parameters.

The influence of the " a " parameter on the shapes of the SWCC and SPF was found to increase as the " a " parameter became smaller. At higher " a " values the SWCC and SPF were less impacted

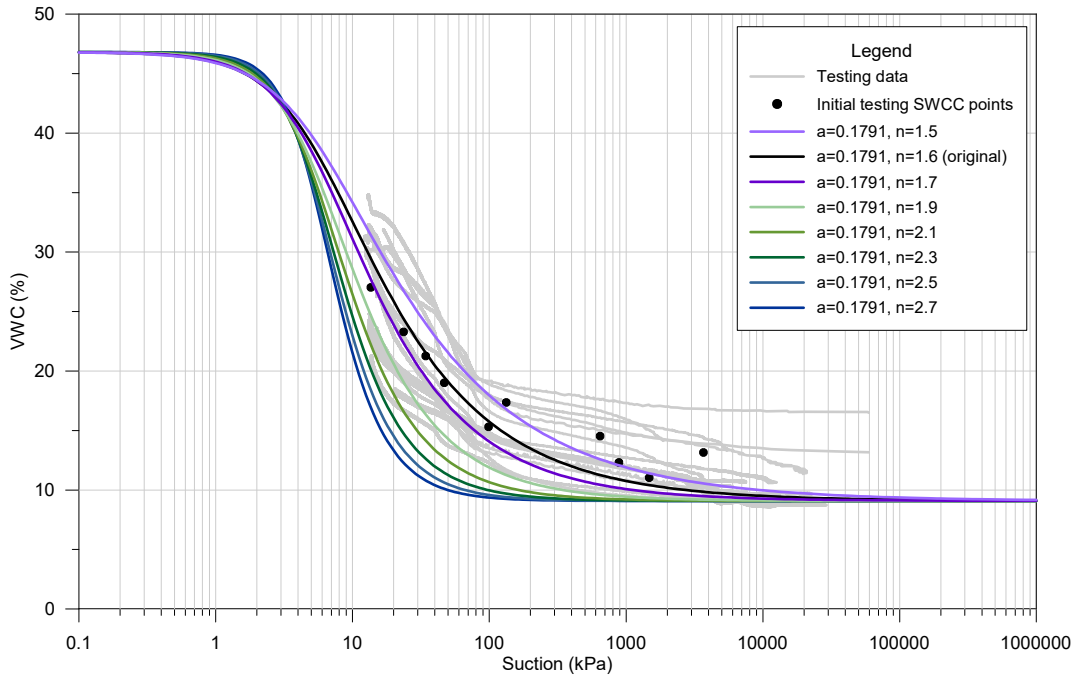


Figure 5.5: Sensitivity of SWCC due to variation in van Genuchten-Mualem " n " parameter

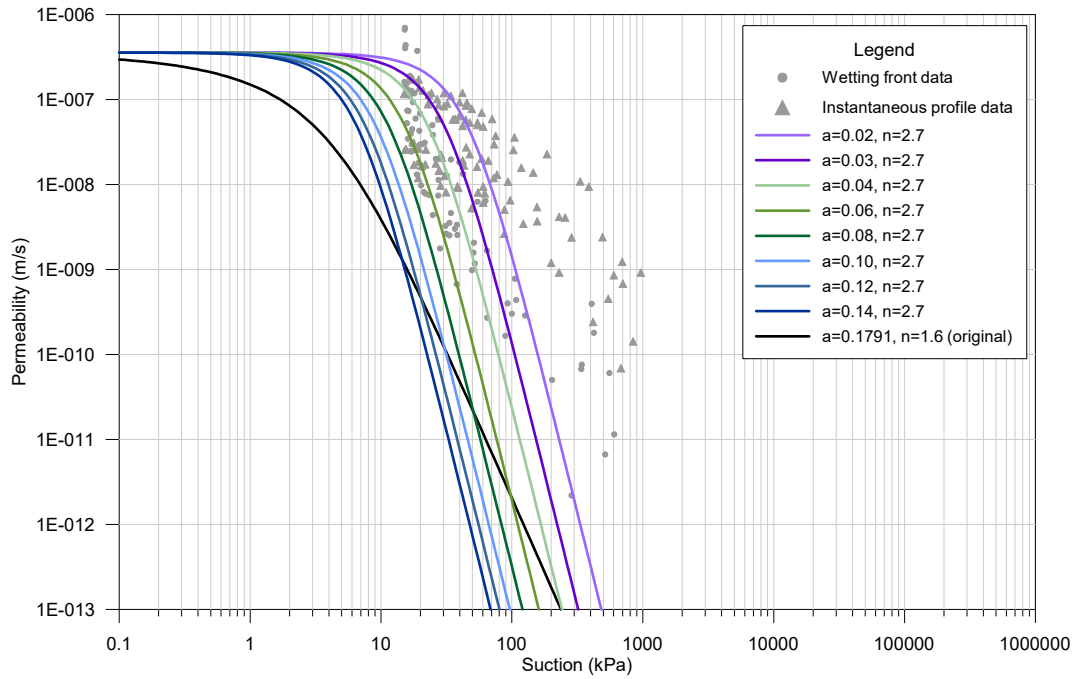


Figure 5.6: Sensitivity of SPF due to variation in van Genuchten-Mualem " a " parameter

by small variations. The " n " parameter had the same effect, with larger influence on the curves with small changes in lower " n " values.

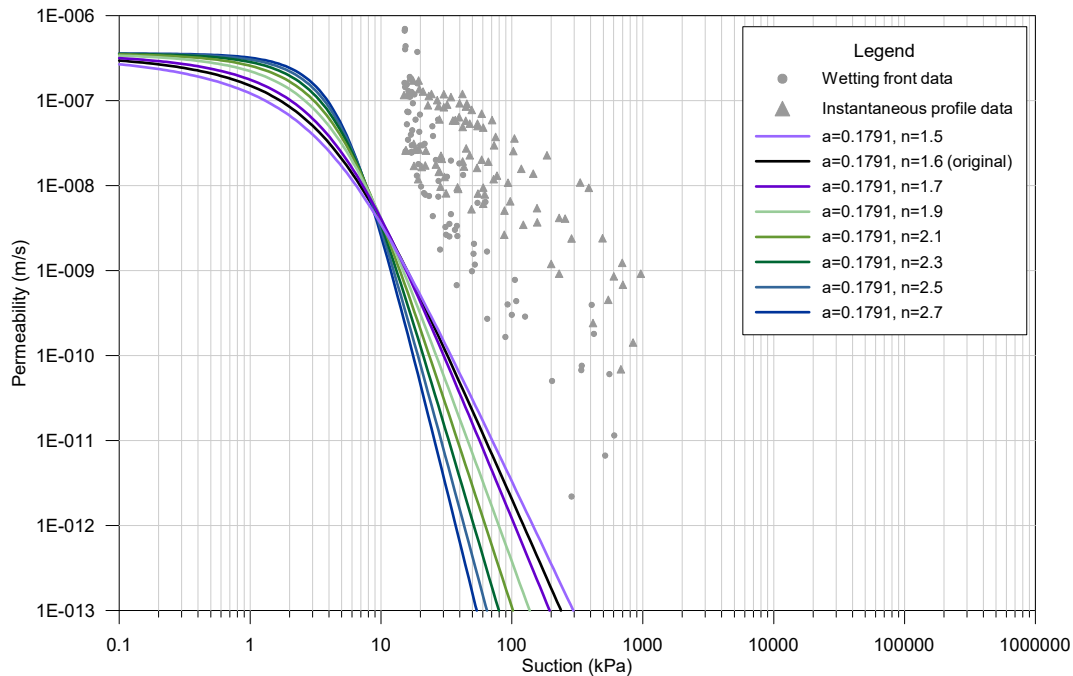


Figure 5.7: Sensitivity of SPF due to variation in van Genuchten-Mualem " n " parameter

5.4.2 Effect of Curve Fitting Parameters on Infiltration Time

As the curve fitting parameters define the shape of the SWCC and SPF, modification of the parameters would also influence infiltration through a soil. Various combinations of " a " and " n " parameters were input to PLAXIS to find the impact on the infiltration time. A contour map with contours representing bands in infiltration time is shown in Figure 5.8, where it can be seen that a higher " n " parameter and lower " a " parameter combination gives the lowest infiltration time. The data points used to generate the contour plot are shown in black within the contours, and labelled with the PLAXIS output time. The contours are wavy in between the defined points due to the inverse distance to a power gridding method used by the software to generate the contour intervals.

The contours show that the combination of a decreasing " a " parameter and an increasing " n " parameter results in the quickest infiltration times. A decreasing " a " parameter translates the SWCC higher on the suction axis, allowing water to begin entering soil pores at a higher suction value. An increasing " n " parameter increases the VWC of the soil quickly with small suction changes, i.e. gives a sharper wetting front. A soil on a wetting curve during infiltration begins with a low VWC and a high suction on the SWCC, meaning the quicker water can enter the soil pores and saturate the material, the quicker the infiltration time. In other words, SPFs with lower " a " parameters and higher " n " parameters have higher permeabilities at higher suctions, or lower VWCs.

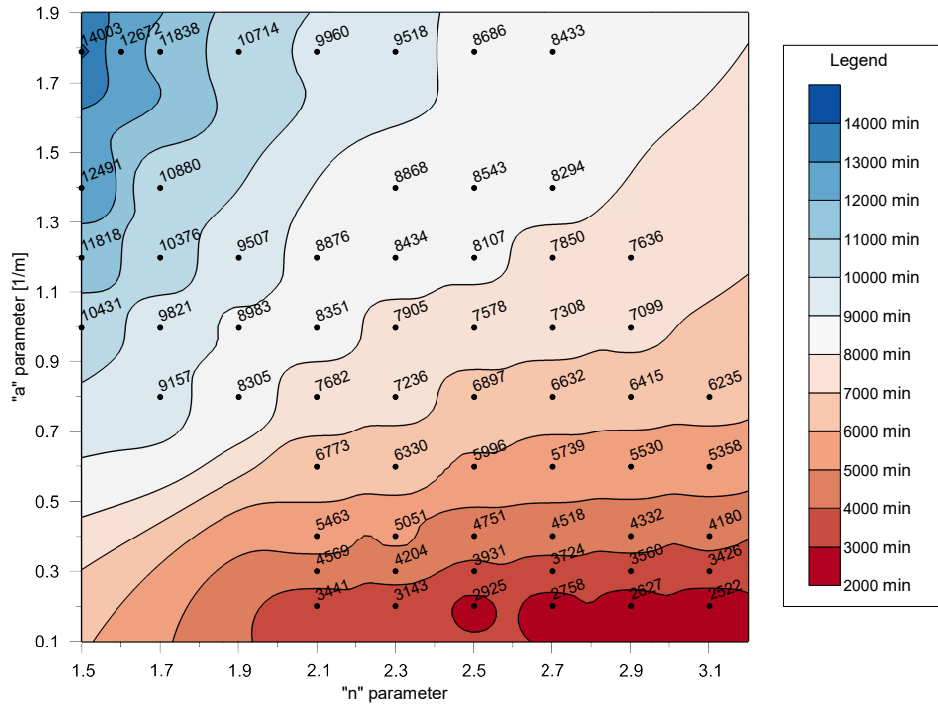


Figure 5.8: Variation of infiltration time by curve fitting parameter modification

The SWCC generated from sensor data gave the parameter set in Table 5.1, with $a=0.1791$ 1/kPa and $n=1.600$. The infiltration time associated with this parameter set overestimated the infiltration time significantly, however in Figure 5.8 it is possible to see several parameter sets which could give the appropriate infiltration time. Therefore, the sensitivity analysis shows an infiltration time from an SWCC is not unique, in that multiple SWCCs could result in the same infiltration time. Figure 5.9 shows in another way the variation of infiltration time with modification to the curve fitting parameters. The actual column infiltration time is also shown on the plot.

Multiple combinations of curve fitting parameters could be used as input parameters and obtain the same infiltration time. The curve fitting parameters which gave an infiltration time to within 20% of the column infiltration time were plotted as SWCCs in Figure 5.10 and as SPFs in Figure 5.11. The original SWCC determined from sensor tests is also shown on the plots for comparison, with all the sensor data in grey behind.

Figure 5.10 shows the SWCCs giving infiltration times close to what was observed during column testing have a higher air entry value and steeper transition zone than what was determined from sensor data. Conversely, the SPFs giving infiltration times close to what was observed in column testing fall within the range of datapoints computed using the instantaneous profile and wetting front advance methods.

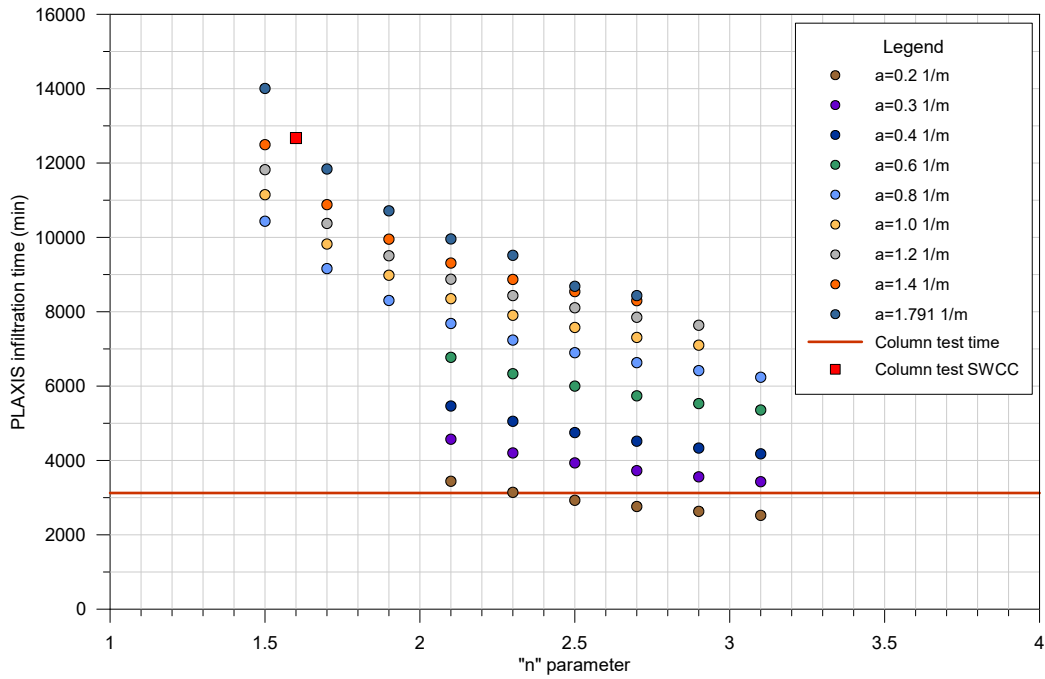


Figure 5.9: Comparison of curve fitting parameter combinations to match column infiltration time

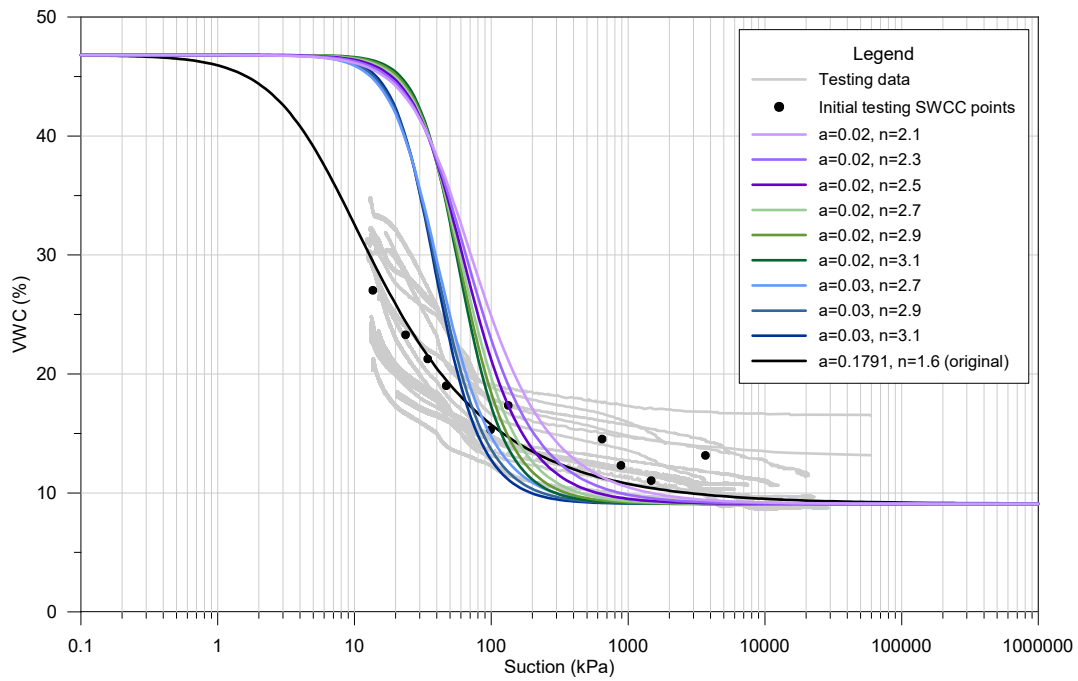


Figure 5.10: SWCCs giving infiltration time close to column experiments

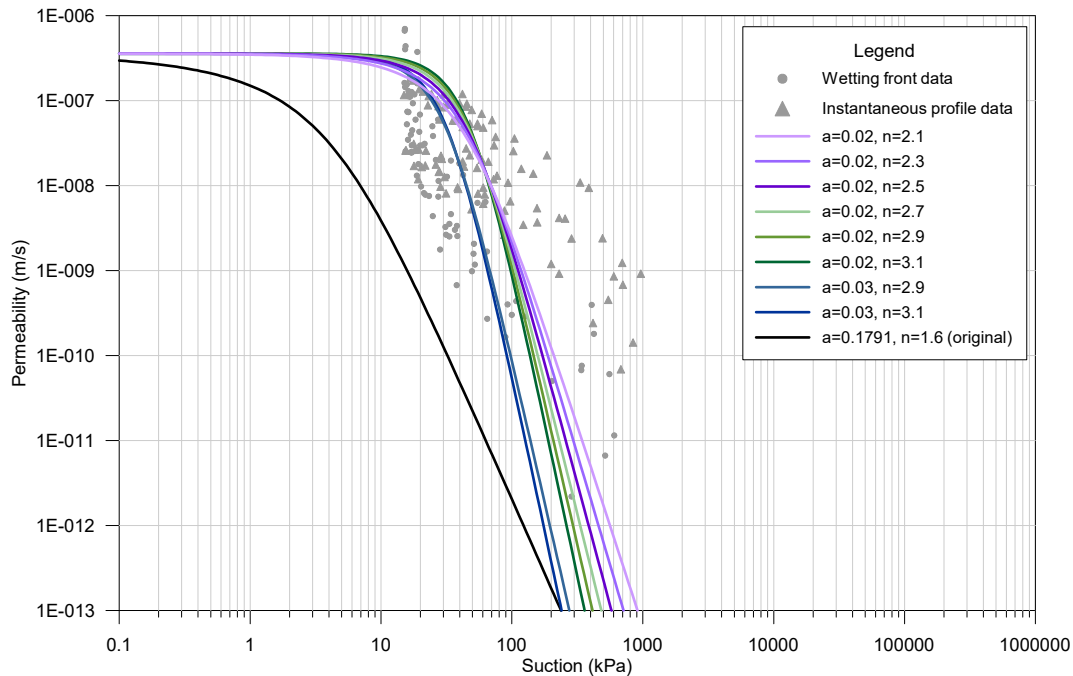


Figure 5.11: SPFs giving infiltration time close to column experiments

5.4.3 Results and Discussion

In the sensitivity analysis the van Genuchten-Mualem curve fitting parameters " a " and " n " were modified in PLAXIS to find parameter combinations which gave similar infiltration times to the time from column testing. The parameters giving similar infiltration times resulted in a SWCC with higher air entry value and steeper transition zone than the average SWCC computed using the VWC sensor and suction sensor data plotted against each other. The SPFs using the selected parameters plotted in the same range as the permeabilities calculated using the instantaneous profile and wetting front advance method.

These results indicate it may be possible to use sensor data to directly compute unsaturated permeability functions for soils from infiltration tests instead of using sensor data to determine a SWCC and from that the SPF. However, the parameters which generate the SPFs matching infiltration times do not give SWCCs which match the sensor data.

The range of " a " parameters in the USDA dataset vary from 0.5 for a silty clay to 14.5 [1/m] for a sand, and the " n " parameter ranges from 1.09 to 2.68 for the same materials. Based on the grain size distribution of the column tested material, the USDA classification is loam, however from the van Genuchten-Mualem parameters the material does not behave as a loam. The tested material has an " a " parameter similar to a silty clay or clay material but an " n " parameter similar to a sand or loamy sand material. The saturated permeability of the tested material is also more in the range of a silty or clayey material. This could be a result of combining three separate

materials together for testing, instead of collecting a naturally occurring loam material. Many properties of the tested material were unknown, and the behaviour could be different than typical naturally occurring materials.

5.5 Limitations of Numerical Model

A numerical infiltration model is a simplification of a complex natural process. Soils are heterogeneous materials with varying properties over time and space, which makes creating a numerical model to mimic reality challenging. In this thesis a simple column experiment was conducted with infiltration occurring in only 1-dimension (vertically) with a constant applied head of water. This is already a simplification to reality, where in slopes infiltration occurs in multiple dimensions with varying hydraulic input. The numerical analysis in this thesis made an initial attempt to create a numerical model which simulated the column experiment infiltration process, with mixed results. The following factors were considered when creating the model and are possible explanations for model divergence from column testing.

The saturated permeability determined from column testing was completed on a non-saturated material. It is likely the saturated permeability is higher, which would increase the PLAXIS infiltration times as permeability is highly dependant on moisture content (Fredlund et al., 2012). The SPF from the column testing SWCC is plotted against saturation level instead of matric suction in Figure 5.12, which shows the permeability change from 100% saturation to 80% saturation is around one order of magnitude.

The PLAXIS model for test 3 with the permeability from column testing gave an infiltration time of 12672 minutes, where with the permeability increased by one order of magnitude the infiltration time decreased to 1330 minutes, which is less than half the actual column test time of 3124 minutes. This shows the measurement of accurate saturated permeability is highly important for numerical model accuracy when using the SWCC parameters to generate the SPF. Further sensitivity analysis could be conducted on the infiltration time by modification of the soil permeability, however this was not completed in this thesis.

A lack of saturation in the sample indicates trapped air within the soil matrix. In terms of water flow, trapped air acts as a solid phase, in that water cannot flow through the pore channels filled with air (Childs et al., 1950). Blocked pore channels mean water must travel horizontally through the sample to find a pore channel which is available for vertical flow, which contributes to infiltration time. PLAXIS assumes all pore channels are available for vertical flow based on the input porosity. The concept of increased distance for water flow due to blocked pore channels is called tortuosity (Fredlund et al., 2012). Tortuosity could be taken into account by using an effective (i.e. reduced) porosity, which would only into account available flow channels for water transport. This modification in PLAXIS would contribute to the overestimation of infiltration

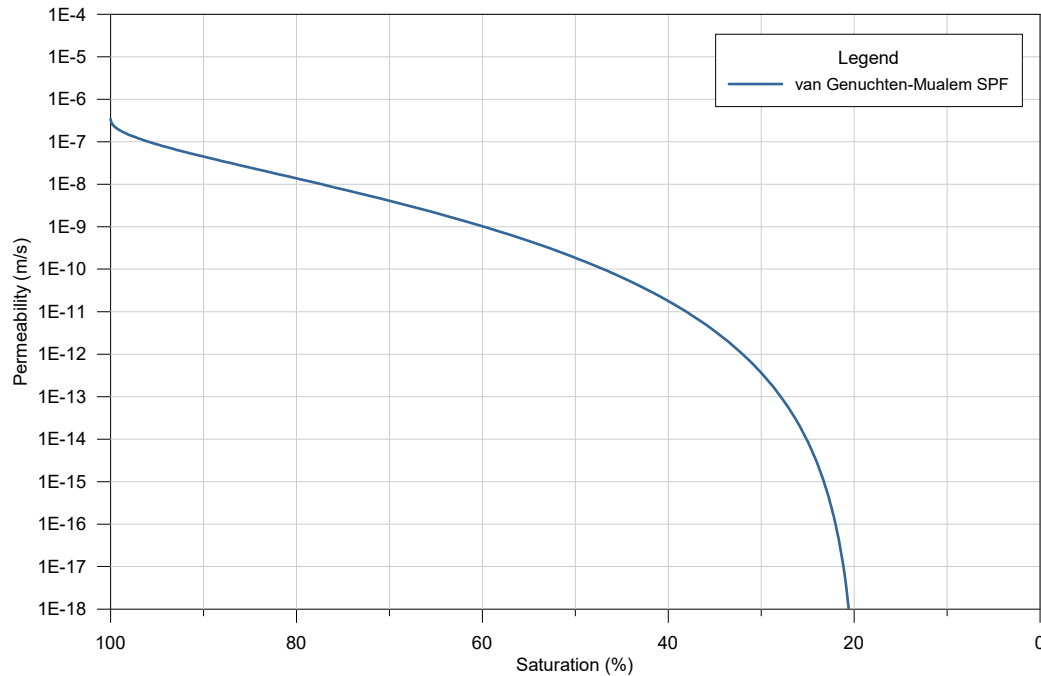


Figure 5.12: SPF plotted against saturation level

time, but would more closely mimic the soil conditions.

The column experiment was prepared manually by placing and compacting conditioned soil in equal lifts. The soil was not left for any amount of time for the moisture condition to equalize in the soil prior to test initiation, which may have led to inconsistencies in moisture content. The PLAXIS model assumes an equal moisture condition throughout the sample. As moisture content affects soil permeability, any irregularities in the column test would not have been modelled numerically (Fredlund et al., 2012).

Compaction into the column was completed in thin layers to try and maintain an equal density with depth. However, it is likely that small pockets of denser and looser material existed within the column, which could have impacted the infiltration rate. In PLAXIS densities are input for dry and saturated material, but no consideration is given to spatial differences in density.

During column testing, consolidation of the samples took place as the sample became saturated. The soil was placed at a relatively low density due to the lack of moisture within the soil, and as the weight of the soil increased due to saturation, and was acted upon by seepage forces, consolidation took place. On average around 5 cm of consolidation occurred by the time infiltration completed. In the PLAXIS flow only analysis no deformation was considered, however the permeability of a soil is influenced by the porosity. A coupled analysis was attempted in PLAXIS, which takes into account flow and deformation in a combined analysis. Numerical difficulties were encountered due to non-linear hydraulic inputs and due to time considerations

this model was not completed. Future work could consider a coupled analysis to better represent the experimental findings.

All of the above considerations for why the numerical model could give differing results from reality show the importance of conducting laboratory and field simulations to properly characterize materials.

Chapter 6

Summary and Main Conclusions

Work began on this thesis with the design and construction of a large-scale infiltration column test setup, and selection and ordering of soil moisture and suction sensors. Initial testing was conducted while the test setup was constructed to finalize the optimal material to be used for large-scale infiltration testing, and resulted in a combination of three materials available at NTNU. The tested material was created to give suctions measurable by the chosen suction sensor while maintaining reasonable infiltration times. Once the sensors were delivered, initial evaluations were completed on the accuracy and stability of the readings through placement in various moisture conditioned samples. A calibration curve was developed for the moisture sensors for the soil to be tested.

Three large-scale infiltration tests were completed in the column test setup, and sensor data was collected throughout the testing period. Evaluation of sensor performance during infiltration tests was completed and compared to results from initial testing with stationary hydraulic conditions. The sensor data from infiltration testing was used to create a SWCC for the tested material and corresponding SPE, and was compared to the Green-Ampt infiltration model. The infiltration process from large-scale testing was modeled using the finite element software program PLAXIS to compare infiltration times and to investigate the sensitivity of model fitting parameters on the infiltration time. A back-analysis was completed following the parameter sensitivity analysis to find curve fitting parameters giving the same infiltration time in PLAXIS as were found in column testing. Finally, a brief discussion on limitations of numerical modeling to represent reality was presented. The main conclusions from this thesis are presented in the following paragraphs.

The infiltration column setup performed well throughout all three column tests, with only one malfunction of the water filling system. The sensors and logging program recorded sensor data consistently, and there were no data gaps during testing. Recommendations on improvements to the infiltration column test setup are given in Section 7.

Evaluation of the VWC sensor performance showed a quick and stable response time to changing moisture contents, and a sensing distance of 2 to 3 cm above the sensor level. This sensor showed some fluctuation in reading stability during column infiltration testing which may have been due to voids forming beneath the sensor heads, however this sensor is still considered acceptable for future laboratory testing or for field installation.

The suction sensor evaluation showed a slow response rate and long equalization time to changing moisture contents, particularly in dry conditions. In the large-scale column tests where the initial VWC was just under 10%, the suction sensors took around 1000 minutes, or nearly 17 hours, to stabilize readings. This likely impacted the determination of the material SWCC, as the suction sensor response time lagged behind the moisture sensor, resulting in falsely high suction measurements at a given VWC.

The wetting front could be sensed slightly above the suction sensor, also at a distance of around 2 to 3 cm, however there was only a short period of time where the sensor recorded suction readings before the sensor measurement range was exceeded on the low suction end. This sensor was insufficient to monitor the full transition zone of the SWCC for the tested material, and was not able to provide suction levels low enough to define an air entry value. This sensor would only be recommended for use in materials with very low permeabilities leading to slow changes in moisture content, with high valued transition zone suctions, such as more clayey material. This sensor could be used in a field setting in clayey material, however a clay material infiltration test in the laboratory may exceed time limitations for future thesis work.

The relationships derived from sensor measurements were dependent on the accuracy of the sensor measurements. Due to the limited range of the suction sensor and the slow response time, the SWCC data contained significant deviation between instrument pairs but followed similar trends, and thus an average SWCC was fit to the data. SWCCs were fitted to the data using the Brooks and Corey, van Genuchten-Mualem and Fredlund-Xing models, which showed good agreement in the transition zone of the SWCC and less agreement near the air entry value and below residual saturation.

SPFs were developed using combinations of instrument readings, visual interpretation and statistical interpretation along the SWCC. The instantaneous profile and wetting front advance methods used direct measurements of wetting front advance through sensor measurements and visual interpretations to find the average unsaturated permeability at various suction levels. The van Genuchten-Mualem SPF model was developed used the same curve fitting parameters from the SWCC and the saturated permeability from column testing. The methods showed somewhat similar permeability results, however due to uncertainty in the sensor measurements and in saturated permeability measurements, permeabilities at one suction value could vary by one order of magnitude.

The Green-Ampt model was fit to the column infiltration data to back-calculate the suction at

the wetting front. The derived wetting front suction was compared to theoretical values proposed by others but was found to differ by two orders of magnitude. This was possibly attributed to the Green-Ampt model assumption of a sharp wetting front, which may not have been the case for the tested material.

A PLAXIS model was created using the average SWCC from sensor data and the saturated permeabilities from each column test as input parameters. The infiltration times were simulated for each column test and were found to overestimate the time by 2.6 to 4 times the actual column infiltration time. A sensitivity analysis was run on the curve fitting parameters to determine the effect of changing parameters on infiltration time. From the sensitivity analysis a back-analysis was conducted to find the parameter set giving the same infiltration time as was determined in the column test.

The back-analysis showed a SWCC parameter set does not give a unique infiltration time, and multiple parameter sets could give equal infiltration times. A series of SWCCs and SPFs with varying parameter sets were plotted which gave PLAXIS infiltration times within 20% of the column infiltration time. The SWCCs were found to be steeper with a higher air entry value than the average SWCC found from sensor data, however the SPFs plotted directly on top of the SPFs found from the instantaneous profile and wetting front advance methods.

The results from the combined experimental and numerical analysis show it may be possible to use installed soil sensors to develop unsaturated soil relationships, however accuracy and measurement range of the sensors are crucial to obtaining consistent results. Numerical analysis is an approximation of a complex physical process, and the combination of uncertainty in input parameters and simplifications during modeling can lead to vastly different results from experimental findings.

Chapter 7

Recommendations for Future Work

The infiltration test setup could be improved before further testing takes place. Recommendations for modifications include:

- Improve the soil mixing machine to be able to break apart clumps when conditioning the soil to the initial moisture content
- Investigate why the water filling system occasionally stops automatically refilling the constant head level
- Improve the water filling system to maintain a more constant head of water
- Section the column into two pieces for ease of filling and removing soil and sensors, as was done by [Bathurst et al. \(2007\)](#) during testing of geotextiles
- Use of a long-battery life video camera to record the wetting front advance, or purchase of an AC adapter for the digital camera to avoid charging breaks
- Multiple video cameras at closer range to the column with accurate depth measurements on the column for better estimation of wetting front location retroactively from photographs

The VWC sensor used for this work is considered acceptable for further testing, however the suction sensor should only be used in certain applications. It is recommended to either change the material type to a clayey material for use with the current suction sensor, or obtain a tensiometer in connection with the current sensor which is able measure the low suction range and is suitable for a laboratory setting. Recommended tensiometers to consider include the T5 tensiometer from METER or the 2100F tensiometer from SoilMoisture Corp.

This thesis focused only on constant head infiltration tests in the column setup, however the column could be used for many other types of research. Some examples of future experiments which could be conducted include:

- Infiltration into layered soils, such as experiments completed by [Yang et al. \(2006\)](#)

- Testing of embedded geotextiles, as completed by [Bathurst et al. \(2007\)](#)
- Influence of variable hydraulic input on infiltration, for example by simulating rainfall on top of the soil column
- Influence on infiltration from of an existing water table creating a vadose zone
- Infiltration tests on natural soils collected from a field location in Norway

Additional work could also be performed with numerical modeling to more accurately represent the conditions in the soil column during testing. In this thesis a flow only analysis was conducted in PLAXIS which neglects any stress and deformation calculations, however since consolidation took place during testing, a coupled analysis would consider the effects of changing void ratio on the soil permeability.

Bibliography

- Albadri, W., Noor, M., and Alhani, I. (2018). The importance of incorporating hysteresis effect in determining shear strength of unsaturated soil.
- ASTM International (2010). *D7664-10(2018)e1 Standard Test Methods for Measurement of Hydraulic Conductivity of Unsaturated Soils*.
- Bathurst, R., F Ho, A., and Siemens, G. (2007). A column apparatus for investigation of 1-d unsaturated-saturated response of sand-geotextile systems. *Geotechnical Testing Journal - GEOTECH TESTING J*, 30.
- Bittelli, M. (2011). Measuring soil water content: A review. *HortTechnology*, 21:293–300.
- Brooks, R. H. and Corey, A. T. (1964). *Hydraulic properties of porous media*. Fort Collins, Colorado: Colorado State University.
- Burdine, N. (1953). Relative permeability calculations from pore size distribution data. *Journal of Petroleum Technology*, 5:71–78.
- Carter, M. and Gregorich, E. (2008). *Soil Sampling and Methods of Analysis, 2nd edition*. Taylor & Francis Group, LLC, Florida.
- Chae, B.-G., Park, H.-J., Catani, F., Simoni, A., and Berti, M. (2017). Landslide prediction, monitoring and early warning: a concise review of state-of-the-art. *Geosciences Journal*, 21(6):1033–1070.
- Childs, E. C., Collis-George, N., and Taylor, G. I. (1950). The permeability of porous materials. *Proceedings of the Royal Society of London. Series A. Mathematical and Physical Sciences*, 201(1066):392–405.
- Cho, S. E. and Lee, S. R. (2002). Evaluation of surficial stability for homogeneous slopes considering rainfall characteristics. *Journal of Geotechnical and Geoenvironmental Engineering*, 128(9):756–763.
- Devoli, G., Tiranti, D., Cremonini, R., Sund, M., and Boje, S. (2018). Comparison of landslide forecasting services in Piedmont (Italy) and Norway, illustrated by events in late spring 2013. *Natural Hazards and Earth System Sciences*, 18(5):1351–1372.

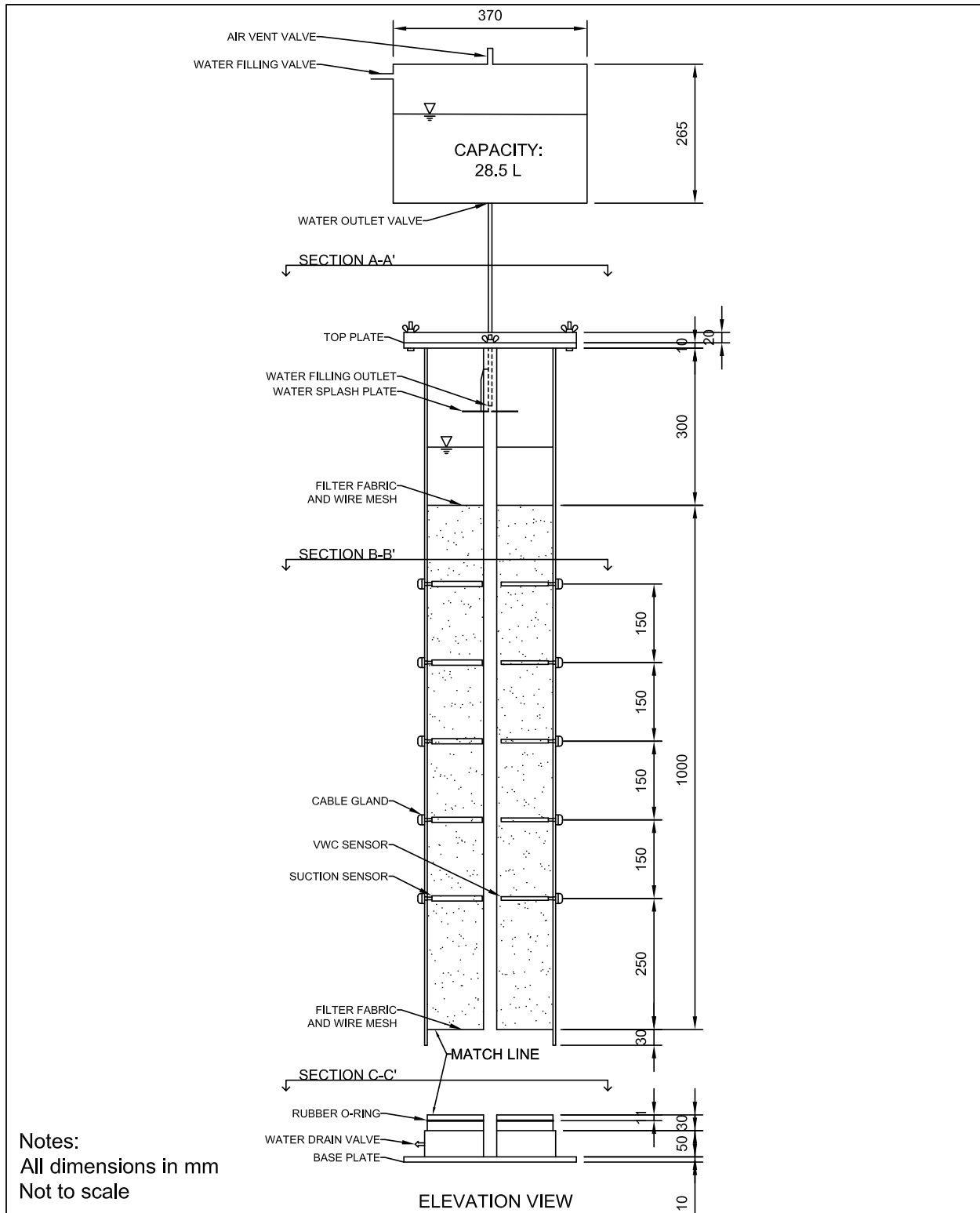
- Dingman, S. (2015). *Physical Hydrology, 3rd edition*. Waveland Press, Inc., Illinois.
- Duong, T., Trinh, V. V., Cui, Y.-J., Tang, A. M., and Calon, N. (2013). Development of a large-scale infiltration column for studying the hydraulic conductivity of unsaturated fouled ballast. volume 36, pages 54–63.
- Fredlund, D., Rahardjo, H., and Fredlund, M. (2012). *Unsaturated Soil Mechanics in Engineering Practice*. John Wiley and Sons, Inc.
- Fredlund, D. and Xing, A. (1994). Equations for the soil-water characteristic curve. *Canadian Geotechnical Journal*, 31(4):521–532.
- Fredlund, D. G., Sheng, D., and Zhao, J. (2011). Estimation of soil suction from the soil-water characteristic curve. *Canadian Geotechnical Journal*, 48:186–198.
- Fredlund, M., Sillers, W., Fredlund, D., and Wilson, G. (1996). Design of a knowledge-based system for unsaturated soil properties. In *3rd Canadian Conference on Computing in Civil and Building Engineering*.
- Froude, M. and Petley, D. (2018). Global fatal landslide occurrence from 2004 to 2016. In Parise, M., editor, *Natural Hazards and Earth System Sciences*, volume 18, pages 2161–2181. European Geosciences Union.
- Gardner, W. R. (1958). Some steady state solutions of the unsaturated moisture flow equation with application to evaporation from a water table. *Soil Science*, 85:228–232.
- GeoCybersafe (2018). NTNU GeoCyberSafe Proposal. Provided text by Dr. Vikas Thakur.
- Hamilton, J., Daniel, D., and Olson, R. (1981). Measurement of hydraulic conductivity of partially saturated soils. *STP746-EB Permeability and Groundwater Contaminant Transport*, pages 182–196.
- Haque, U., Blum, P., and da Silva, P. e. a. (2016). Fatal landslides in Europe. *Landslides*, 13:1545 – 1554.
- Kizito, F., Campbell, C., Campbell, G., Cobos, D., Teare, B., Carter, B., and Hopmans, J. (2008). Frequency, electrical conductivity and temperature analysis of a low-cost capacitance soil moisture sensor. *Journal of Hydrology*, 352(3):367 – 378.
- Li, X., Zhang, L. M., and Fredlund, D. G. (2009). Wetting front advancing column test for measuring unsaturated hydraulic conductivity. *Canadian Geotechnical Journal*, 46(12):1431–1445.
- Lu, N. and Godt, J. (2008). Infinite slope stability under steady unsaturated seepage conditions. *Water Resources Research*, 44(11).
- Lu, N. and Likos, W. J. (2006). Suction stress characteristic curve for unsaturated soil. *Journal of Geotechnical and Geoenvironmental Engineering*, 132(2):131–142.

- Lu, N. and Likos, W. J. (2013). *Origin of Cohesion and Its Dependence on Saturation for Granular Media*, pages 1669–1675.
- Makonto, O. T. (2013). Vadose zone classification and aquifer vulnerability of the Molototsi and Middle Letaba Quaternary Catchments, Limpopo Province, South Africa. Master's thesis, University Pretoria, South Africa.
- Matula, S., Bát'ková, K., and Legese, W. L. (2016). Laboratory performance of five selected soil moisture sensors applying factory and own calibration equations for two soil media of different bulk density and salinity levels. *Sensors*, 16.
- McCartney, J., Villar, L., and Zornberg, J. (1981). Estimation of the hydraulic conductivity function of an unsaturated clay using an infiltration column test.
- Mein, R. G. and Larson, C. L. (1973). Modeling infiltration during a steady rain. *Water Resources Research*, 9(2):384–394.
- METER Group (2019a). *EC-5 manual*.
- METER Group (2019b). ECH2O EC-5.
- METER Group (2019c). TEROS 21.
- METER Group (2019d). *TEROS 21 manual*.
- Mishra, S., Tyagi, J., and Singh, V. (2003). Comparison of infiltration models. *Hydrological Processes - HYDROL PROCESS*, 17:2629–2652.
- Mualem, Y. (1976). A new model for predicting hydraulic conductivity of unsaturated porous-media. *Water Resources Research*, 12:513–522.
- PLAXIS bv (2019a). *2D Reference Manual*.
- PLAXIS bv (2019b). *Material Models Manual*.
- Rawls, W. J., Brakensiek, D. L., and Miller, N. (1983). Green-Ampt infiltration parameters from soils data. *Journal of Hydraulic Engineering-ASCE*, 109(1):62–70.
- Richards, L. (1931). Capillary conduction of liquids in porous mediums. *Physics*, 1:318 – 333.
- Rossi, C. and Nimmo, J. R. (1994). Modeling of soil water retention from saturation to oven dryness. *Water Resources Research*, 30(3):701–708.
- Sillers, W., Fredlund, D., and Zakerzaher, N. (2001). Mathematical attributes of some soil-water characteristic curve models. *Geotechnical and Geological Engineering*, 19:243–283.
- Sillers, W. S. and Fredlund, D. G. (2001). Statistical assessment of soil-water characteristic curve models for geotechnical engineering. *Canadian Geotechnical Journal*, 38(6):1297–1313.

- SINTEF. Klima digital. <https://www.sintef.no/projectweb/klimadigital>. Accessed: 2018-11-19.
- Soltani, A., Azimi, M., Deng, A., and Taheri, A. (2019). A simplified method for determination of the soil-water characteristic curve variables. *International Journal of Geotechnical Engineering*, 13(4):316–325.
- Srivastava, R. and Jim Yeh, T.-C. (1991). Analytical solutions for one-dimensional, transient infiltration toward the water table in homogeneous and layered soils. *Water Resources Research*, 27(5):753–762.
- stackoverflow. Usda ternary diagram. <https://stackoverflow.com/questions/12520003/representing-ternary-plot-data-for-lookups>. Accessed: 2019-03-22.
- Tuller, M. and Or, D. (2003). Retention of water in soil and the soil water characteristic curve.
- van Genuchten, M. (1980). A closed-form equation for predicting the hydraulic conductivity of unsaturated soils. *Soil Science Society of America Journal*, 44:892–898.
- Watson, K. K. (1966). An instantaneous profile method for determining the hydraulic conductivity of unsaturated porous materials. *Water Resources Research*, 2(4):709–715.
- Yang, H., Rahardjo, H., and Leong, E.-C. (2006). Behavior of unsaturated layered soil columns during infiltration. *Journal of Hydrologic Engineering*, 11(4):329–337.
- Zapata, C. E., Houston, W. N., Houston, S. L., and Walsh, K. D. (1999). *Soil Water Characteristic Curve Variability*.
- Zhang, L., Li, J., Li, X., Zhang, J., and Zhu, H. (2016). *Rainfall-Induced Soil Slope Failure: Stability Analysis and Probabilistic Assessment*. CRC Press, Taylor and Francis Group.

Appendix A

Drawings



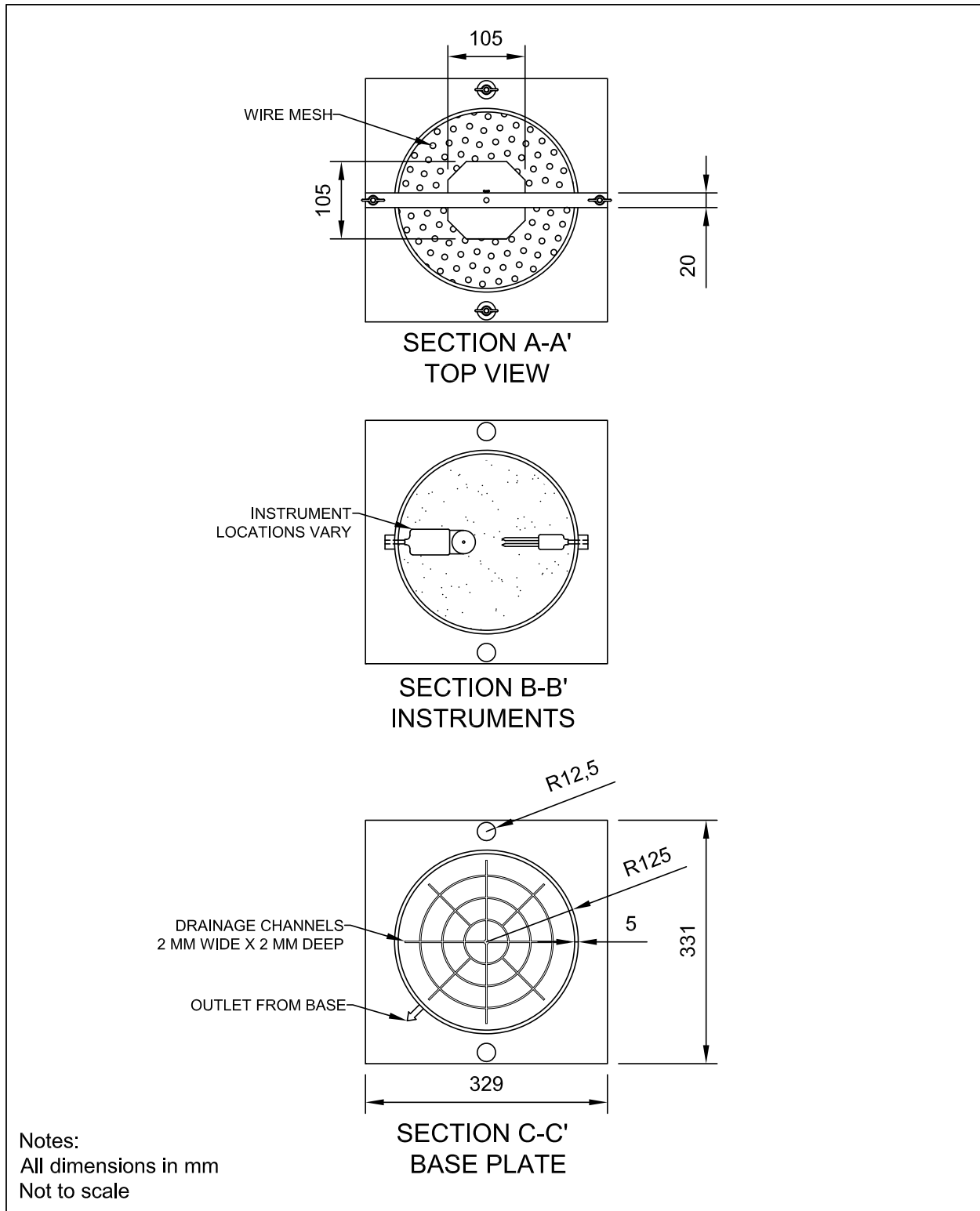
Infiltration Column

DATE: 30 MAY 2019

DRAWN BY: KATE ROBINSON

REVISION: 003

PAGE: 1 OF 2



Infiltration Column	DATE: 30 MAY 2019	DRAWN BY: KATE ROBINSON
	REVISION: 003	PAGE: 2 OF 2

Appendix B

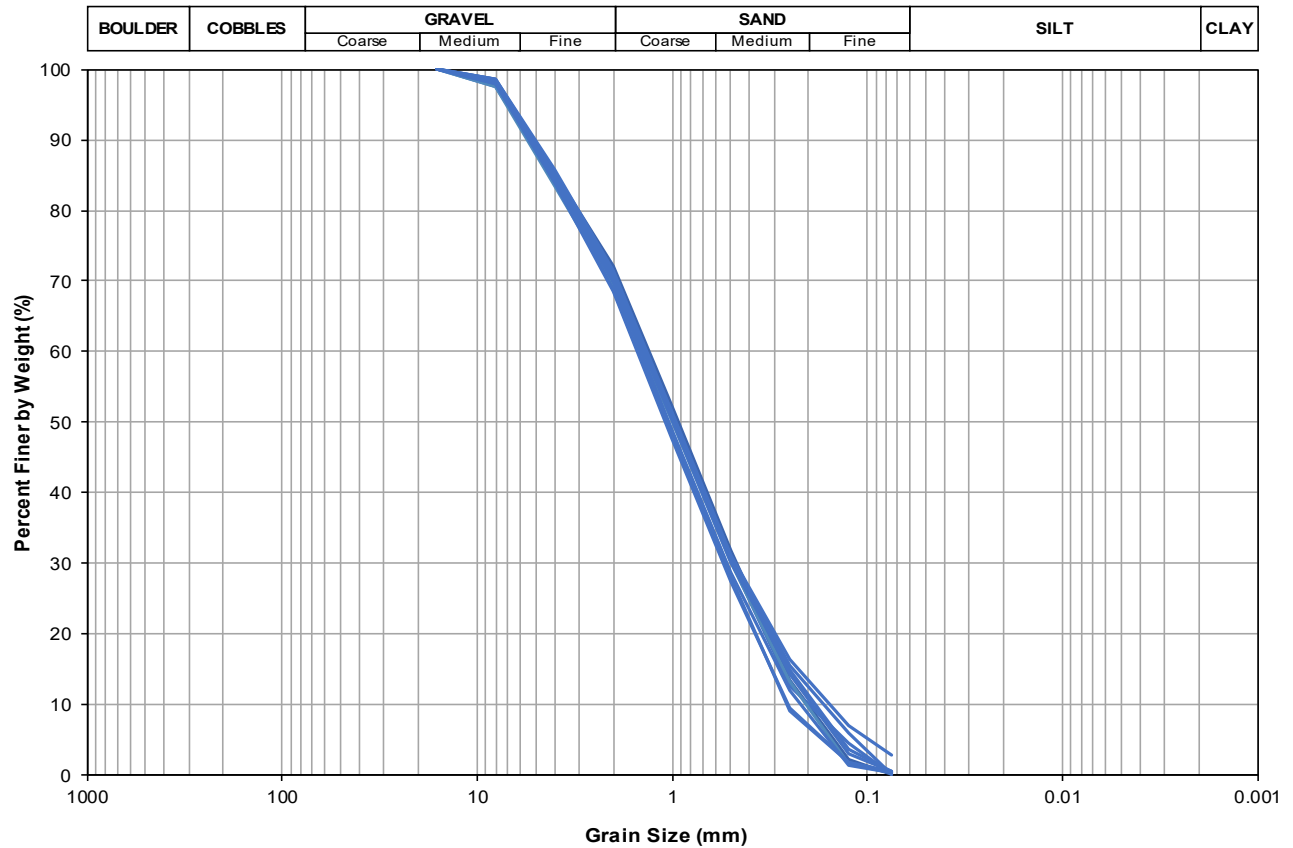
Laboratory Testing Results

Testing date: 18 to 22 Feb 2019

Tested material: Sand and gravel from NTNU

Project: TBA4900 - Master Thesis

Operator: K.Robinson



GRAIN SIZE DISTRIBUTION SUMMARY

Test No.	d ₆₀ (mm)	d ₃₀ (mm)	d ₁₀ (mm)	C _u	C _c	Classification
1	1.39	0.47	0.21	6.6	0.8	Medium Graded
2	1.44	0.50	0.21	6.9	0.8	Medium Graded
3	1.44	0.48	0.17	8.7	1.0	Medium Graded
4	1.47	0.48	0.18	8.2	0.9	Medium Graded
5	1.51	0.50	0.22	7.0	0.8	Medium Graded
6	1.43	0.49	0.20	7.1	0.8	Medium Graded
7	1.59	0.54	0.26	6.2	0.7	Medium Graded
8	1.48	0.50	0.20	7.6	0.9	Medium Graded
9	1.58	0.53	0.26	6.0	0.7	Medium Graded
10	1.53	0.52	0.23	6.7	0.8	Medium Graded

Testing date: 03.Mar.19

Tested material: Silt from NTNU basement

Project: TBA4900 - Master Thesis

Operator: K.Robinson

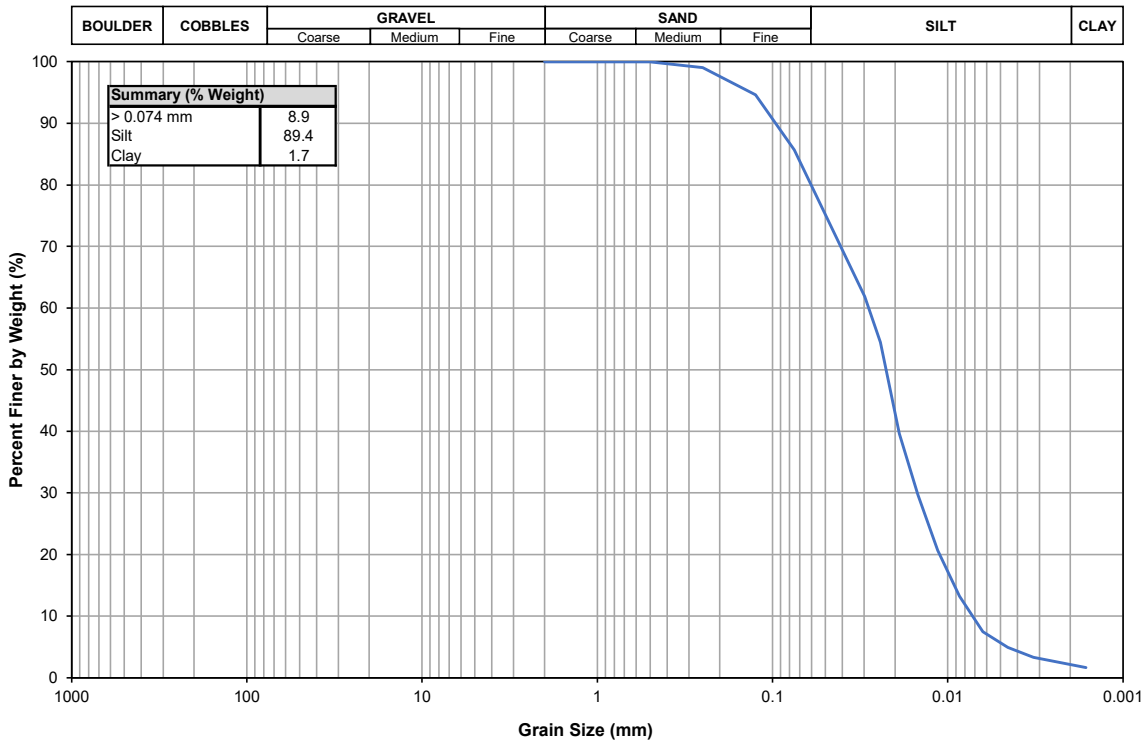
Initial Sieving			
Sieve opening (mm)	Mass retained (g)	% Retained	% Passing
2	0	0.00	100.00
1	0	0.00	100.00
0.5	0	0.00	100.00
0.25	0.57	0.96	99.04
0.125	2.62	4.43	94.61
0.075	5.29	8.94	85.66
Pan	50.66	-	-

Input Parameters	
Mass, total wet sample (grams):	59.14
Moisture content (%):	0.74
Mass, dry soil > #200 sieve (grams):	8.42
Mass, dry soil < #200 sieve (grams):	50.29
Mass, soil into hydrometer (grams):	50.29
Mass, dispersant (grams):	1.00
Analysis parameters	
G _s	2.77
a	97.6

Date and Time (yyyy-mm-dd hh:mm)	Elapsed Time, t (min)	Temp. (C)	R (g/L)	Zero Correction (g/L)	Corrected R (g/L)	Z _r (cm)	K $\sqrt{\text{min/cm}}$	$\sqrt{Z_r/t}$ $\sqrt{\text{min/cm}}$	Grain Diameter (mm)	Relative Mass < d (0.074 mm) N %	Relative Mass Total Sample N' %
26.03.2019 10:00	0										
26.03.2019 10:01	1	23.9	40.5	-3	37.5	5.2	0.01310	2.27	0.030	72.78	61.89
26.03.2019 10:02	2	23.9	36	-3	33.0	6.9	0.01310	1.86	0.024	64.05	54.46
26.03.2019 10:05	5	23.3	27	-3	24	10.3	0.01315	1.44	0.019	46.58	39.61
26.03.2019 10:10	10	22.7	21	-3	18	12.6	0.01320	1.12	0.015	34.94	29.71
26.03.2019 10:20	20	21.9	15.5	-3	13	14.7	0.01330	0.86	0.011	24.26	20.63
26.03.2019 10:40	40	21.5	11	-3	8	16.4	0.01335	0.64	0.009	15.53	13.20
26.03.2019 11:20	80	21.1	7.5	-3	5	17.8	0.01340	0.47	0.006	8.73	7.43
26.03.2019 12:40	160	21.2	6	-3	3	18.4	0.01340	0.34	0.005	5.82	4.95
26.03.2019 15:20	320	21.2	5	-3	2	18.7	0.01340	0.24	0.003	3.88	3.30
27.03.2019 08:00	1320	19.9	4	-3	1	19.1	0.01353	0.12	0.002	1.94	1.65

Notes:

Note 1: The a coefficient corresponds to the specific gravity of 2.77 for this material.



Testing date: 01.Apr.19

Tested material: Clay cuttings from Flotten, Tiller

Project: TBA4900 - Master Thesis

Operator: K.Robinson

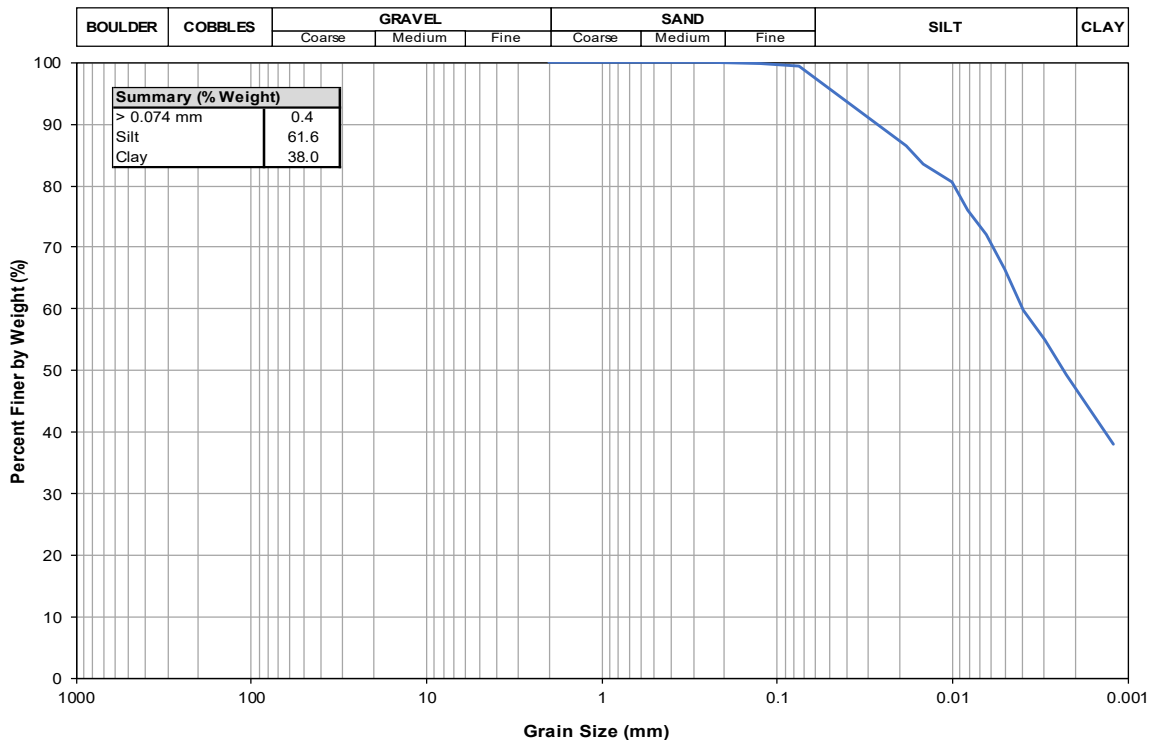
Initial Sieving			
Sieve opening (mm)	Mass retained (g)	% Retained	% Passing
2	0	0.00	100.00
1	0	0.00	100.00
0.5	0.01	0.02	99.98
0.25	0.02	0.04	99.94
0.125	0.04	0.08	99.86
0.075	0.22	0.44	99.43
Pan	50.15	-	-

Input Parameters	
Mass, total wet sample (grams):	50.44
Moisture content (%):	0.00
Mass, dry soil > #200 sieve (grams):	0.29
Mass, dry soil < #200 sieve (grams):	50.15
Mass, soil into hydrometer (grams):	50.15
Mass, dispersant (grams):	1.00
Analysis parameters	
G _s	2.86
a	95.8

Date and Time (yyyy-mm-dd hh:mm)	Elapsed Time, t (min)	Temp. (C)	R (g/L)	Zero Correction (g/L)	Corrected R (g/L)	Z _r (cm)	K $\sqrt{\text{min/cm}}$	$\sqrt{Z_r/t}$ $\sqrt{\text{min/cm}}$	Grain Diameter (mm)	Relative Mass < d (0.074 mm) N %	Relative Mass Total Sample N %
01.04.2019 10:30	0										
01.04.2019 10:31	1	22.0	48.0	-2.5	45.5	2.1	0.01259	1.45	0.018	86.92	86.42
01.04.2019 10:32	2	22.0	46.5	-2.5	44.0	2.7	0.01259	1.16	0.015	84.05	83.57
01.04.2019 10:35	5	21.8	45.0	-2.5	43	3.3	0.01252	0.81	0.010	81.19	80.72
01.04.2019 10:40	10	21.3	42.5	-2.5	40	4.2	0.01268	0.65	0.008	76.41	75.97
01.04.2019 10:50	20	20.6	40.5	-2.5	38	5.0	0.01281	0.50	0.006	72.59	72.17
01.04.2019 11:10	40	20.2	37.5	-2.5	35	6.1	0.01288	0.39	0.005	66.86	66.48
01.04.2019 11:50	80	20.0	34.0	-2.5	32	7.5	0.01290	0.31	0.004	60.17	59.83
01.04.2019 13:10	160	20.1	31.5	-2.5	29	8.4	0.01289	0.23	0.003	55.40	55.08
01.04.2019 15:50	320	20.3	28.5	-2.5	26	9.6	0.01286	0.17	0.002	49.67	49.38
02.04.2019 08:30	1320	20.6	22.5	-2.5	20	11.9	0.01281	0.09	0.001	38.21	37.99

Notes:

Note 1: The a coefficient corresponds to the specific gravity of 2.86 for this material.



Testing date: 05.Apr.19

Tested material: Infiltration Test 1 Material

Project: TBA4900 - Master Thesis

Operator: K.Robinson

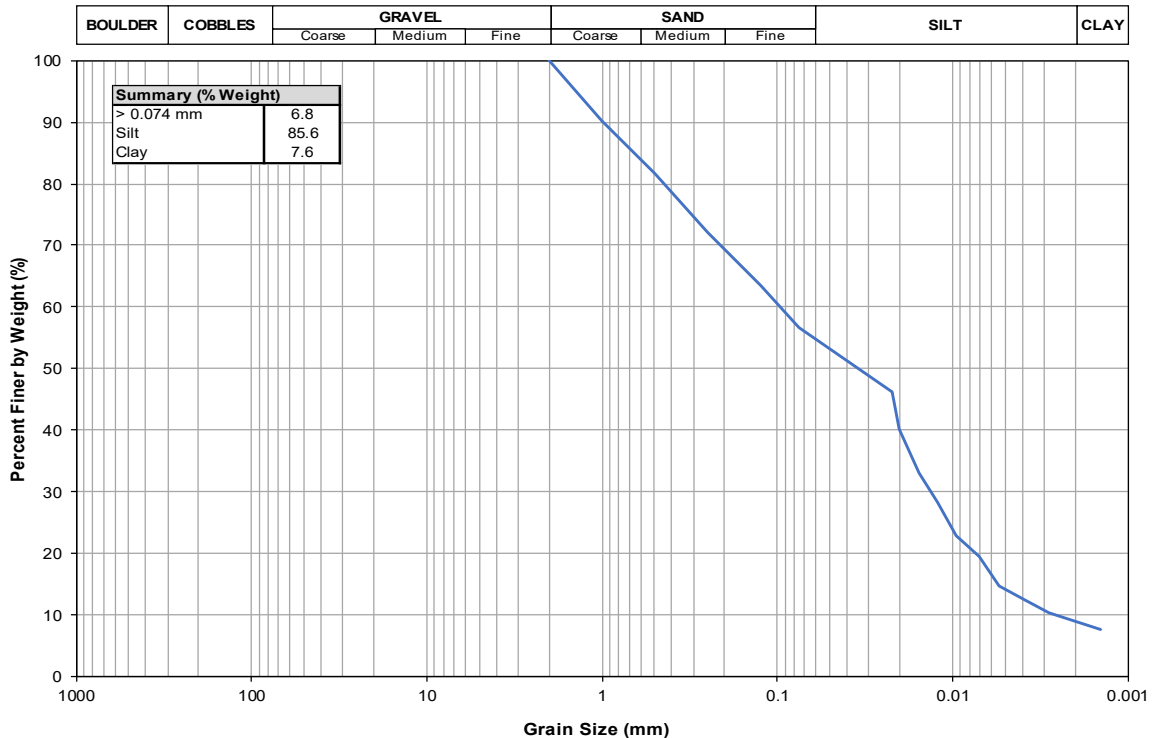
Initial Sieving			
Sieve opening (mm)	Mass retained (g)	% Retained	% Passing
2	0	0.00	100.00
1	119.87	9.70	90.30
0.5	105.84	8.56	81.74
0.25	119.76	9.69	72.05
0.125	105.45	8.53	63.52
0.075	84.2	6.81	56.71
Pan	700.91	-	-

Input Parameters	
Mass, total wet sample (grams):	1236.03
Moisture content (%):	0.00
Mass, dry soil > #200 sieve (grams):	535.12
Mass, dry soil < #200 sieve (grams):	700.91
Mass, soil into hydrometer (grams):	50.00
Mass, dispersant (grams):	1.00
Analysis parameters	
G _s	2.86
a	95.8

Date and Time (yyyy-mm-dd hh:mm)	Elapsed Time, t (min)	Temp. (C)	R (g/L)	Zero Correction (g/L)	Corrected R (g/L)	Z _r (cm)	K $\sqrt{\text{min/cm}}$	$\sqrt{Z_r/t}$ $\sqrt{\text{min/cm}}$	Grain Diameter (mm)	Relative Mass < d (0.074 mm) N %	Relative Mass Total Sample N %
05.04.2019 10:30	0										
05.04.2019 10:31	1	23.9	44.0	-1.5	42.5	3.3	0.01235	1.80	0.022	81.43	46.18
05.04.2019 10:32	2	23.9	38.5	-1.5	37.0	5.4	0.01235	1.64	0.020	70.89	40.20
05.04.2019 10:35	5	23.1	32.0	-1.5	31	7.8	0.01245	1.25	0.016	58.44	33.14
05.04.2019 10:40	10	22.8	27.5	-1.5	26	9.6	0.01248	0.98	0.012	49.82	28.25
05.04.2019 10:50	20	22.1	22.5	-1.5	21	11.5	0.01256	0.76	0.010	40.24	22.82
05.04.2019 11:10	40	21.6	19.5	-1.5	18	12.6	0.01265	0.56	0.007	34.49	19.56
05.04.2019 11:50	80	21.5	15.0	-1.5	14	14.3	0.01268	0.42	0.005	25.87	14.67
05.04.2019 13:10	160	21.5	13	-1.5	12	15.1	0.01268	0.31	0.004	22.03	12.49
05.04.2019 15:50	320	21.5	11	-1.5	10	15.9	0.01268	0.22	0.003	18.20	10.32
06.04.2019 08:30	1320	20.9	8.5	-1.5	7	16.8	0.01277	0.11	0.001	13.41	7.61

Notes:

Note 1: The a coefficient corresponds to the specific gravity of 2.86 for this material.



Testing date: 05.May.19

Tested material: Infiltration Test 2 Material

Project: TBA4900 - Master Thesis

Operator: K.Robinson

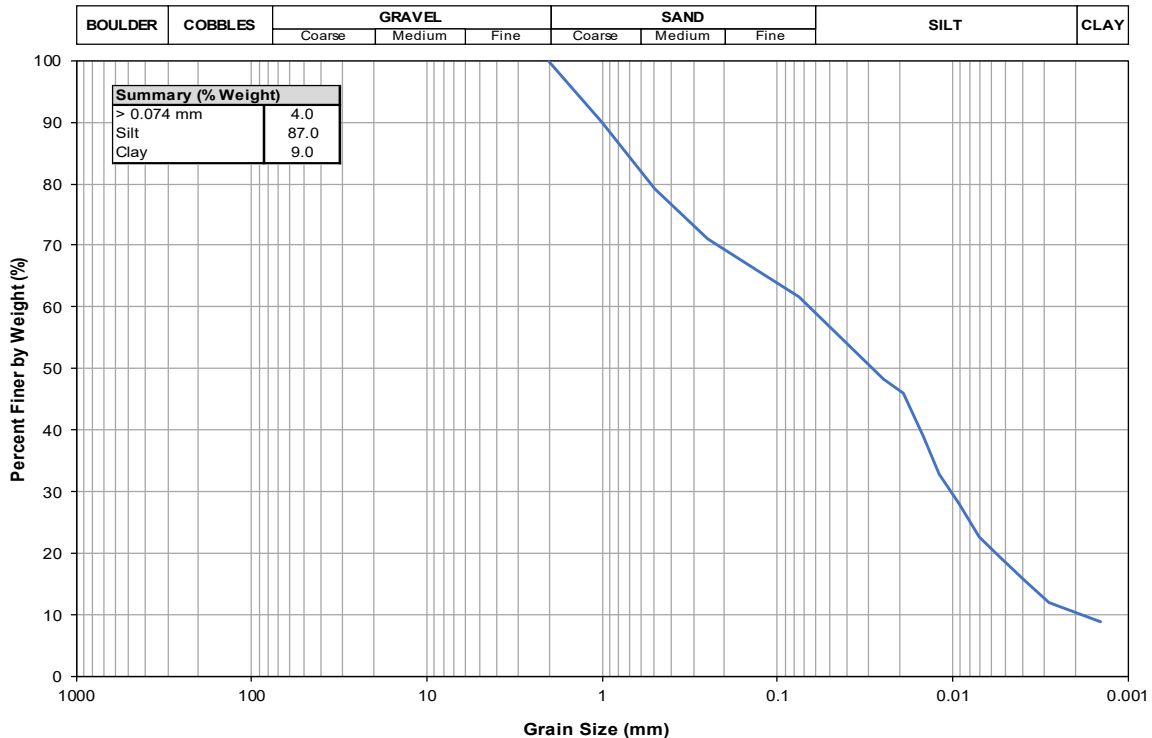
Initial Sieving			
Sieve opening (mm)	Mass retained (g)	% Retained	% Passing
2	0.14	0.19	99.81
1	7.1	9.68	90.13
0.5	8.05	10.98	79.15
0.25	5.99	8.17	70.98
0.125	3.91	5.33	65.65
0.075	2.95	4.02	61.63
Pan	52.43	-	-

Input Parameters	
Mass, total wet sample (grams):	80.57
Moisture content (%):	0.00
Mass, dry soil > #200 sieve (grams):	28.14
Mass, dry soil < #200 sieve (grams):	52.43
Mass, soil into hydrometer (grams):	52.18
Mass, dispersant (grams):	1.00
Analysis parameters	
G _s	2.86
a	95.8

Date and Time (yyyy-mm-dd hh:mm)	Elapsed Time, t (min)	Temp. (C)	R (g/L)	Zero Correction (g/L)	Corrected R (g/L)	Z _r (cm)	K $\sqrt{\text{min/cm}}$	$\sqrt{Z_r/t}$ $\sqrt{\text{min/cm}}$	Grain Diameter (mm)	Relative Mass < d (0.074 mm) N %	Relative Mass Total Sample N %
05.05.2019 11:35	0										
05.05.2019 11:36	1	24.2	42.0	-1.5	40.5	4.0	0.01228	2.00	0.025	74.36	48.39
05.05.2019 11:37	2	24.2	40	-1.5	38.5	4.8	0.01228	1.55	0.019	70.68	46.00
05.05.2019 11:40	5	24.2	34.0	-1.5	33	7.1	0.01228	1.19	0.015	59.67	38.83
05.05.2019 11:45	10	22.7	29.0	-1.5	28	9.0	0.01248	0.95	0.012	50.49	32.85
05.05.2019 11:55	20	22.0	25.0	-1.5	24	10.5	0.01259	0.73	0.009	43.14	28.08
05.05.2019 12:15	40	21.2	20.5	-1.5	19	12.2	0.01269	0.55	0.007	34.88	22.70
05.05.2019 12:55	80	21.1	17.5	-1.5	16	13.4	0.01272	0.41	0.005	29.38	19.12
05.05.2019 14:15	160	21.0	14.5	-1.5	13	14.5	0.01273	0.30	0.004	23.87	15.53
05.05.2019 16:55	320	21.0	11.5	-1.5	10	15.7	0.01273	0.22	0.003	18.36	11.95
06.05.2019 09:35	1320	21.0	9	-1.5	8	16.6	0.01273	0.11	0.001	13.77	8.96

Notes:

Note 1: The a coefficient corresponds to the specific gravity of 2.86 for this material.



Testing date: 05.May.19

Tested material: Infiltration Test 3 Material

Project: TBA4900 - Master Thesis

Operator: K.Robinson

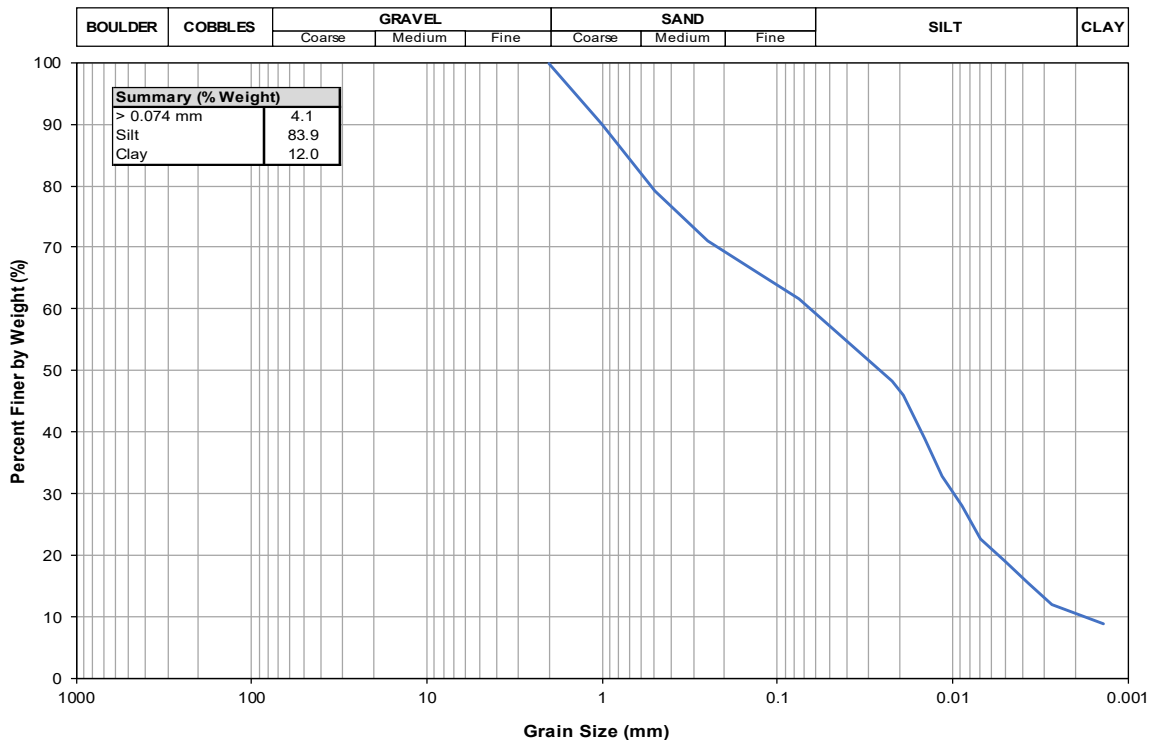
Initial Sieving			
Sieve opening (mm)	Mass retained (g)	% Retained	% Passing
2	0.09	0.12	99.88
1	7.31	10.11	89.76
0.5	7.95	11.00	78.76
0.25	5.59	7.73	71.03
0.125	3.66	5.06	65.97
0.075	2.96	4.10	61.87
Pan	52.12	-	-

Input Parameters	
Mass, total wet sample (grams):	79.68
Moisture content (%):	0.00
Mass, dry soil > #200 sieve (grams):	27.56
Mass, dry soil < #200 sieve (grams):	52.12
Mass, soil into hydrometer (grams):	52.03
Mass, dispersant (grams):	1.00
Analysis parameters	
G _s	2.86
a	95.8

Date and Time (yyyy-mm-dd hh:mm)	Elapsed Time, t (min)	Temp. (C)	R (g/L)	Zero Correction (g/L)	Corrected R (g/L)	Z _r (cm)	K $\sqrt{\text{min/cm}}$	$\sqrt{Z_r/t}$ $\sqrt{\text{min/cm}}$	Grain Diameter (mm)	Relative Mass < d (0.074 mm) N %	Relative Mass Total Sample N %
05.05.2019 11:42	0										
05.05.2019 11:43	1	23.9	44.0	-1.5	42.5	3.3	0.01235	1.80	0.022	78.25	51.19
05.05.2019 11:44	2	23.4	40	-1.5	38.5	4.8	0.01240	1.55	0.019	70.89	46.37
05.05.2019 11:47	5	23.1	35.0	-1.5	34	6.7	0.01245	1.16	0.014	61.68	40.35
05.05.2019 11:52	10	22.6	30.5	-1.5	29	8.4	0.01250	0.92	0.011	53.40	34.93
05.05.2019 12:02	20	21.8	26.5	-1.5	25	9.9	0.01252	0.71	0.009	46.03	30.11
05.05.2019 12:22	40	21.2	22.0	-1.5	21	11.7	0.01269	0.54	0.007	37.75	24.69
05.05.2019 13:02	80	21.0	20.0	-1.5	19	12.4	0.01273	0.39	0.005	34.06	22.28
05.05.2019 14:22	160	21.0	16.5	-1.5	15	13.8	0.01273	0.29	0.004	27.62	18.07
05.05.2019 17:02	320	21.0	15	-1.5	14	14.3	0.01273	0.21	0.003	24.86	16.26
06.05.2019 09:42	1320	21.0	11.5	-1.5	10	15.7	0.01273	0.11	0.001	18.41	12.04

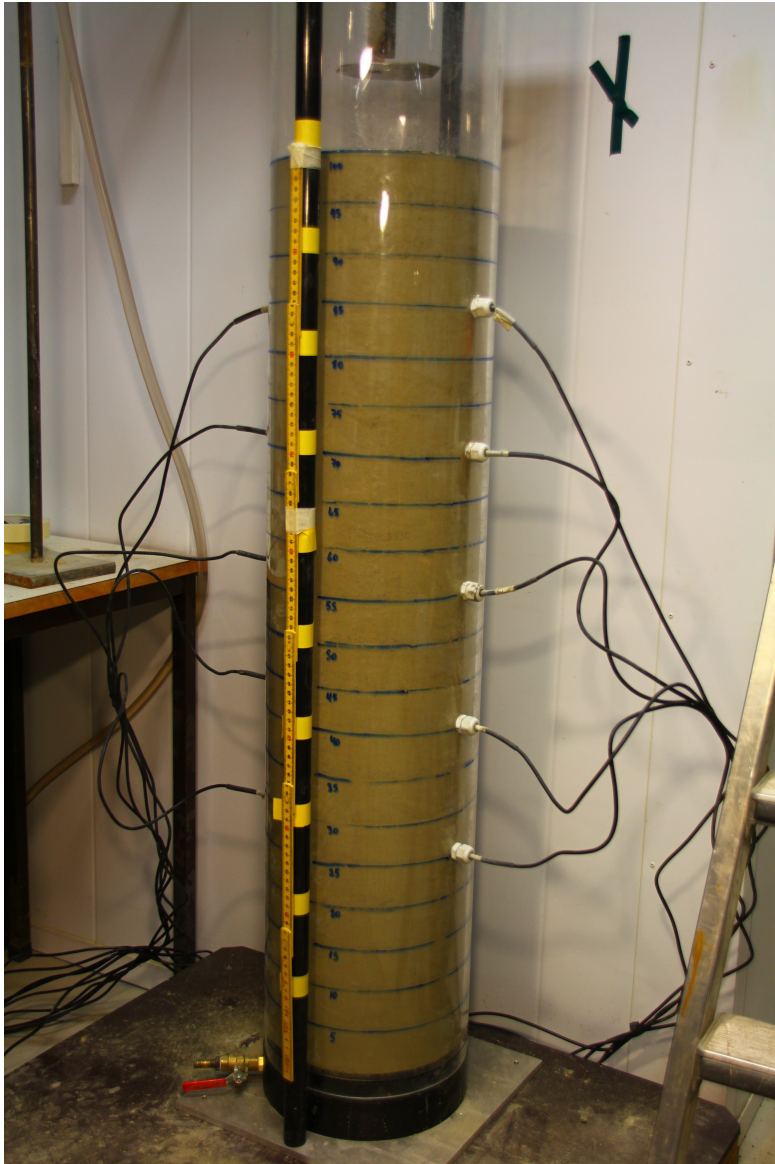
Notes:

Note 1: The a coefficient corresponds to the specific gravity of 2.86 for this material.

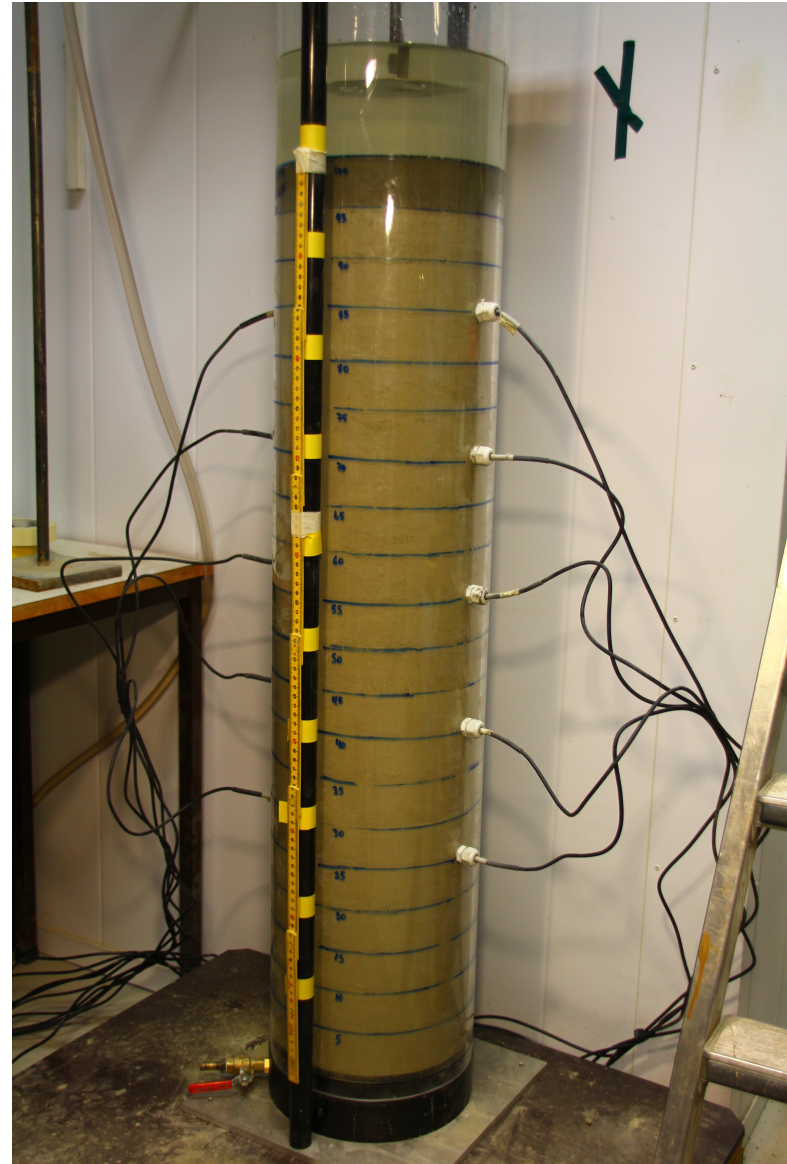


Appendix C

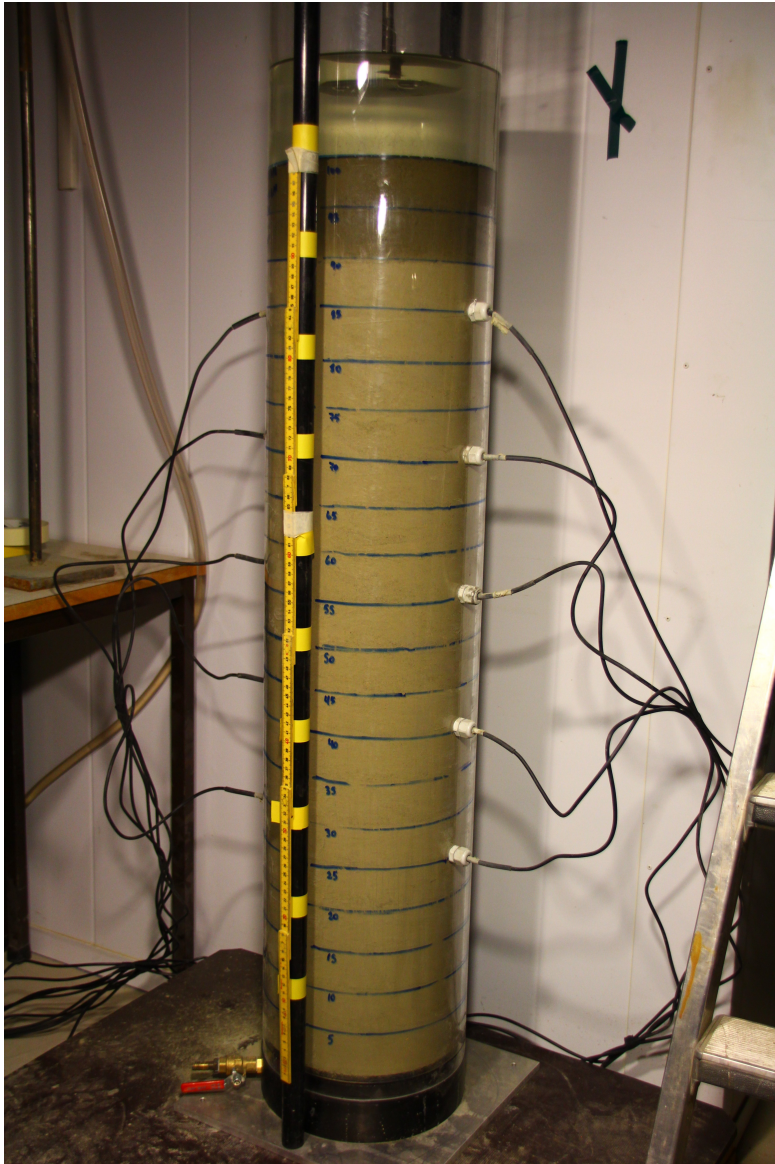
Sample Photos from Test 2



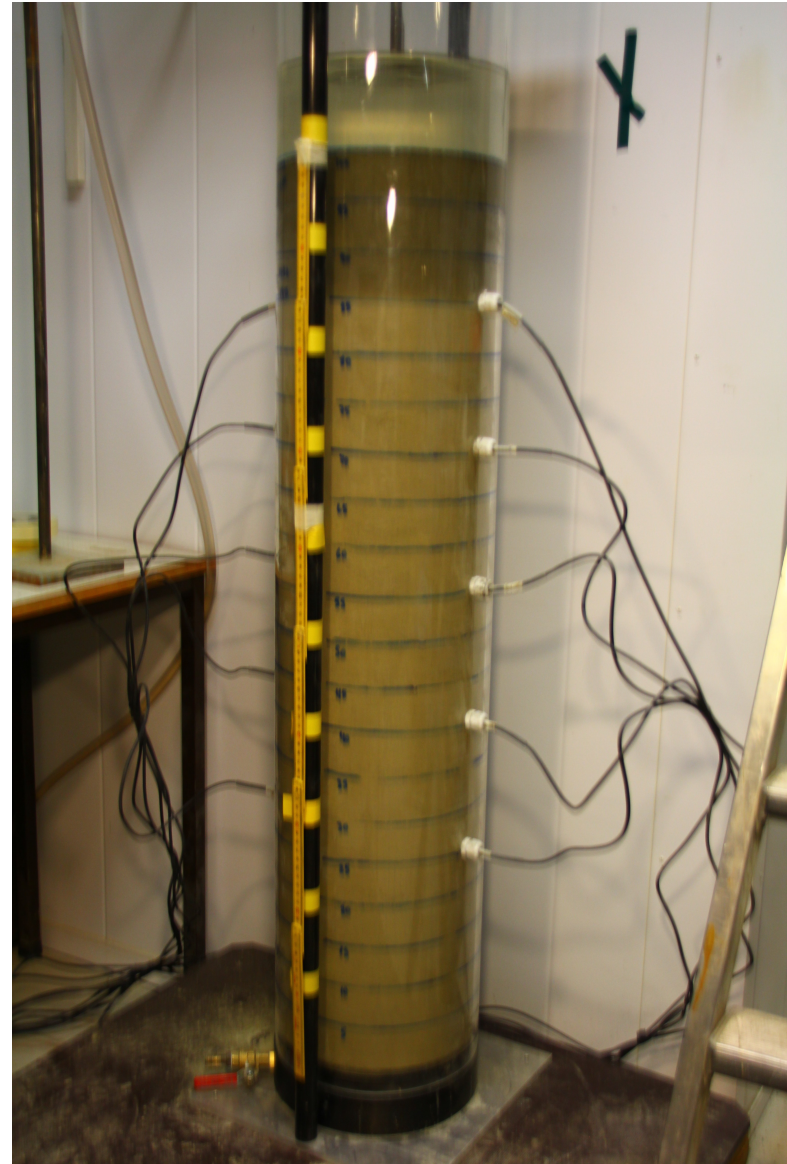
(a) Test initiation: 21.04.2019 16:22



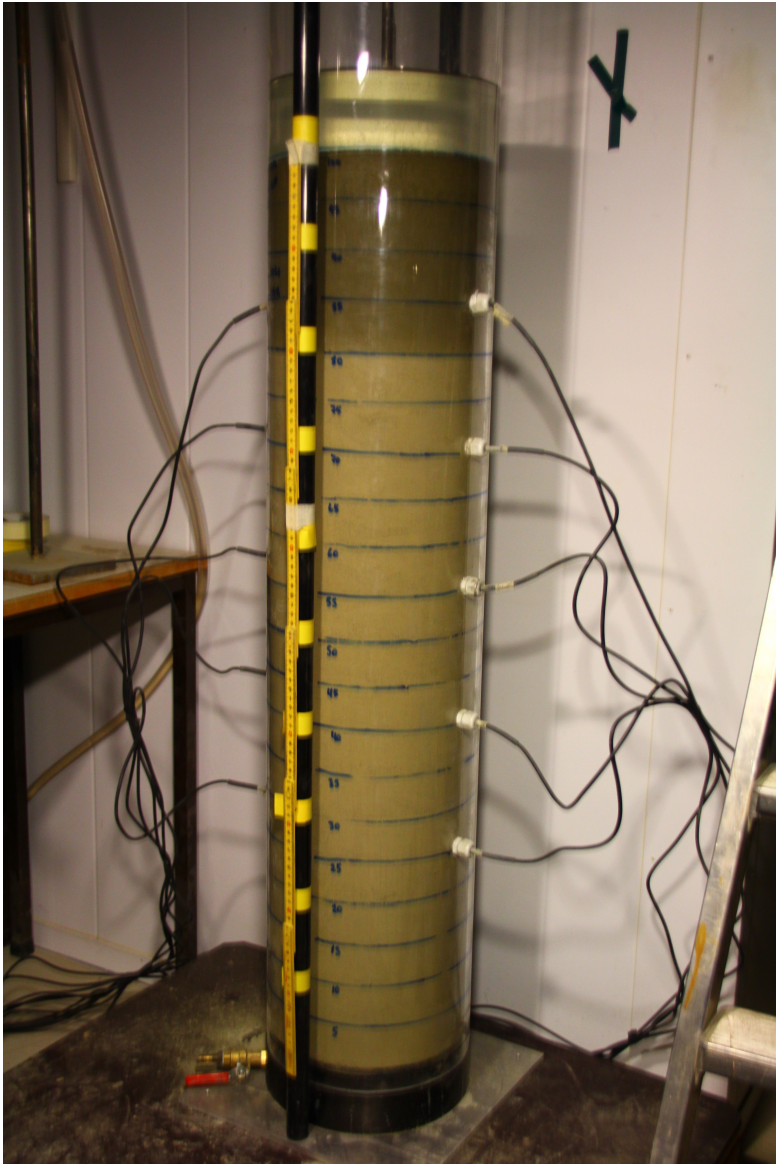
(b) 5 cm: 21.04.2019 16:46



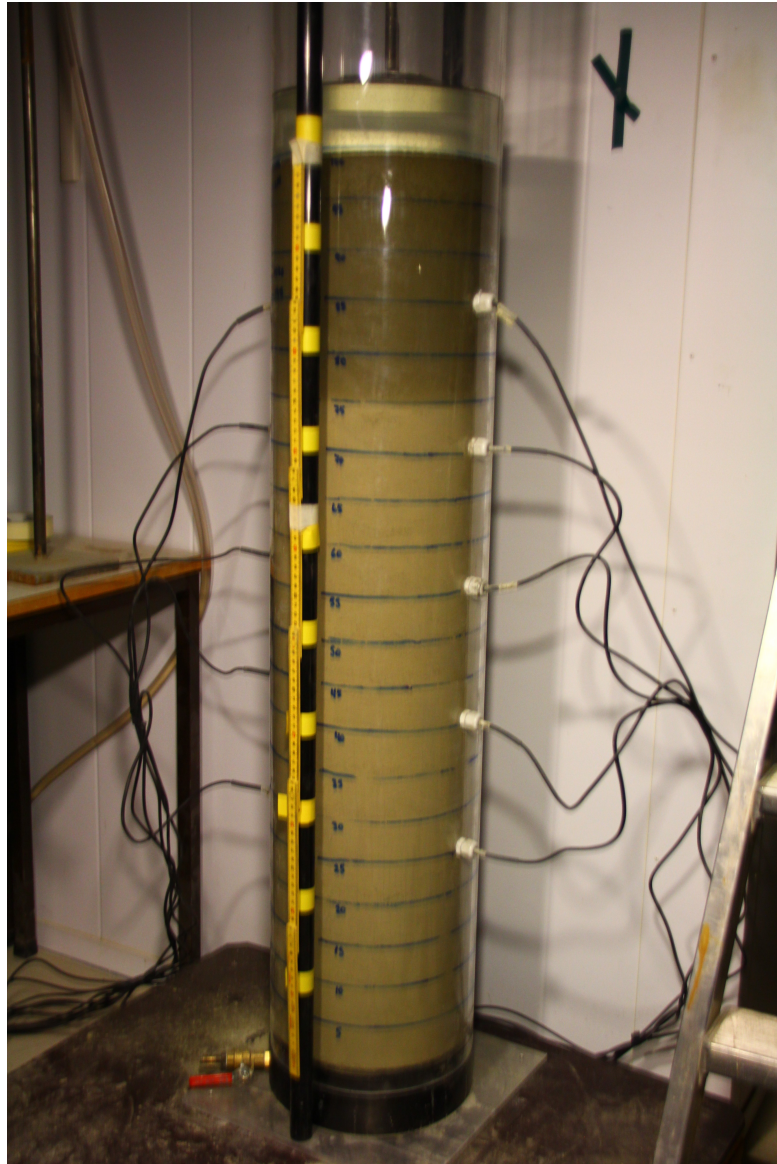
(a) 10 cm: 21.04.2019 17:46



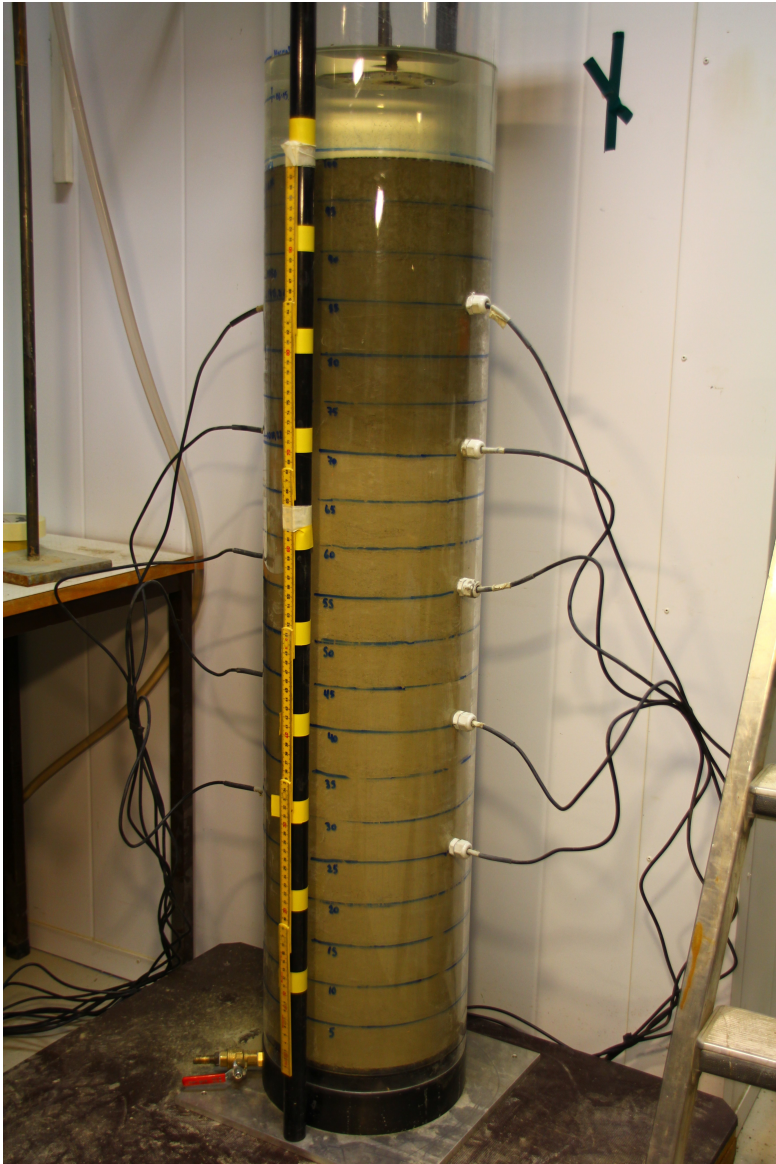
(b) 15 cm: 21.04.2019 19:38



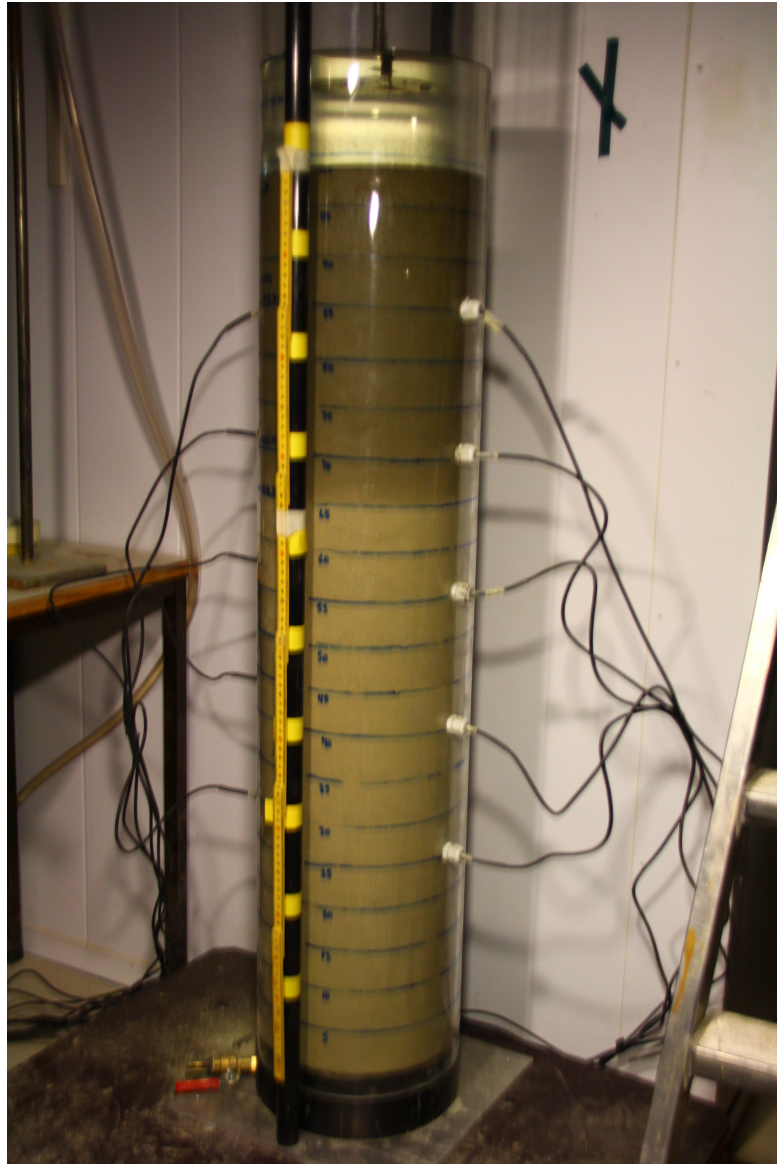
(a) 20 cm: 21.04.2019 22:48



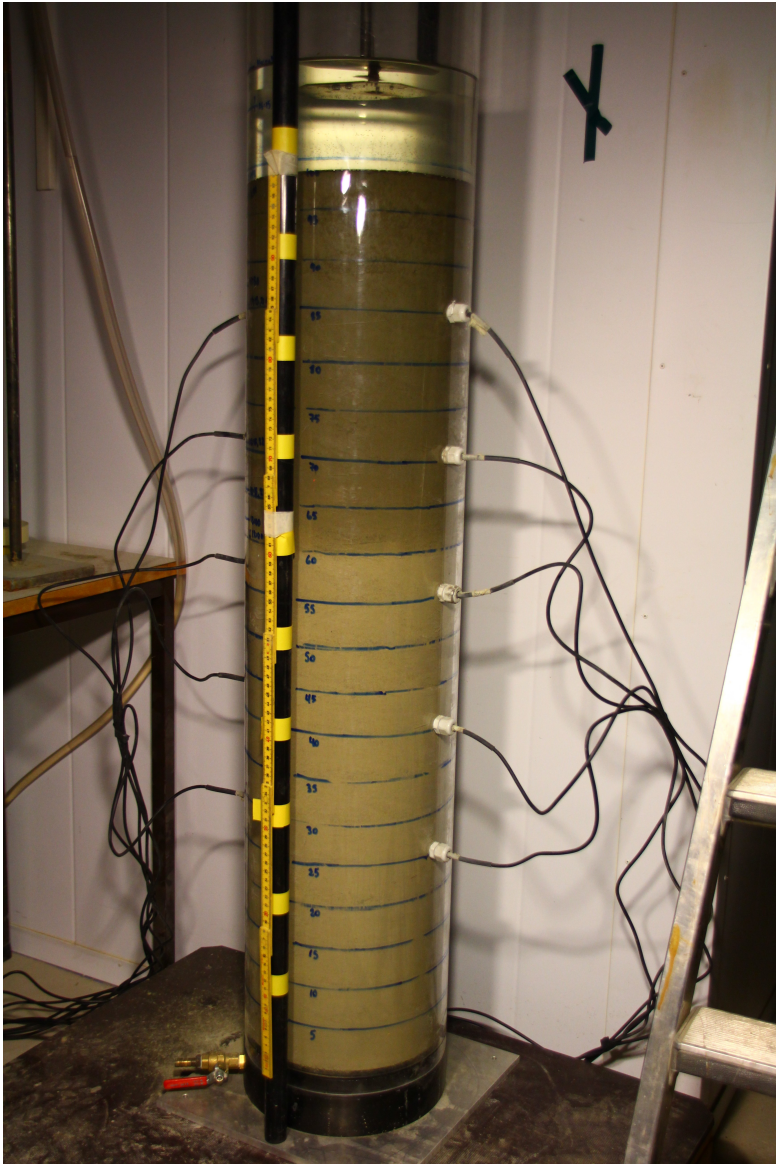
(b) 25 cm: 22.04.2019 02:28



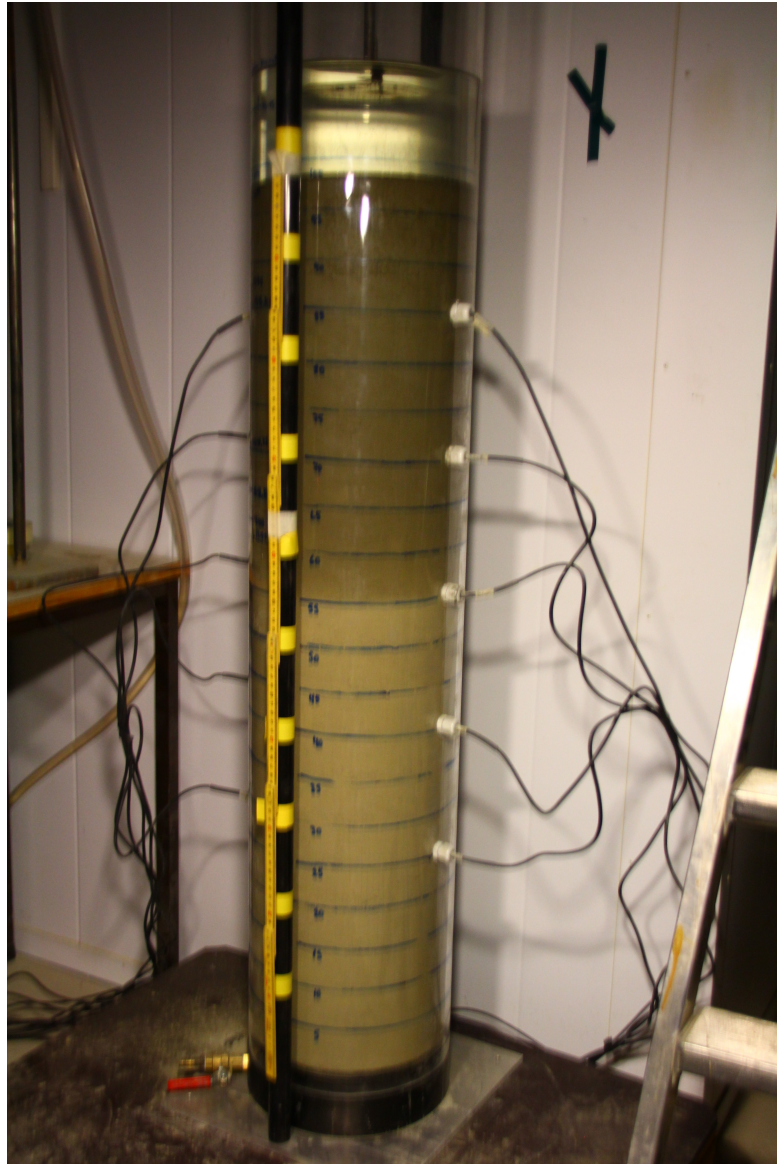
(a) 30 cm: 22.04.2019 06:56



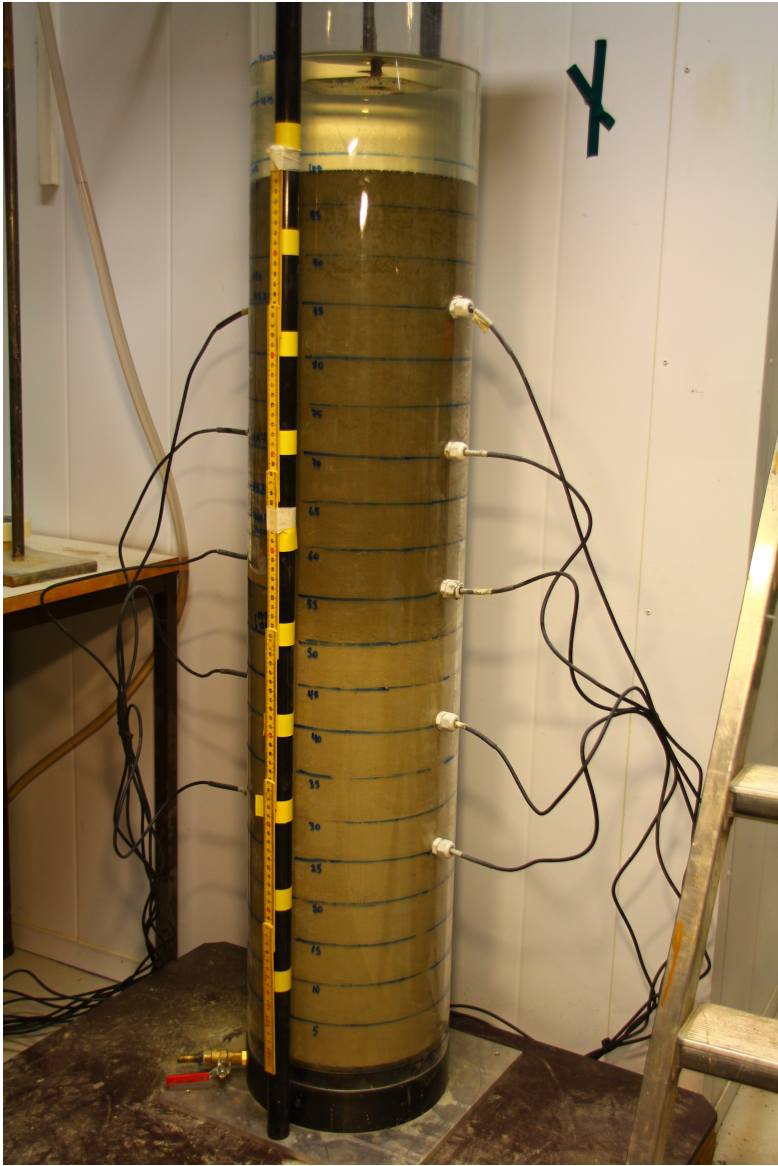
(b) 35 cm: 22.04.2019 11:51



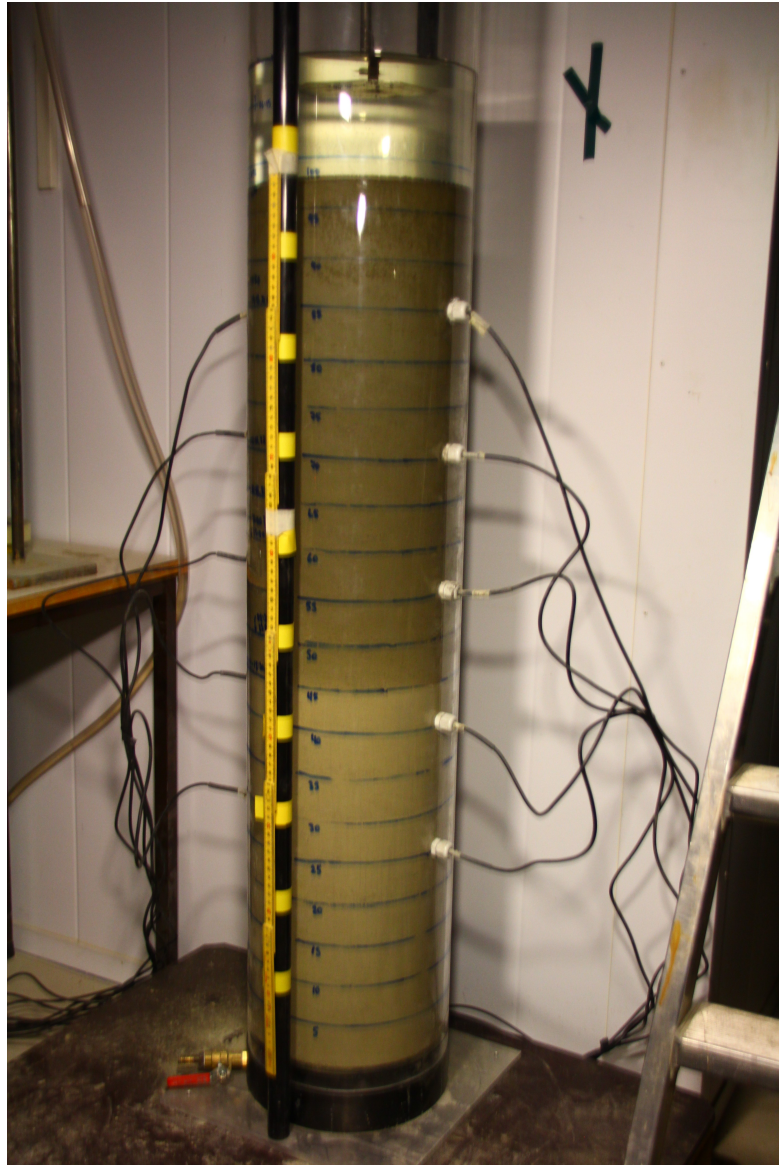
(a) 40 cm: 22.04.2019 18:07



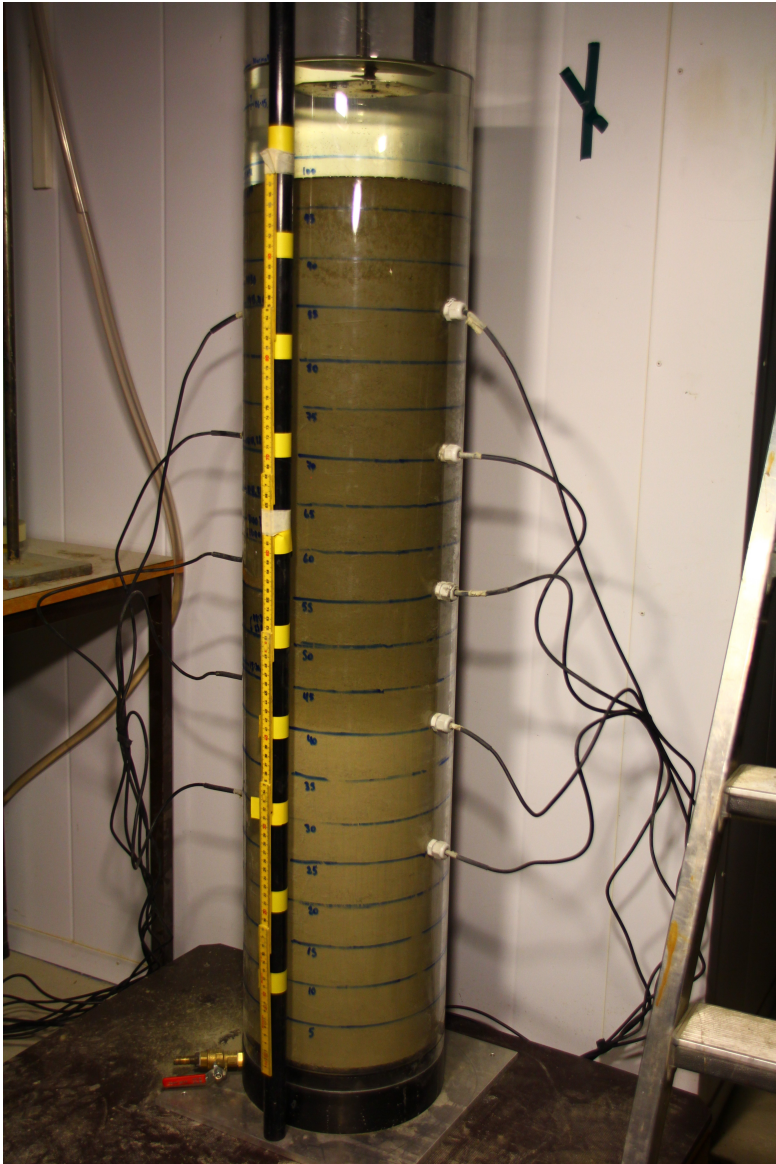
(b) 45 cm: 23.04.2019 00:49



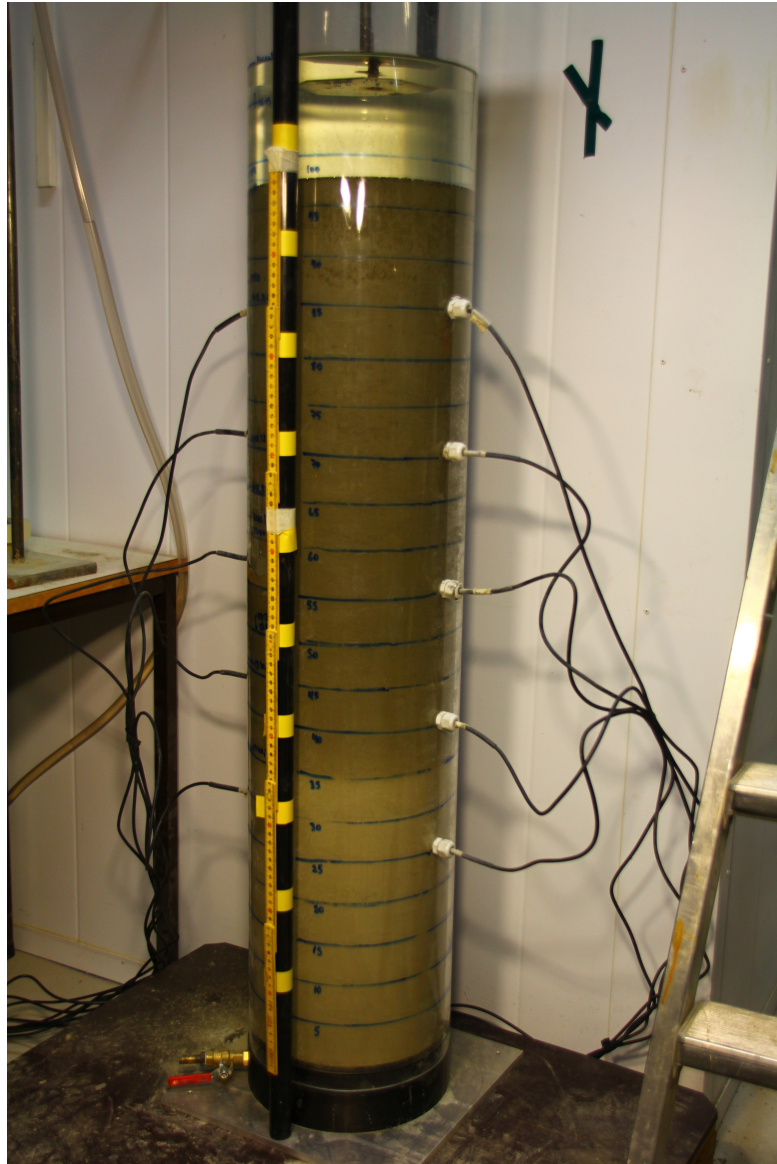
(a) 50 cm: 23.04.2019 08:37



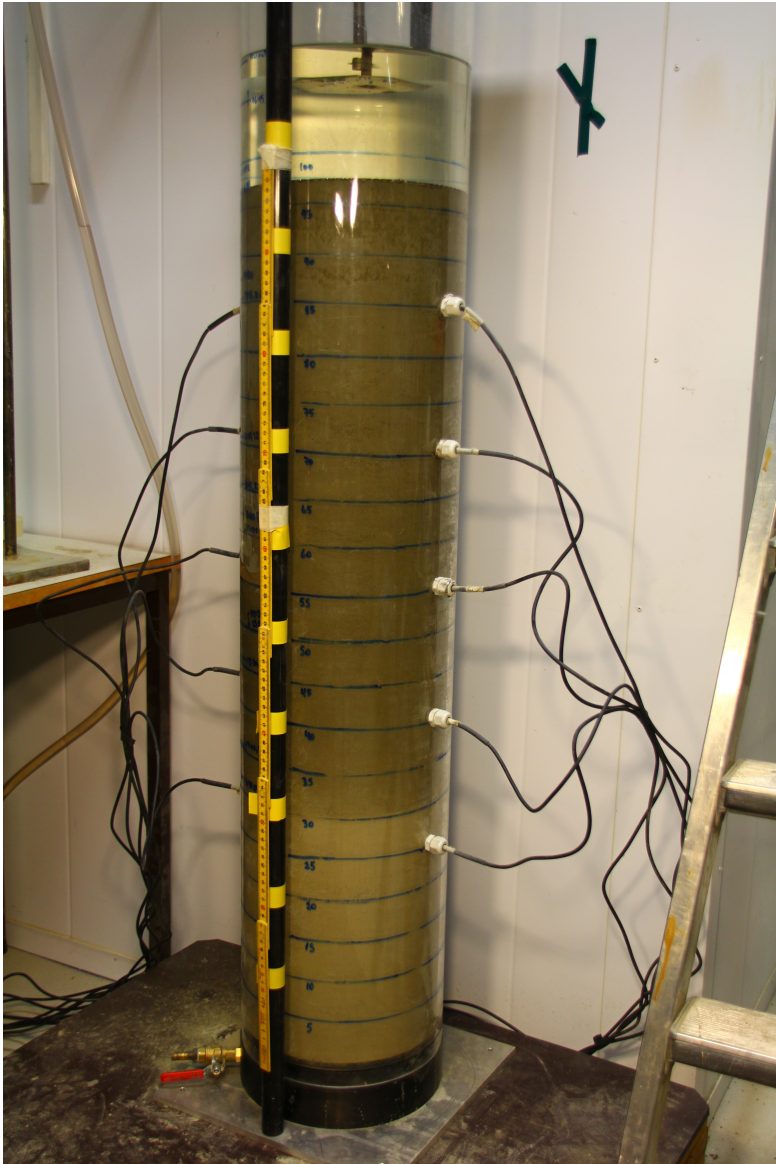
(b) 55 cm: 23.04.2019 17:15



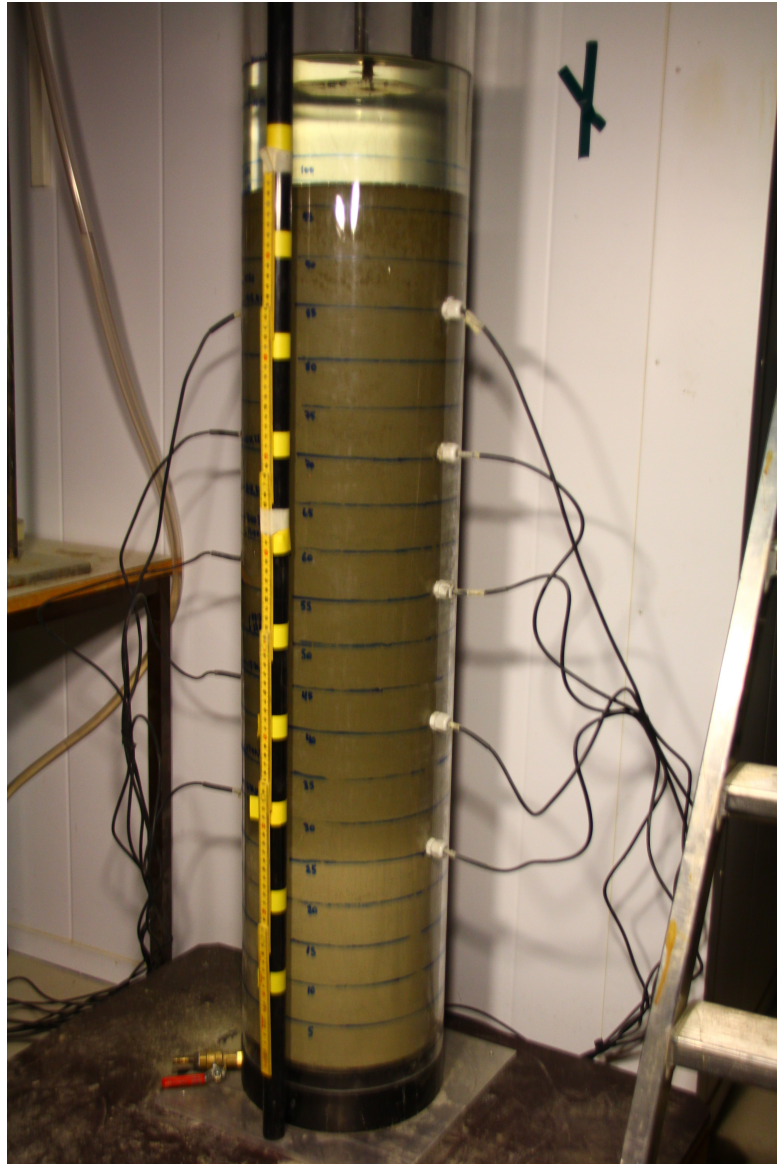
(a) 60 cm: 24.04.2019 00:37



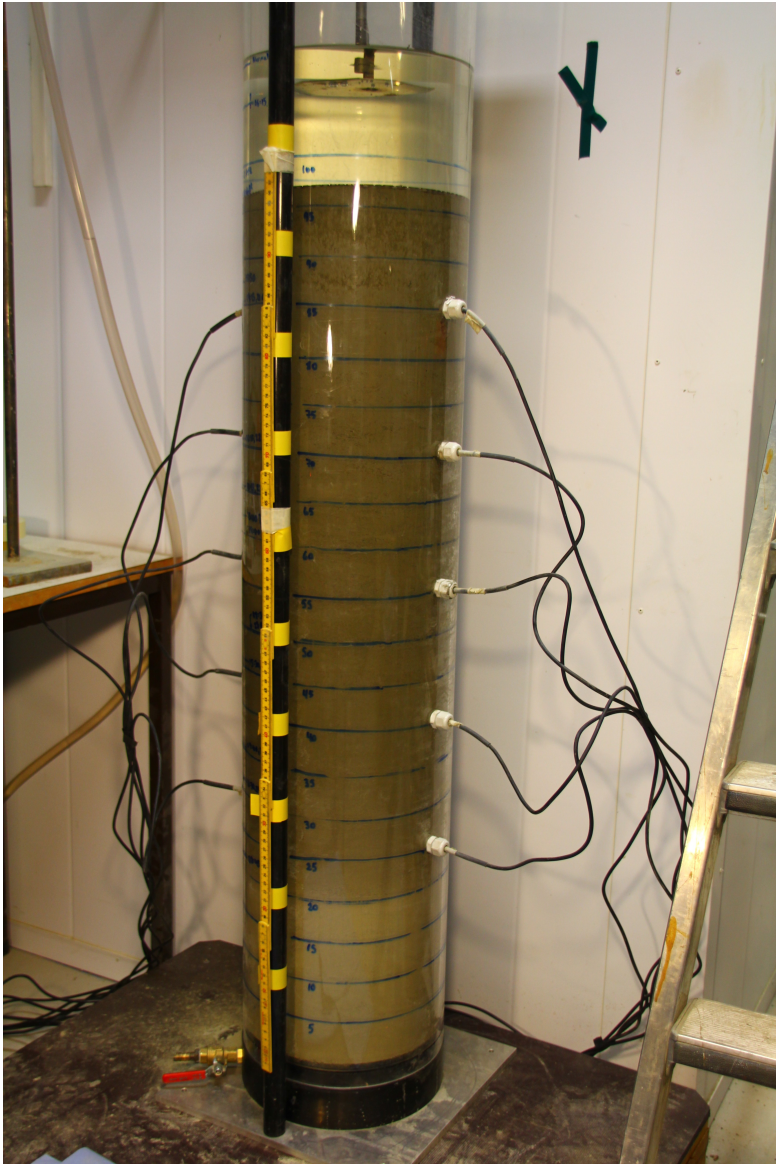
(b) 65 cm: 24.04.2019 11:23



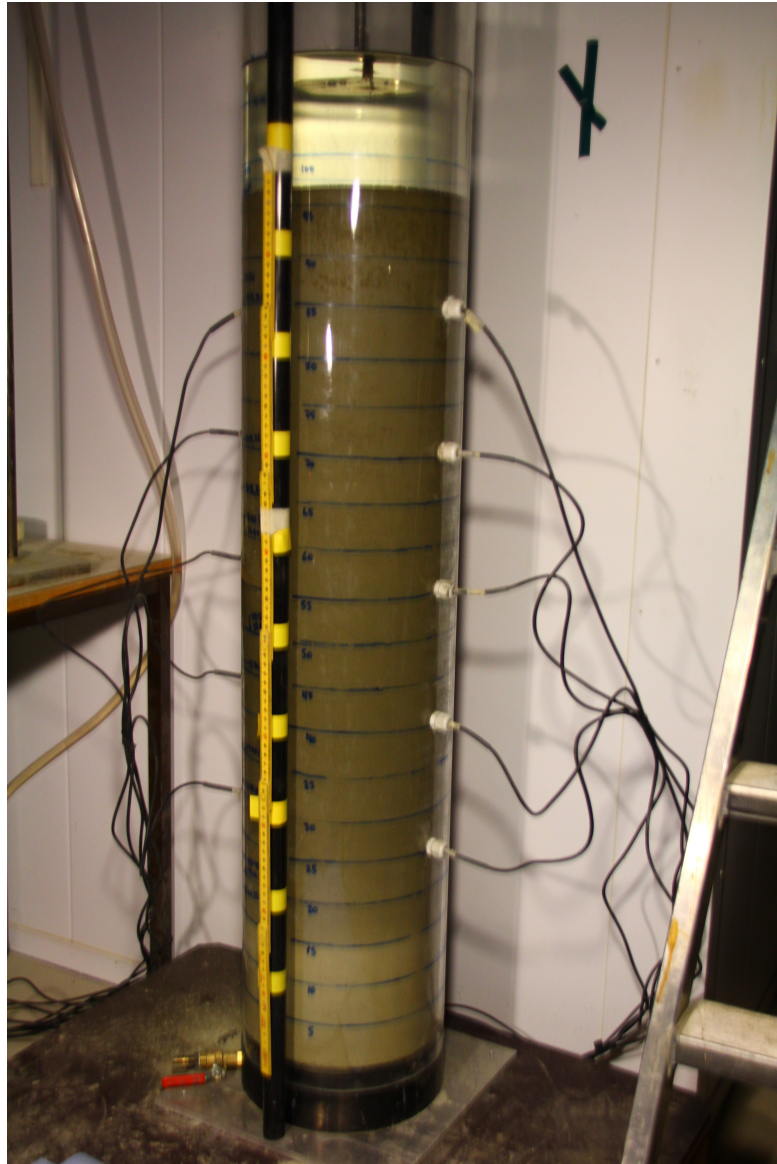
(a) 70 cm: 24.04.2019 20:22



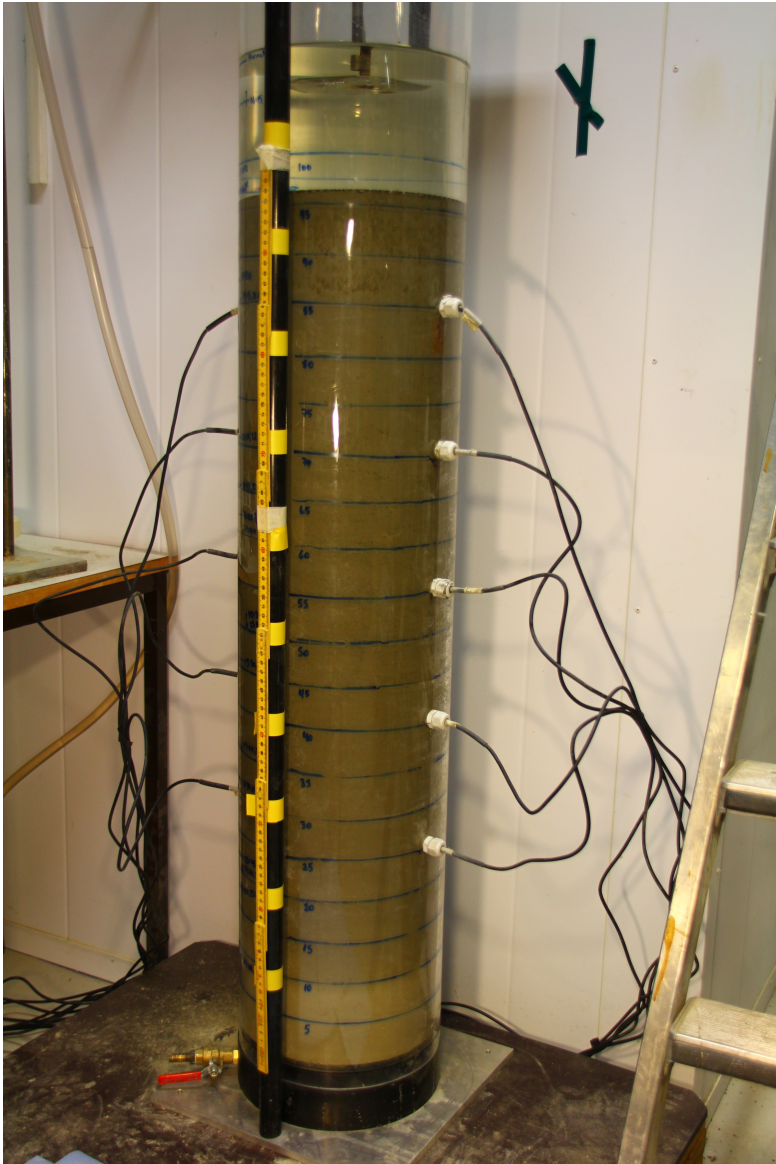
(b) 75 cm: 25.04.2019 04:01



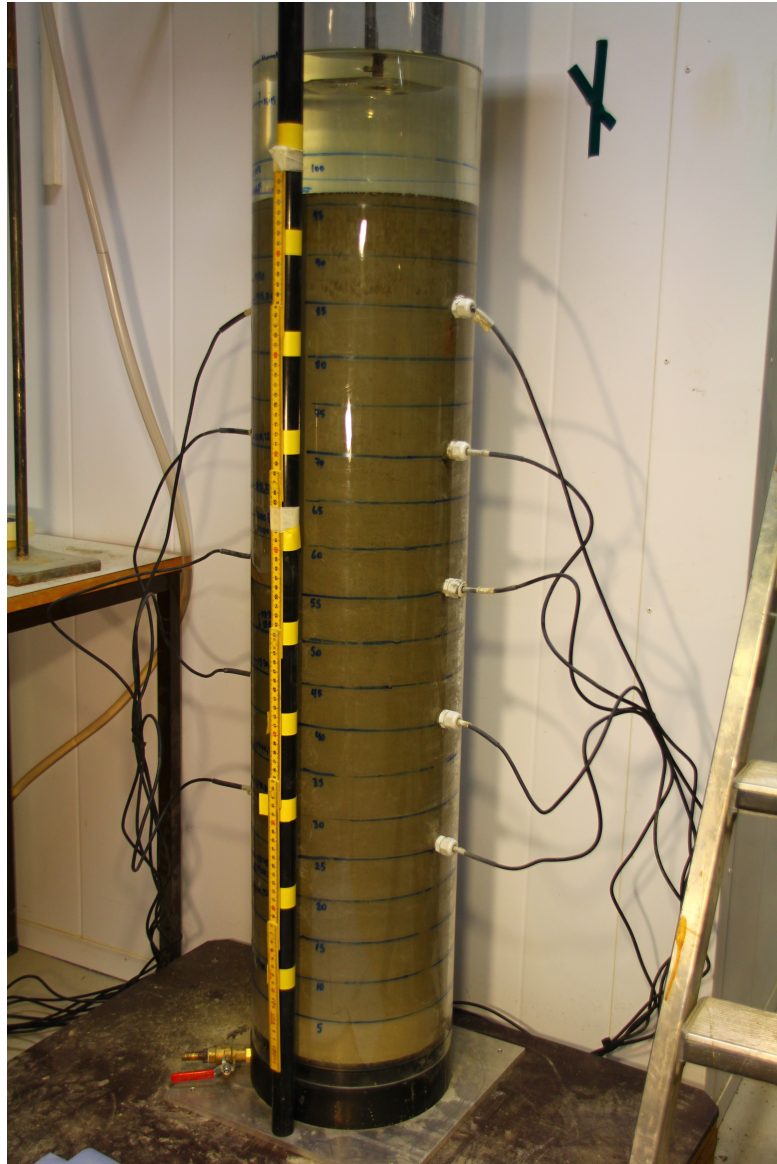
(a) 80 cm: 25.04.2019 13:57



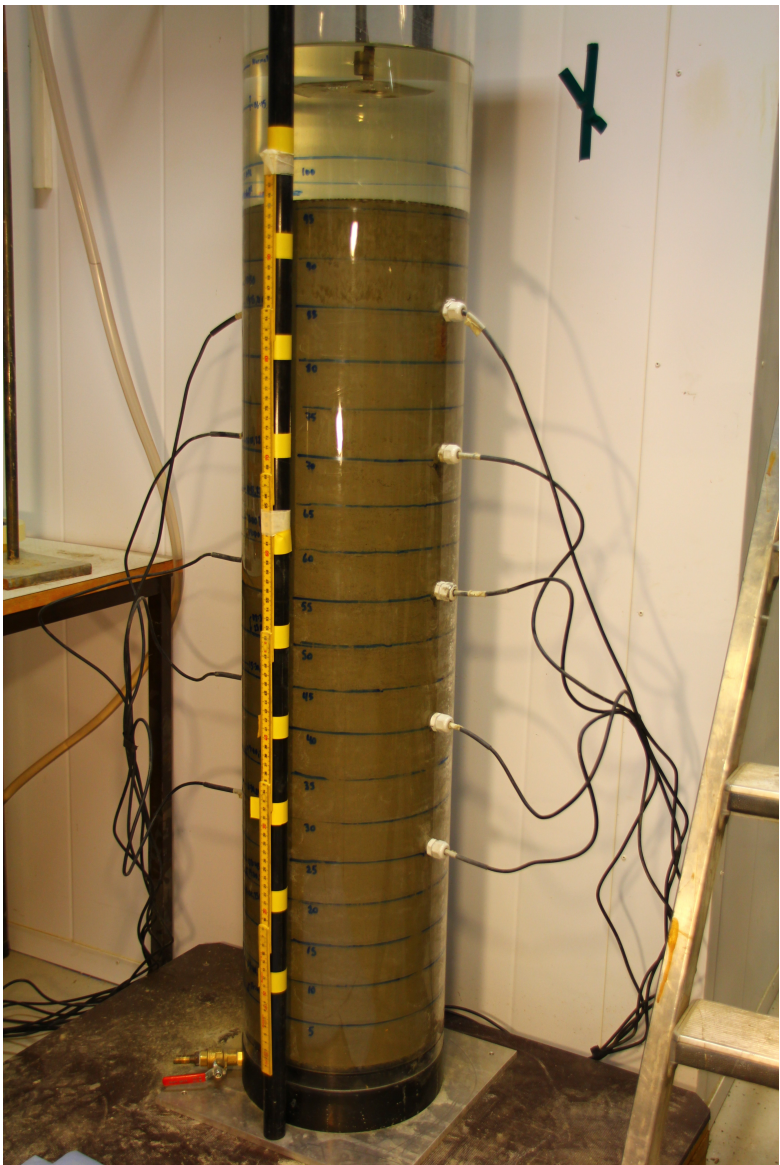
(b) 85 cm: 25.04.2019 22:47



(a) 90 cm: 26.04.2019 09:08



(b) 95 cm: 26.04.2019 17:43



(a) Test completion: 27.04.2019 09:11